

Lawrence Berkeley National Laboratory

Recent Work

Title

QUANTUM ELECTRODYNAMICS IN STRONG AND SUPERCRITICAL FIELDS

Permalink

<https://escholarship.org/uc/item/1hm3w3b3>

Author

Brodsky, Stanley J.

Publication Date

1977-02-01

To be published in "Heavy Ion Atomic
Physics," Ivan A. Sellin, ed.,
Springer-Verlag, (1977)

LBL-6087 *2 c.1*
X SLAC-PUB-1889

RECEIVED
LAWRENCE
BERKELEY LABORATORY

APR 26 1977

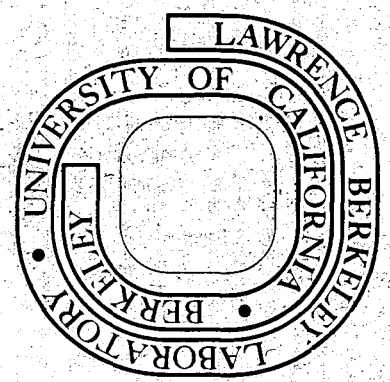
LIBRARY AND
DOCUMENTS SECTION

QUANTUM ELECTRODYNAMICS IN STRONG AND
SUPERCritical FIELDS

For Reference
Not to be taken from this room

Stanley J. Brodsky and Peter J. Mohr

February 1977



Prepared for the U. S. Energy Research and
Development Administration under Contract W-7405-ENG-48

DISCLAIMER

This document was prepared as an account of work sponsored by the United States Government. While this document is believed to contain correct information, neither the United States Government nor any agency thereof, nor the Regents of the University of California, nor any of their employees, makes any warranty, express or implied, or assumes any legal responsibility for the accuracy, completeness, or usefulness of any information, apparatus, product, or process disclosed, or represents that its use would not infringe privately owned rights. Reference herein to any specific commercial product, process, or service by its trade name, trademark, manufacturer, or otherwise, does not necessarily constitute or imply its endorsement, recommendation, or favoring by the United States Government or any agency thereof, or the Regents of the University of California. The views and opinions of authors expressed herein do not necessarily state or reflect those of the United States Government or any agency thereof or the Regents of the University of California.

0

LBL-6087
SLAC-PUB-1889

QUANTUM ELECTRODYNAMICS IN STRONG AND SUPERCRITICAL FIELDS

Stanley J. Brodsky
Stanford Linear Accelerator Center
Stanford University
Stanford, California 94305

Peter J. Mohr
Department of Physics and
Lawrence Berkeley Laboratory
University of California
Berkeley, California 94720

February 1977

TABLE OF CONTENTS

Introduction	1
A.1 The Electrodynamics of High-Z Electronic Atoms	4
A.1.1 Lamb Shift in Hydrogenlike Ions	4
A.1.2 Lamb Shift in Heliumlike Ions	9
A.1.3 Quantum Electrodynamics in High-Z Neutral Atoms	11
A.1.4 High-Z Atoms and Limits on Nonlinear Modifications of QED	14
A.1.5 Wichmann-Kroll Approach to Strong-Field Electrodynamics	15
A.2 The Electrodynamics of High-Z Muonic Atoms	21
A.2.1 General Features	21
A.2.2 Vacuum Polarization	24
A.2.3 Additional Radiative Corrections	32
A.2.4 Nuclear Effects	34
A.2.5 Electron Screening	35
A.2.6 Summary and Comparison with Experiment	37
A.2.7 Muonic Helium	41
A.2.8 Nonperturbative Vacuum Polarization Modification and Possible Scalar Particles	45
A.3 Quantum Electrodynamics in Heavy-Ion Collisions and Supercritical Fields	48
A.3.1 Electrodynamics for $Z\alpha > 1$	48
A.3.2 Spontaneous Pair Production in Heavy-Ion Collisions	55
A.3.3 Calculation of the Critical Internuclear Distance	61
A.3.4 Calculation of the Spontaneous Positron Production Rate	62
A.3.5 Induced Versus Adiabatic Pair Production	69
A.3.6 Vacancy Formation in Heavy-Ion Collisions	72
A.3.7 Nuclear Excitation and Other Background Effects	73
A.3.8 Radiative Corrections in Critical Fields	75
A.3.9 Coherent Production of Photons in Heavy-Ion Collisions	77
A.3.10 Self-Neutralization of Matter	78
A.3.11 Very Strong Magnetic Field Effects	79
Conclusion	81
Acknowledgments	83
References	84
Figure Captions	95
Figures	99

02104708934

INTRODUCTION

Quantum electrodynamics (QED), the theory of the interactions of electrons and muons via photons, has now been tested both to high precision – at the ppm level – and to short distances of order 10^{-14} - 10^{-15} cm. The short distance tests, particularly the colliding beam measurements of $e^+e^- + \mu^+\mu^-$, $\gamma\gamma$, and e^+e^- [A.1], are essentially tests of QED in the Born approximation. On the other hand, the precision anomalous magnetic moment and atomic physics measurements check the higher order loop corrections and predictions dependent on the renormalization procedure. Despite the extraordinary successes, it is still important to investigate the validity of QED in the strong field domain. In particular, high- $Z\alpha$ atomic physics tests, especially the Lamb shift in high- Z hydrogenic atoms, test the QED amplitude in the situation where the fermion propagator is far off the mass shell and cannot be handled in perturbation theory in $Z\alpha$, but where the renormalization program for perturbation theory in α must be used. High- Z heavy-ion collisions can be used to probe the Dirac spectrum in the non-perturbative domain of high $Z\alpha$, where spontaneous positron production can occur, and where two different vacuum states must be considered.

Another reason to pursue the high- $Z\alpha$ domain is that the spectrum of radiation emitted when two colliding heavy ions (temporarily) unite can lead to a better understanding of relativistic molecular physics. This physics is reviewed in the accompanying articles of this volume. Furthermore, the atomic spectra of the low-lying electron states and outgoing positron continua reflect the nature of the nuclear charge distribution, and could be a useful tool in unraveling the nuclear physics and dynamics of a close

heavy-ion collision. Somewhat complementary to these tests are the studies of Delbrück scattering (elastic scattering of photons by a strong Coulomb field) reviewed in Ref. A.2.

One of the intriguing aspects of high field strength quantum electrodynamics is the possibility that it may provide a model for quark dynamics. Present theoretical ideas for the origin of the strong interactions have focused on renormalizable field theories, such as quantum chromodynamics (QCD), where the quarks are the analogues of the leptons, and the gluons – the generalizations of the photon – are themselves charged (non-abelian Yang-Mills theory). In contrast to QED where the vacuum polarization strengthens the charged particle interaction at short distances, in QCD the interactions weaken at short distances, and (presumably) become very strong at large separations.

To see the radical possibilities in strong fields, suppose α is large in QED and the first bound state of positronium has binding energy $\epsilon > m$. The total mass of the atom \mathcal{M} is then less than the mass of a free electron $\mathcal{M} = 2m - \epsilon < m$. Consider then an experiment in which an e^+e^- pair is produced near threshold – e.g. via a weak current process. Since an additional virtual pair may be present, the produced pair can spontaneously decay to two positronium atoms in the ground state, each with finite kinetic energy. Thus bound states, and not free fermions, are produced! It is clearly an interesting question whether strong field strength in QED can provide a mechanism analogous to quark confinement in hadron dynamics. The work of K. WILSON [A.3] and J. MANDULA [A.4] is especially relevant here. The studies of spontaneous pair production in heavy-ion collisions (see Section A.3) provide a simple phenomenological framework where some of the effects of strong fields can be tested.

00004708935

It should be noted that our review only touches a limited aspect of high- $Z\alpha$ electrodynamics. We consider only the cases of a fixed or heavy source for a high- $Z\alpha$ Coulomb potential. An important open question concerns the behavior of the Bethe-Salpeter equation for positronium in the large α domain, and in particular, whether the binding energy can become comparable to the mass of the constituents so that $\mathcal{M} = 2m - \epsilon \rightarrow 0$.

The organization of this article is as follows: We review in detail the recent work on the atomic spectra of high- Z electronic (Section A.1) and muonic atoms (Section A.2), including muonic helium, with emphasis on the Lamb shift and vacuum polarization corrections which test strong field quantum electrodynamics. The theoretical framework of the QED calculations for strong fields is discussed in Section A.1.5. The constraints on non-perturbative vacuum polarization modifications and possible scalar particles are presented in Section A.2.8. A review of recent work on the quantum electrodynamics of heavy-ion collisions, particularly the dynamics of positron production, is presented in Section A.3. In addition to reviewing the phenomenology and calculational methods (Sections A.3.2 - A.3.4), we also discuss the parameters for possible experiments, with a brief review of vacancy formation (Section A.3.6) and background effects (Section A.3.7). In our review of heavy-ion collisions we will also touch on several new topics, including the coherent production of photons in heavy-ion collisions (Section A.3.9) and the self-neutralization of charged matter (Section A.3.10). We also point out some questions which are not completely resolved, including the relative importance of induced versus adiabatic pair production (Section A.3.5) and the nature of radiative corrections in α to spontaneous pair production (Section A.3.8).

A.1 THE ELECTRODYNAMICS OF HIGH- Z ELECTRONIC ATOMS

A.1.1 Lamb Shift in Hydrogenlike Ions

At present the most precise and sensitive way to test quantum electrodynamics at high field strength is to compare the theory and measurements of the classic Lamb shift interval, the $2S_{1/2} - 2P_{1/2}$ separation in hydrogenlike ions. In recent work on the Lamb shift, measurements have been extended to hydrogenlike argon ($Z = 18$) by an experiment at the Berkeley SuperHILAC [A.5]. As we shall see, such experiments provide an important test of QED in strong fields. The higher order binding terms in the theory which are small in hydrogen become relatively more important at high Z . For example, the terms of order $\alpha(Z\alpha)^6$ which contribute 0.016% of the Lamb shift in hydrogen give 12% of the Lamb shift in hydrogenlike argon. The theoretical contributions to the Lamb shift are by now well established [A.6,7]. Our purpose here will be to summarize these contributions as an aid to testing the validity of the theory.

The dominant part of the Lamb shift is given by the self-energy and vacuum polarization of order α , corresponding to the Feynman diagrams in Fig. A.1(a) and (b). In the past, most of the theoretical work on the self-energy has been concerned with the evaluation of terms of successively higher order in $Z\alpha$. However, ERICKSON [A.8] has given an analytic approximation which can be used as a guide for the Lamb shift for any Z . This is discussed in detail in Ref. A.9.

More recently, MOHR [A.10] has made a comprehensive numerical evaluation of the $2S_{1/2}$ and $2P_{1/2}$ self-energy to all orders in $Z\alpha$. The method of evaluation is based on the expansion of the bound electron propagation function in terms of the known Coulomb radial Green's functions [A.11], and is described in

more detail in Section A.1.5. In order to display the results for the order α self-energy contribution $S_{SE}^{(2)}$ to the Lamb shift $S = \Delta E(2S_{1/2}) - \Delta E(2P_{1/2})$, it is convenient to isolate the exactly known low-order terms by writing

$$S_{SE}^{(2)} = \frac{\alpha}{\pi} \frac{(Z\alpha)^4}{6} m \left[\ln(Z\alpha)^{-2} - \ln \frac{K_0(2,0)}{K_0(2,1)} + \frac{11}{24} + \frac{1}{2} \right. \\ \left. + 3\pi \left(1 + \frac{11}{128} - \frac{1}{2} \ln 2 \right) (Z\alpha) - \frac{3}{4} (Z\alpha)^2 \ln^2(Z\alpha)^{-2} \right. \\ \left. + \left(\frac{299}{240} + 4 \ln 2 \right) (Z\alpha)^2 \ln(Z\alpha)^{-2} + (Z\alpha)^2 G_{SE}(Z\alpha) \right] \quad (A.1)$$

We shall always distinguish radiative terms in α from terms in $Z\alpha$ which arise from the nuclear field strength. Values of the remainder $G_{SE}(Z\alpha)$ in Eq. (A.1) corresponding to the calculated values of $S_{SE}^{(2)}$ for Z in the range 10 - 50, appear in Fig. A.2. The error bars in that figure represent a conservative estimate of the uncertainty associated with the numerical integration in the evaluation of self-energy and, at $Z=1$, the uncertainty resulting from extrapolation from $Z=10$.

Evaluation of the energy level shift associated with the vacuum polarization of order α is facilitated by considering the expansion of the vacuum polarization potential in powers of the external Coulomb potential (see WICHMANN and KROLL [A.12]). Only odd powers of the external potential contribute as a consequence of Furry's theorem [A.13]. The first term in the expansion gives rise to the Uehling potential [A.14,15]; the associated level shift is easily evaluated numerically. The second nonvanishing term in the expansion is third order in the external potential. The two lowest order contributions to the Lamb shift from this term are given by [A.12,16].

$$\frac{\alpha}{\pi} \frac{(Z\alpha)^6}{6} m \left[\frac{19}{60} - \frac{\pi^2}{36} + \left(\frac{3}{64} - \frac{31\pi^2}{3840} \right) \pi(Z\alpha) \right] \quad (A.2)$$

A substantial discrepancy between theory and experiment was eliminated when APPELQUIST and BRODSKY [A.17] corrected the fourth order Lamb shift terms by a numerical evaluation. Since then, the terms have been evaluated analytically. The total of the fourth order radiative corrections to the Lamb shift is given by

$$S^{(4)} = \left(\frac{\alpha}{\pi} \right)^2 \frac{(Z\alpha)^4}{6} m \left[\pi^2 \ln 2 - \frac{37\pi^2}{144} - \frac{3767}{1728} - \frac{3}{2} \zeta(3) \right] \quad (A.3)$$

Recent work on the evaluation of this term is summarized in Ref. A.7. Note that only the lowest order term in $Z\alpha$ has been evaluated.

The lowest order reduced mass and relativistic recoil contributions to the Lamb shift are given by (see Ref. A.7)

$$S_{RM} = \frac{\alpha}{\pi} \frac{(Z\alpha)^4}{6} m \left(-3 \frac{m}{M} \right) \left[\ln(Z\alpha)^{-2} - \ln \frac{K_0(2,0)}{K_0(2,1)} + \frac{23}{60} \right] \quad (A.4)$$

and

$$S_{RR} = \frac{(Z\alpha)^5}{6\pi} m \left(\frac{m}{M} \right) \left[\frac{1}{4} \ln(Z\alpha)^{-2} - 2 \ln \frac{K_0(2,0)}{K_0(2,1)} + \frac{97}{12} \right] \quad (A.5)$$

where M is the nuclear mass.

The finite nuclear size correction to the Lamb shift is given, for Z not too large, by the perturbation theory expression

$$S_{NS} = \left[1 + 1.70(Z\alpha)^2 \right] \frac{(Z\alpha)^2}{12} m \left(\frac{Z\alpha R}{\chi} \right)^{2s} \quad (A.6)$$

assuming a nuclear model in which the charge is distributed uniformly inside a sphere; where $s = \sqrt{1 - (Z\alpha)^2}$ and R is the r.m.s. charge radius of the nucleus. An estimate of the error due to neglected higher order terms in perturbation theory is given in Ref. A.16.

102004708936

The sum of contributions listed above gives the total Lamb shift S . Values for the individual contributions are listed in Table I for hydrogen-like argon. Theoretical and experimental values for $Z > 3$ are compared in Table II. The theoretical values for $Z < 30$ are listed in Ref. A.16.

TABLE I. Contributions to the Lamb shift at $Z = 18$, $R = 3.45(5)$ fm assumed.

Source	Order	Value
Self energy	$\alpha(Z\alpha)^4 [\ln(Z\alpha)^{-2}, 1, Z\alpha, \dots]$	40,544(15) GHz
Vacuum polarization	$\alpha(Z\alpha)^4 [1, Z\alpha, \dots]$	-2,598(3)
Fourth order	$\alpha^2(Z\alpha)^4$	11(14)
Reduced mass	$\alpha(Z\alpha)^4 m/M$	-1
Relativistic recoil	$(Z\alpha)^5 m/M$	12(9)
Nuclear size	$(Z\alpha)^4 (R/\lambda)^2 [1, (Z\alpha)^2 \ln(R/\lambda), \dots]$	283(12)
		38,250(25) GHz

TABLE II. Comparison between theory and measurement of the Lamb shift $E(2S_{1/2}) - E(2P_{1/2})$ for $Z > 3$.

	Theory (1σ)	Experiment (1σ)	Ref.
${}^6\text{Li}^{2+}$	62,737.5(6.6) MHz	62,765(21) MHz 62,790(70) MHz 63,031(327) MHz	[A.18] [A.19] ^a [A.20]
${}^{12}\text{C}^{5+}$	781.99(21) GHz	780.1(8.0) GHz	[A.21]
${}^{16}\text{O}^{7+}$	2,196.21(92) GHz	2,215.6(7.5) GHz 2,202.7(11.0) GHz	[A.22] [A.23]
${}^{19}\text{F}^{8+}$	3,343.1(1.6) GHz	3,339(35) GHz	[A.24] ^a
${}^{40}\text{Ar}^{17+}$	38.250(25) THz	38.3(2.4) THz	[A.5] ^a

^aImproved experimental precision is expected.

Most of the experiments listed in Table II were done by the so-called static field quenching method [A.20]. This method is based on the large difference between the $2S_{1/2}$ and $2P_{1/2}$ lifetimes and the small separation of the levels. The ratio of the lifetimes is roughly $\tau(2S_{1/2})/\tau(2P_{1/2}) \sim 10^8 Z^{-2}$. Atoms in the metastable $2S_{1/2}$ state are passed through an electric field which causes the lifetime of the $2S_{1/2}$ state to decrease by mixing the S and P states. The change in the lifetime as a function of electric field strength leads to a value for the Lamb shift according to the Bethe-Lamb theory. The quenching experiments at higher Z ($Z > 6$) depend on the electric field in the rest frame of a fast beam of ions passing through a magnetic field to produce the 2S-2P mixing.

The experiments of LEVENTHAL [A.18] and DIETRICH et al [A.19] with lithium are based on the microwave resonance method. The experiment of KUGEL et al [A.24] with fluorine measures the frequency of the $2S_{1/2} - 2P_{3/2}$ separation which is in the infrared range. The Lamb shift is deduced with the aid of the theoretical $2P_{1/2} - 2P_{3/2}$ splitting which is relatively weakly dependent on QED. In the experiment, one-electron ions of fluorine in the metastable $2S_{1/2}$ state are produced by passing a 64 MeV beam through carbon foils. The metastable atoms are excited to the $2P_{3/2}$ state by a laser beam which crosses the atomic beam, and the x rays emitted in the transition $2P_{3/2} \rightarrow 1S_{1/2}$ are observed. A novel feature of the experiment is that the resonance curve is swept out by varying the angle between the laser beam and the ion beam which Doppler-tunes the frequency seen by the atoms.

A.1.2 Lamb Shift in Heliumlike Ions

It would be of considerable interest to extend accurate Lamb shift measurements to hydrogenic systems with very high Z in order to test strong field QED. However, it appears unlikely that the hydrogenlike Lamb shift can be measured by the quenching methods in ions with $Z \geq 30$ [A.25].

A different possibility for accurate checking of QED at very high Z is the study of two- and three-electron ions with high- Z nuclei. When Z is very large, the electron-nucleus interaction dominates over the electron-electron interaction. Therefore, a theoretical approach which considers noninteracting electrons bound to the nucleus according to the single particle Dirac equation, and treats interactions of the electrons and radiative corrections as perturbations, should be capable of making accurate theoretical predictions [A.26].

As an example, consider the energy separation $2^3P_0 - 2^3S_1$ in heliumlike ions. In the high- Z jj -coupling limit, the energy separation is given by $(1s_{1/2}2p_{1/2})^0 - (1s_{1/2}2s_{1/2})^1$, so that if the electron-electron interaction is neglected compared to the electron-nucleus interaction, the absolute energy separation is just the hydrogenic Lamb shift $E(2S_{1/2}) - E(2P_{1/2})$. The electron-electron interaction must still be taken into account. The largest term, corresponding to one-photon exchange between the bound electrons, is of the form $\alpha[a(Z\alpha) + b(Z\alpha)^3 + c(Z\alpha)^5 + \dots]m$, with the leading term coming from the nonrelativistic Coulomb interaction of the electrons. The dominant energy separation is given by the first two terms which grow more slowly with Z than the Lamb shift $\sim \alpha(Z\alpha)^4$. Hence, the Lamb shift becomes an increasing fraction of the energy separation as Z increases. The ratio of the Lamb shift to the total energy separation is 0.002% for $Z=2$, 0.8% for

$Z=18$, and 9% for $Z=54$. At high Z , the main QED corrections in heliumlike ions correspond to Feynman diagrams such as those pictured in Figs. A.3(a) and (b). The energy shift associated with these diagrams is just the hydrogenlike ion Lamb shift. Diagrams with an exchanged photon such as the one in Fig. A.3(c) are less important (of relative order Z^{-1}), but need to be calculated for a precise comparison with experiment.

From the experimental standpoint, the heliumlike Lamb shift has the advantage that both the 2^3P_0 and 2^3S_1 states are long-lived compared to the hydrogenlike $2P$ states so that the natural width of the states is not the main limitation to the accuracy which may be achieved. In addition, in contrast to the hydrogenlike case, there is no strongly favored decay mode (for zero spin nuclei) to the ground state to depopulate the upper level, which makes direct observation of the decay photons feasible in a beam-foil experiment.

Studies of the fine structure in heliumlike argon ($Z=18$) have been carried out by DAVIS and MARRUS [A.27], who measured the energy of photons emitted in the decays $2^3P_2 + 2^3S_1$ and $2^3P_0 + 2^3S_1$ in a beam-foil experiment at the Berkeley SuperHILAC. Their results are shown in Table III. In that table, the theoretical values for the QED corrections are the hydrogenlike corrections for $Z=18$, and are seen to be already tested to the 25% level.

TABLE III
Fine structure in heliumlike argon, from DAVIS and MARRUS [A.27], in eV.

Transition	Self energy and vacuum polarization	ΔE_{th}	ΔE_{exp}
$2^3P_2 + 2^3S_1$	-0.15	22.14(3)	22.13(4)
$2^3P_0 + 2^3S_1$	-0.16	18.73(3)	18.77(3)

708937

GOULD and MARRUS [A.28] have measured the transition rate for the radiative decay $2^3P_0 \rightarrow 2^3S_1$ in heliumlike krypton ($Z = 36$) by observing the x rays emitted in the subsequent M1 decay $2^3S_1 \rightarrow 1^1S_0$. Interestingly, the QED corrections to the $2^3P_0 - 2^3S_1$ energy splitting produce an observable effect in the decay rate. The observed lifetime of the 2^3P_0 state is $\tau = 1.66(6)$ nsec. Assuming that the decay rate is given by the relativistic dipole length formula [A.29]

$$A(2^3P_0 \rightarrow 2^3S_1) = \frac{4}{3} \alpha \omega^3 \sum_M |\langle 2^3S_1, M | \vec{r}_1 + \vec{r}_2 | 2^3P_0, 0 \rangle|^2 \quad (\text{A.7})$$

the theoretical value for the lifetime is $\tau = 1.59(3)$ nsec ($\tau = 1.42(3)$ nsec) with (without) the QED corrections included in the energy separation ω .

A.1.3 Quantum Electrodynamics in High-Z Neutral Atoms

Binding energies of inner electrons in heavy atoms are measured to high accuracy by means of electron spectroscopy of photoelectrons or internal conversion electrons [A.30]. Because of the extraordinary precision of the measurements, surprisingly sensitive tests of QED as well as the many-electron calculations can be made.

Precise calculations of the ground state energies have been given by DESIDERIO and JOHNSON [A.31] and MANN and JOHNSON [A.32]. DESIDERIO and JOHNSON [A.31] have calculated the self-energy level shift of the 1S state in a Dirac-Hartree-Fock potential for atoms with Z in the range 70 - 90 (see Section A.1.5). They estimated the vacuum polarization correction to the 1S level by employing the Uehling potential contribution for a Coulomb potential reduced by 2% to account for electron screening. MANN and JOHNSON [A.32] have done a calculation of the binding energy of a K electron for W, Hg,

Pb, and Rn which takes into account the Dirac-Hartree-Fock eigenvalue, the lowest order transverse electron-electron interaction, and an empirical estimate of the correlation energy. The binding energy is taken as the difference between the energy of the atom and the energy of the ion with a 1S vacancy. Their comparison of theory to the experimental values [A.30] corrected for the photoelectric work function is shown in Table IV. The inclusion of the QED terms dramatically improves the agreement between theory and experiment.

TABLE IV. K-electron energy levels (in Ry) from MANN and JOHNSON [A.32].

Element	Self-energy and vacuum polarization ^a	E_{th}	E_{expt}
^{74}W	8.65	-5110.50	-5110.46 ± .02
^{80}Hg	11.28	-6108.52	-6108.39 ± .06
^{82}Pb	12.27	-6468.79	-6468.67 ± .05
^{86}Rn	14.43	-7233.01	-7233.08 ± .90

^aCalculated by DESIDERIO and JOHNSON [A.31]. These numbers include an estimated correlation energy of -0.08 Ry.

A similar comparison of theory and experiment has been made for Fm ($Z = 100$). FREEDMAN, PORTER, and MANN [A.33] and FRICKE, DESCLAUX, and WABER [A.34] have calculated the K-electron binding energy in fermium. The results of FREEDMAN, PORTER, and MANN are compared to the experimental value obtained by PORTER and FREEDMAN [A.35] in Table V. They used extrapolations of the results for $Z = 70-90$ of MANN and JOHNSON for the rearrangement energy, and of DESIDERIO and JOHNSON for the QED corrections. If the

extrapolated value for the self-energy in that table is replaced by the recently calculated value of CHENG and JOHNSON [A.56], the theoretical energy level is -141.957 keV.

TABLE V. Calculated K-electron energy level in ${}_{100}\text{Fm}$ (in keV), from FREEDMAN, PORTER, and MANN [A.33].

Source	Amount
E_{1S} (neutral-atom eigenvalue)	-143.051
Magnetic	+0.709
Retardation	-0.040
Rearrangement	+0.088
Self-energy	+0.484
Vacuum polarization	-0.154
Electron correlation	-0.001
E_{1S} (Z = 100)	-141.965 ± 0.025
Experimental value	-141.967 ± 0.013

Extensive calculations of electron binding energies for all the elements in the range $2 < Z < 106$ have recently been done by HUANG, AOYAGI, CHEN, CRASEMANN, and MARK [A.37]. They used relativistic Hartree-Fock-Slater wave functions to calculate the expectation value of the total Hamiltonian. They assumed complete relaxation and included the Breit interaction and vacuum polarization corrections, as well as finite nuclear size effects.

By comparing their results to experiment, it is possible to see the effect of the self-energy radiative corrections to the $2S_{1/2} - 2P_{1/2}$ ($L_I - L_{II}$) level splitting in heavy atoms. Figure A.4 shows the relative difference between the theoretical splitting without the self-energy and the experimental values compiled by BEARDEN and BURR [A.30]. The solid line shows theoretical

values for the Coulomb self-energy splitting [A.10], and the dashed line shows values modified with a screening correction [A.37].

A.1.4 High-Z Atoms and Limits on Nonlinear Modifications of QED

Various reformulations of classical electrodynamics have been proposed which attempt to eliminate the problem of an infinite self-energy of the electron. Among these is the nonlinear theory of BORN and INFELD [A.38,39]. They proposed that the usual Lagrangian $L = \frac{1}{2}(H^2 - E^2)$ be replaced by

$$L_{BI} = E_0^2 \left\{ \left[1 + (H^2 - E^2) / E_0^2 \right]^{1/2} - 1 \right\} \quad (\text{A.8})$$

This formulation reduces to the usual form for field strengths much smaller than an "absolute field" E_0 . Within the Born-Infeld theory, the electric field of a point charge is given by

$$E_r = \frac{e}{r^2} \left[1 + \left(\frac{e}{r^2} \right)^2 / E_0^2 \right]^{-1/2} \quad (\text{A.9})$$

The magnitude of E_0 is determined by the condition that the integral of the energy density of the electric field associated with a point charge at rest is just the rest energy of the electron m . This results in a value $E_0 = 1.2 \times 10^{18}$ V/cm and a characteristic radius $r_0 = 3.5$ fm inside of which the electric field deviates substantially from the ordinary form e/r^2 . Due to the large magnitude of E_0 , the observable deviations from linear electrodynamics should be most evident in situations involving strong fields.

There has been recent interest in the experimental consequences of the Born-Infeld modification. RAFELSKI, FULCHER, and GREINER [A.40] have found that the critical charge Z_{cr} (see Section A.3.1) is increased from about 174

in ordinary electrodynamics to 215 within the Born-Infeld electrodynamics. FREEDMAN, PORTER, and MANN [A.33] and FRICKE, DECLAUN, and WABER [A.34] have pointed out that the excellent agreement between the theoretical and experimental 1S binding energies in fermium ($Z = 100$), discussed in Section A.1.3, is evidence against deviations from the linear theory of electrodynamics. In Fm, the difference in 1S energy eigenvalues between the Born-Infeld theory and ordinary electrodynamics is 3.3 keV, based on a calculation using the Thomas-Fermi electron distribution with a Fermi nuclear charge distribution. This is two orders of magnitude larger than the combined uncertainty in theory and experiment listed in Table V. Although the other corrections listed in that table might be modified by the Born-Infeld theory, e.g., the self-energy, the linear theory produces agreement with experiment in a case where the effects of possible nonlinearities are large. SOFF, RAFELSKI, and GREINER [A.41] have found that unless E_0 is greater than 1.7×10^{20} V/cm which is 140 times the Born-Infeld value, the modification due to L_{BI} [Eq. (A.8)] would disrupt agreement between measured and calculated values for low-n transition energies in muonic lead.

A.1.5 Wichmann-Kroll Approach to Strong-Field Electrodynamics

A common aspect of calculations of strong field QED effects is the problem of finding a useful representation of the bound interaction (Furry) picture propagator $S_F^e(x_2, x_1)$ for a particle in a strong external potential $A_\mu(x)$. The approaches based on expanding $S_F^e(x_2, x_1)$ in powers of either the potential $A_\mu(x)$ or the field strength $\partial_\mu A_\nu(x) - \partial_\nu A_\mu(x)$ suffer from two main drawbacks. First, in the case of the self-energy radiative correction, the power series generated in this way converges slowly numerically. Second,

for both the self-energy and the vacuum polarization, the expressions corresponding to successively higher order terms in the expansion become increasingly more complicated and difficult to evaluate.

In their classic study of the vacuum polarization in a strong Coulomb field, WICHMANN and KROLL [A.12] employed an alternative approach to the problem of finding a useful expression for the bound particle propagator. Their method and variations of it have been the basis for studies of strong field QED effects, so we describe the method in some detail here. We also give a brief survey of calculations of strong field QED effects based on these methods.

For a time-independent external potential, which we assume has only a nonvanishing fourth component $-eA_0(x) = V(\vec{x})$, $\vec{A}(x) = 0$, the bound electron propagation function is

$$S_F^e(x_2, x_1) = \begin{cases} \sum_{E_n > E_0} \phi_n(\vec{x}_2) \bar{\phi}_n(\vec{x}_1) \exp[-iE_n(t_2 - t_1)] & t_2 > t_1 \\ -\sum_{E_n < E_0} \phi_n(\vec{x}_2) \bar{\phi}_n(\vec{x}_1) \exp[-iE_n(t_2 - t_1)] & t_2 < t_1 \end{cases} \quad (\text{A.10})$$

where the $\phi_n(\vec{x})$ are the bound state and continuum solutions of the Dirac equation for the external potential. It has an integral representation given by [A.12,42]

$$S_F^e(x_2, x_1) = \frac{1}{2\pi i} \int_C dz G(\vec{x}_2, \vec{x}_1, z) \gamma^0 e^{-iz(t_2 - t_1)} \quad (\text{A.11})$$

where $G(\vec{x}_2, \vec{x}_1, z)$ is the Green's function for the Dirac equation

$$[-i\vec{\alpha} \cdot \vec{\nabla}_2 + V(\vec{x}_2) + \beta m - z] G(\vec{x}_2, \vec{x}_1, z) = \delta^3(\vec{x}_2 - \vec{x}_1) \quad (\text{A.12})$$

and the contour C in (A.11) extends continuously from $-\infty$ to $+\infty$ below the real axis for $\text{Re}(z) < E_0$, through E_0 , and above the real axis in the region $\text{Re}(z) > E_0$. The crossing point E_0 depends on the definition of the vacuum (see Section A.3.1). For the Coulomb potential with $(Z\alpha) < 1$, it is convenient to choose $E_0 = 0$. Two possible contours of integration for $(Z\alpha) > 1$ are shown in Fig. A.5. In that figure, the branch points of $G(\vec{x}_2, \vec{x}_1, z)$ at $z = \pm im$ and the bound state poles are also shown.

The Green's function is formally given by the spectral representation

$$G(\vec{x}_2, \vec{x}_1, z) = \sum_E \frac{\phi_E(\vec{x}_2) \phi_E^\dagger(\vec{x}_1)}{E - z} \quad (\text{A.13})$$

where the sum in (A.13) is over bound state and continuum solutions as in Eq. (A.10).

For a spherically symmetric external potential $V(r)$, the Green's function may be written as a sum over eigenfunctions (with eigenvalue $-\kappa$) of the Dirac operator $K = \beta(\vec{\sigma} \cdot \vec{L} + 1)$. Each term in the sum can be factorized into a part which depends in a trivial way on the directions of \vec{x}_2 and \vec{x}_1 and a radial Green's function which contains the nontrivial dependence on r_2 and r_1 , the magnitudes of \vec{x}_2 and \vec{x}_1 . The radial Green's function $G_\kappa(r_2, r_1, z)$, written as a 2×2 matrix, satisfies the inhomogeneous radial equation

$$\begin{bmatrix} V(r_2) + m - z & -\frac{1}{r_2} \frac{d}{dr_2} r_2 + \frac{\kappa}{r_2} \\ \frac{1}{r_2} \frac{d}{dr_2} r_2 + \frac{\kappa}{r_2} & V(r_2) - m - z \end{bmatrix} G_\kappa(r_2, r_1, z) = \frac{1}{r_2 r_1} \delta(r_2 - r_1) \quad (\text{A.14})$$

The utility of this formulation is that the radial Green's functions G_κ can be constructed explicitly from solutions of the homogeneous version of (A.14). Let $A(r)$ and $B(r)$ be the two linearly independent two-component solutions of

(A.14) with the right hand side replaced by 0, where $A(r)$ is regular at $r=0$ and $B(r)$ is regular at $r=\infty$. Then for z in the cut plane (Fig. A.5) and not a bound state eigenvalue, the Green's function G_κ is given by

$$G_\kappa(r_2, r_1, z) = \frac{1}{J(z)} [\theta(r_2 - r_1) B(r_2) A^\dagger(r_1) + \theta(r_1 - r_2) A(r_2) B^\dagger(r_1)] \quad (\text{A.15})$$

with the Wronskian $J(z)$ given by ($J(z)$ is independent of r)

$$J(z) = r^2 [A_2(r) B_1(r) - A_1(r) B_2(r)] \quad (\text{A.16})$$

In (A.16), $1(2)$ denotes the upper(lower) component of A or B . Note that the radial Green's function can also be expressed in the form of a spectral representation, in analogy with Eq. (A.13), as

$$G_\kappa(r_2, r_1, z) = \sum_E \frac{F_E(r_2) F_E^\dagger(r_1)}{E - z} \quad (\text{A.17})$$

where $F_E(r)$ is a bound state or continuum solution of the homogeneous radial equation.

In the case of a Coulomb potential, the solutions $A(r)$ and $B(r)$ can be expressed in terms of confluent hypergeometric (or Whittaker) functions [A.12,11]. WICHMANN and KROLL [A.12] employed integral representations for these functions, carried out some of the integrations involved in evaluation of the vacuum polarization, and arrived at relatively compact expressions for the Laplace transform of the vacuum polarization charge density times r^2 . Their starting point was the expression for the unrenormalized vacuum polarization charge density of order e

$$\rho_{VP}(r) = -i \frac{em^3}{(2\pi)^2} \sum_{\kappa=1}^{\infty} \kappa \int_C dz [\text{Tr} G_\kappa(r, r, z) + \text{Tr} G_{-\kappa}(r, r, z)] \quad (\text{A.18})$$

This expression, which is valid to all orders in $Z\alpha$, may be further expanded in a power series in $Z\alpha$. Many of the calculations relevant to high- Z muonic atoms (see Section A.2) are based on results obtained by WICHMANN and KROLL in their extensive study of $\rho_{VP}(r)$.

ARAFUNE [A.43] and BROWN, CAHN, and McLERRAN [A.44,45] employed an approximation based on setting $m=0$ in the radial Green's function G_κ to study finite nuclear size effects on the vacuum polarization in muonic atoms. This approximation considerably simplifies the calculation and corresponds to including only the short-range effect of the vacuum polarization.

GYULASSY [A.46-48] constructed Green's functions for a finite nucleus potential in a numerical study of the effect of finite size on the higher order vacuum polarization in muonic atoms and in electronic atoms with Z near the critical value (see Section A.3.8). In these studies, it was found that the main correction due to nuclear size arises from the $\kappa=1$ ($j=\frac{1}{2}$) term in Eq. (A.18). BROWN, CAHN, and McLERRAN [A.49,50] have constructed approximate analytic expressions for the radial Green's functions for a Coulomb potential in order to estimate the effect of the spatial distribution of the vacuum polarization charge density in muonic atoms.

BROWN, LANGER, and SCHAEFER [A.51] have developed a method of calculating the 1S self-energy radiative correction for large Z , in which the solutions $A(r)$ and $B(r)$ are generated by numerical integration of a set of coupled differential equations. This method has been generalized to non-Coulomb potentials by DESIDERIO and JOHNSON [A.31] who evaluated the self-energy in a screened Coulomb potential for the 1S state with Z in the range 70-90. More recently, CHENG and JOHNSON [A.36] have evaluated the self-energy, with finite nuclear size and electron screening taken into account for Z in the range 70-160, and with a Coulomb potential for Z in the range 50-130.

MOHR [A.10,11] has evaluated the self-energy radiative correction for the 1S, 2S, and $2P_{1/2}$ states over the range $Z = 10-110$ for a Coulomb potential. In that calculation, the radial Green's functions are evaluated numerically by taking advantage of power series and asymptotic expansions of the explicit expressions for the radial Green's functions in terms of confluent hypergeometric functions. In terms of the radial Green's functions, the (unrenormalized) self-energy has the form

$$\begin{aligned} \Delta E_{SE} = & -\frac{i\alpha}{2\pi} \int_C dz \int_0^\infty dr_2 r_2^2 \int_0^\infty dr_1 r_1^2 \\ & \times \sum_\kappa \sum_{i,j=1}^2 [f_i(r_2) G_\kappa^{ij}(r_2, r_1, z) f_j(r_1) A_\kappa(r_2, r_1) \\ & - f_i(r_2) G_\kappa^{ij}(r_2, r_1, z) f_j(r_1) A_\kappa^{ij}(r_2, r_1)] \end{aligned} \quad (A.19)$$

where $\bar{i}=3-i$, $\bar{j}=3-j$; $f_i(r)$, $i=1,2$ are the large and small components of the Dirac radial wave functions, and the A 's are functions associated with the angular momentum expansion of the photon propagator and consist of spherical Bessel and Hankel functions. In the numerical evaluation of (A.19), particular care is required in isolating the mass renormalization term [A.11].

A.2 THE ELECTRODYNAMICS OF HIGH-Z MUONIC ATOMS

A.2.1 General Features

Muons, impinging on a solid target, can become trapped in bound states in the target atoms [A.52]. Because the Bohr radius of a particle in a Coulomb potential scales as the inverse of the mass of the particle, the radii of the muon orbits are 1/207 times the radii of the corresponding electron orbits. Thus the muon and the nucleus form a small high-Z hydrogen-like system inside the atomic electron cloud. Observation of the transition x rays of the muon yields the energy level spacings of the system. The lowest levels of the muon, which have radii comparable to the radius of the nucleus, are sensitive to properties of the nucleus such as charge distribution and polarization effects [A.52]. We are here concerned instead with higher circular orbits of the muon, such as the $4f_{7/2}$ and $5g_{9/2}$ states in lead atoms, which have the property

$$\text{nuclear radius} \ll \text{muon Bohr radius} \ll \text{electron Bohr radius.}$$

For these states, the effect of the structure of the nucleus and of the bound atomic electrons is small. Hence precise theoretical predictions for the energy levels can be made and, in comparison with the experimental transition energies, provide a means of testing the effects of QED. In particular, the effect of electron vacuum polarization, which is large for muon levels, is tested to better than 1% with present-day experimental precision.

Experimental determination of the $3d \rightarrow 2p$ transition energy in muonic phosphorus by KOSLOV, FITCH, and RAINWATER [A.53] showed the effect of the

lowest order vacuum polarization. More recently, with the use of lithium drifted germanium detectors to measure the x-ray energies, which are typically in the range 100-500 keV for the transitions considered here, experiments have become sufficiently accurate to be sensitive to higher order vacuum polarization effects [A.54-59]. The experiments of DIXIT et al [A.55] and of WALTER et al [A.56] reported in 1971-2 showed a significant discrepancy with theory; however, more recent experiments of TAUSCHER et al [A.57], of DIXIT et al [A.58], and of VUILLEUMIER et al [A.59] reported in 1975-6 are in agreement with theory for the muonic transition energies. The accurate experiments, and particularly the apparent discrepancy with theory, led to a considerable amount of work on the theory of muonic energy levels. In the following discussion, we describe the present status of the theory, with attention focused on the well-studied transition $5g_{9/2} \rightarrow 4f_{7/2}$ in muonic ^{208}Pb . Numerical values for the various contributions to the energy levels are collected in Table VI of Section A.2.6.

The main contribution to the energy levels is the Dirac energy of a muon in a Coulomb potential. A small correction must be added to account for the finite charge radius of the nucleus. This can be calculated either by first order perturbation theory, or by numerical integration of the Dirac equation with a finite nuclear potential. The latter procedure is necessary for low n states where the finite size correction is large. For high n circular states, the correction is small and insensitive to the details of the nuclear charge distribution. For the $5g_{9/2} - 4f_{7/2}$ transition in lead, the correction is -4 eV compared to the reduced mass Coulomb energy difference of 429,344 eV. The other small non-QED corrections from electron screening, and nuclear polarization and motion are discussed in subsequent sections.

The largest correction to the Dirac Coulomb energy levels is the effect

: 0 9 1 0 4 7 0 8 9 3 9

of electron vacuum polarization which is discussed in the following section. In the remainder of this section, we make some general remarks about the magnitude of the radiative corrections in muonic atoms.

If we restrict our attention to interactions of photons with electrons and muons, the QED corrections to the energy levels of a bound muon, to lowest order in α , are given by the Feynman diagrams in Fig. A.6. In that figure, the double lines represent electrons or muons in the static field of the nucleus. The diagrams (a), (b), and (c) represent the muon self-energy, the muon vacuum polarization, and the electron vacuum polarization, respectively.

It is of interest to compare the QED corrections to muon levels to the corresponding corrections to electron levels. The lowest order diagrams for a bound electron are given by the diagrams in Fig. A.6 with the μ 's and e 's interchanged. For a point nucleus, the electron diagrams corresponding to (a) and (b) give exactly the same corrections, relative to the electron Dirac energy, as (a) and (b) give, relative to the muon Dirac energy. On the other hand, diagram (c) gives the large vacuum polarization correction in muonic atoms, while its analog, with μ and e interchanged, is negligible in electron atoms.

The relatively greater effect of the electron vacuum polarization in muonic atoms is due to the short-range nature of the vacuum polarization potential. The leading (Uehling) term of the potential falls off exponentially in distance from the nucleus with a characteristic length of $\lambda_e/2$. Hence, the overlap of the vacuum polarization potential with the muon wavefunction, which has a radius of $0.2\lambda_e$ for the $n=5$ state in lead, is much greater than the overlap of the potential with the electron wavefunction, which has a radius of about $550\lambda_e$ in the $n=2$ state of hydrogen.

The difference in scale between muon and electron atoms has another

consequence. The short-ranged muon wavefunction is sensitive to the short-range behavior of the electron vacuum polarization potential, while the long-range electron wavefunction is sensitive only to the zero and first radial moments of the potential. Hence while the hydrogen Lamb shift, with presently measured precision [A.60,61], tests the vacuum polarization to 0.1%, it is sensitive to a different aspect of the vacuum polarization than the muonic atom tests.

A further difference between muon and electron atoms is that the high- Z muonic atom measurements test higher order than Uehling potential contributions to the vacuum polarization, which are negligible in the hydrogen Lamb shift [A.12].

A.2.2 Vacuum Polarization

The electron vacuum polarization of lowest order in α and all orders in $Z\alpha$ is represented by the Feynman diagram in Fig. A.6(c). For a stationary nuclear field corresponding to the charge density $\rho_N(\vec{r})$, the effect of the vacuum polarization is equivalent to the interaction of the bound muon with an induced charge distribution given by ($-e$ is the charge of the electron) [A.12,62]

$$\begin{aligned} \rho_{VP}(\vec{r}) &= \langle 0 | j_0(\vec{r}, t) | 0 \rangle = \frac{e}{2} \left[\sum_{E>0} |\phi_E(\vec{r})|^2 - \sum_{E<0} |\phi_E(\vec{r})|^2 \right] \\ &= \frac{e}{2\pi i} \int_C dz \text{Tr} G(\vec{r}, \vec{r}', z) \Big|_{\vec{r}' \rightarrow \vec{r}} \end{aligned} \quad (\text{A.20})$$

(see also Eq. (A.18)), where G is the Green's function for the external field Dirac equation discussed in Section A.1.5. (The vacuum $|0\rangle$ is the state

corresponding to no electrons or positrons in the external potential; $j_{\mu}(x) = -\frac{e}{2} [\bar{\psi}(x), \gamma_{\mu} \psi(x)]$ has a vanishing vacuum expectation value only in the limit $Z\alpha \rightarrow 0$.) The three expressions for the charge density in (A.20) are formal expressions and require regularization and charge renormalization in order to be well defined. A practical method of regularization is the Pauli-Villars scheme with two auxiliary masses [A.63]. The sum-over-states formula for the charge density in Eq. (A.20) is related to the last expression in (A.20) by choosing a suitable contour of integration C and evaluating the residue of the pole in the spectral representation, Eq. (A.13), of G [A.12].

In order to facilitate the evaluation of the charge density (A.20), it is convenient to expand it in powers of the external field. The Feynman diagrams corresponding to this expansion are shown in Fig. A.7. The \times 's in Fig. A.7 represent interaction with the external nuclear field. Only odd powers of the external field contribute due to Furry's theorem [A.13]. The expansion in powers of the external field in Fig. A.7 corresponds to the Neumann series generated by iteration of the integral equation for the Green's function

$$G(\vec{r}, \vec{r}', z) = G^0(\vec{r}, \vec{r}', z) - \int d^3\vec{r}'' G^0(\vec{r}, \vec{r}'', z) V(\vec{r}'') G(\vec{r}'', \vec{r}', z) \quad (A.21)$$

In (A.21), $G^0(\vec{r}, \vec{r}', z)$ is the Green's function in the absence of an external potential and $V(\vec{r})$ is the potential energy of the electron in the nuclear field. The term in the expansion of $G(\vec{r}, \vec{r}', z)$ linear in $V(\vec{r})$, when substituted for G in (A.20), gives, after charge renormalization, the charge density associated with the Uehling potential [A.15]

$$V_{11}^0(\vec{r}) = -\frac{\alpha e}{\pi} \int_1^{\infty} dt (t^2 - 1)^{-1/2} \left(\frac{2}{3t^2} + \frac{1}{3t^4} \right) \int d^3\vec{r}'' e^{-2m_e |\vec{r} - \vec{r}''| t} \frac{\rho_N(\vec{r}'')}{|\vec{r} - \vec{r}''|} \quad (A.22)$$

In (A.22), the charge distribution of the nucleus normalized such that $\int d^3\vec{r} \rho_N(\vec{r}) = Ze$, and the subscripts on V refer to the order of the vacuum polarization, i.e., $V_{nm} = 0 (\alpha^n (Z\alpha)^m)$. The effect of V_{11}^0 on a muon energy level is accurately taken into account by adding V_{11}^0 to the external nuclear potential V in the Dirac equation

$$[\vec{\alpha} \cdot \vec{p} + V(\vec{r}) + V_{11}^0(\vec{r}) + \beta m_{\mu} - E_n] \phi_n(\vec{r}) = 0 \quad (A.23)$$

and solving for the bound state energy E_n numerically. This procedure is equivalent to summing over the higher order reducible contributions of the Uehling potential; Fig. A.8 shows the first three terms in this sum.

For the high- l states under consideration here, the Uehling contribution is well approximated by the point charge value, V_{11} , obtained by making the replacement $\rho_N(\vec{r}) \rightarrow Ze\delta^3(\vec{r})$ in the right-hand side of (A.22), evaluated in first order perturbation theory with Dirac wavefunctions for a point nucleus. Only the short distance behavior of the electron vacuum polarization is important ($m_e r \approx 0.2$ for $r \approx$ radius of the $n=5$ state in lead) [A.64-66]:

$$V_{11}(r) = \frac{\alpha Z \alpha}{\pi} \left\{ \frac{2}{3r} [\ln(m_e r) + \gamma] + \frac{5}{9r} - \frac{\pi m_e}{2} + m_e^2 r - \frac{2\pi}{9} m_e^3 r^2 + \frac{1}{6} m_e^4 r^3 [\ln(m_e r) + \gamma] + \frac{7}{18} m_e^4 r^3 + \dots \right\} \quad (A.24)$$

($\gamma = 0.57721 \dots$ is Euler's constant.) There are two non-negligible corrections to V_{11} . The first is the correction due to the finite extent of the nucleus. The small r form of the correction is [A.65]

$$\delta V_{11}(r) = V_{11}^0(r) - V_{11}(r) = \frac{\alpha Z \alpha}{\pi} \left[-\frac{1}{9r^3} \langle r^2 \rangle + \frac{1}{3} \frac{m_e^2}{r} \langle r^2 \rangle - \frac{1}{30r^5} \langle r^4 \rangle + \dots \right] \quad (A.25)$$

where the notation $\langle \rangle$ denotes an average over the nuclear charge density.

09004708940

The other correction is the second order perturbation correction of the main term corresponding to the diagram in Fig. A.8(b)

$$\Delta E = \sum_{n \neq 0} \langle 0 | V_{11} | n \rangle \frac{1}{E_0 - E_n} \langle n | V_{11} | 0 \rangle \quad (\text{A.26})$$

The energy shifts for the $5g_{9/2} - 4f_{7/2}$ transition arising from these corrections are listed separately in Table VI [A.65].

We next consider the vacuum polarization of order α and third and higher order in $Z\alpha$, corresponding to diagrams with three or more \times 's in the series in Fig. A.7. The point nucleus approximation is considered first. WICHMANN and KROLL [A.12] obtained an explicit expression for the Laplace transform of r^2 times the vacuum polarization charge density of order $\alpha(Z\alpha)^3$. BLOMQUIST [A.65] has used their result to obtain the vacuum polarization potential $V_{13}(r)$ exactly in coordinate space and found the small r series expansion which is sufficient to evaluate the muon energy shifts

$$\begin{aligned} V_{13}(r) = & \frac{\alpha(Z\alpha)^3}{\pi} \left\{ \left(-\frac{2}{3} \zeta(3) + \frac{1}{6} \pi^2 - \frac{7}{9} \right) \frac{1}{r} + \left(2\pi\zeta(3) - \frac{1}{4} \pi^3 \right) m_e \right. \\ & + \left(-6\zeta(3) + \frac{1}{16} \pi^4 + \frac{1}{6} \pi^2 \right) m_e^2 r + \frac{2\pi}{9} m_e^3 r^2 [\ln(m_e r) + \gamma] \\ & \left. + \left(\frac{2}{3} \pi\zeta(3) + \frac{4}{9} \pi \ln 2 - \frac{31}{27} \pi \right) m_e^3 r^2 + \dots \right\} \quad (\text{A.27}) \end{aligned}$$

This term contributes -43 eV to the $5g_{9/2} - 4f_{7/2}$ transition energy in muonic lead. VOGEL [A.67] has tabulated numerical values of $V_{13}(r)$ as a function of r based on BLOMQUIST's exact expression. Calculations by BELL [A.68] and by SUNDARESAN and WATSON [A.69], based on interpolation of the asymptotic forms of the Laplace transform of the third order vacuum polarization charge density given by WICHMANN and KROLL, are in agreement with the values obtained by BLOMQUIST. An earlier calculation by FRICKE [A.70] had the wrong sign for

this term, which accounted for part of the apparent original discrepancy between theory and experiment (see Section A.2.1).

The vacuum polarization of order $\alpha(Z\alpha)^5$ and higher can be accounted for by considering the small distance behavior of the induced charge density. For a point nuclear charge density, the effect of the vacuum polarization of third and higher order is to produce a finite change δQ in the magnitude of the charge at the origin and a finite distribution of charge with a mean radius of approximately $0.86\lambda_e$ [A.12]. The integral over all space of the induced charge density of order $(Z\alpha)^3$ and higher must, of course, vanish. The induced point charge, which gives rise to a leading term proportional to r^{-1} in the vacuum polarization potential, has the dominant effect on the muon energy. The magnitude of the induced charge was calculated by WICHMANN and KROLL [A.12] to all orders (≥ 3) in $Z\alpha$. Their result has been confirmed by an independent method by BROWN, CAHN, and McLERRAN [A.71,49]. WICHMANN and KROLL obtained this result as a special case in a general study of the vacuum polarization, while BROWN, CAHN, and McLERRAN were able to simplify the calculation by setting $m_e = 0$ from the beginning. That this procedure produces the leading r^{-1} term in third order is seen by inspection of $V_{13}(r)$ in Eq. (A.27). The lowest order terms in δQ are given by

$$\delta Q = \frac{e}{3\pi} \left\{ \left[2\zeta(3) + \frac{7}{3} - \frac{\pi^2}{2} \right] (Z\alpha)^3 - \left[2\zeta(5) + \frac{71}{5} \zeta(3) - \frac{47\pi^4}{240} \right] (Z\alpha)^5 + \dots \right\} \quad (\text{A.28})$$

The numerical value of the charge to all orders in $Z\alpha$ is displayed by writing

$$\delta Q = -e[0.020940(Z\alpha)^3 + 0.007121(Z\alpha)^5 F_0(Z\alpha)] \quad (\text{A.29})$$

where $F_0(Z\alpha)$ appears in Fig. A.9. The leading terms of the fifth and seventh order vacuum polarization potential are [A.12,65]

$$\begin{aligned}
 V_{15}(r) &= \frac{\alpha(Z\alpha)^5}{\pi r} \left[\frac{2}{3} \zeta(5) - \frac{21}{4} \zeta(4) + \frac{71}{15} \zeta(3) - \frac{1}{4} \zeta^2(2) + O(m_e r) \right] \\
 V_{17}(r) &= \frac{\alpha(Z\alpha)^7}{\pi r} \left[-\frac{2}{3} \zeta(7) + \frac{445}{24} \zeta(6) - \frac{286}{21} \zeta(5) - \frac{1}{4} \zeta(2)\zeta(4) \right. \\
 &\quad \left. - \frac{5}{2} \zeta^2(3) + O(m_e r) \right] \quad (A.30)
 \end{aligned}$$

The fifth and seventh order leading terms contribute -7 eV to the $5g_{9/2} - 4f_{7/2}$ energy separation in lead.

We briefly examine the contribution of terms of higher order in $m_e r$ to the fifth and higher order (in $Z\alpha$) vacuum polarization. The order α potential (excluding the r^{-1} term of the Uehling part) is given by [A.50]

$$V_{11^+}(r) = A(Z\alpha) \frac{1}{r} + B(Z\alpha)m_e + C(Z\alpha)m_e(m_e r)^{2\lambda} + D(Z\alpha)m_e^2 r + \dots \quad (A.31)$$

where $\lambda = (1 - (Z\alpha)^2)^{1/2}$, and the terms omitted from (A.31) are higher order in $m_e r$. The term $A(Z\alpha)r^{-1}$ corresponds to the induced point charge discussed earlier. $B(Z\alpha)$ has not been calculated in fifth or higher order in $Z\alpha$, but gives the same contribution for all states and therefore does not effect the transition energies. The coefficients $C(Z\alpha)$ and $D(Z\alpha)$ have been calculated numerically to all orders in $Z\alpha$ by BROWN, CAHN, and McLERRAN [A.50]. Their results show that the part of order fifth and higher in $(Z\alpha)$ in these terms (the third order parts are included in (A.27)) gives a small (of order 1 eV) contribution to the transition energy. A similar conclusion was reached by BELL [A.68].

A correction to the vacuum polarization of third and higher order must be made to account for the finite size of the nucleus. ARAFUNE [A.43] and BROWN, CAHN, and McLERRAN [A.44] have independently obtained approximate analytic expressions for the potential corresponding to the finite size correction to the vacuum polarization. ARAFUNE's expression [A.43]

$$\begin{aligned}
 \delta V_{11^+}(r) \approx & -\frac{\alpha(Z\alpha)}{15\pi r} \left[1 - \left(\frac{\pi^2}{3} - 3 - \frac{349}{13860} \right) (Z\alpha)^2 - \frac{865}{2016} (Z\alpha)^2 \frac{R}{r} \right] \left(\frac{R}{r} \right)^{2\lambda} \\
 & \text{for } r > R \quad (A.32)
 \end{aligned}$$

where $\lambda = (1 - (Z\alpha)^2)^{1/2}$, is based on the following approximations: Terms of relative order $(m_e r)^2$ are neglected, terms of order R^4/r^5 are neglected, higher order terms in $(Z\alpha)^2$ are neglected except in the exponent, and the nucleus is approximated by a uniformly charged sphere of radius R . The effect of the potential inside the radius R is negligible for high- ℓ states. In order to isolate the contribution of (A.32) to the third and higher order vacuum polarization, it is necessary to subtract from (A.32) the term

$$-\frac{\alpha(Z\alpha)}{15\pi r} \left(\frac{R}{r} \right)^2 \quad (A.33)$$

which corresponds to the Uehling potential portion and appears as the first term on the right-hand side of (A.25), ($R^2 = \frac{5}{3} \langle r^2 \rangle$).

BROWN, CAHN, and McLERRAN [A.44,45] have done a similar calculation. Their expression allows for an arbitrary nuclear charge distribution and is valid to all orders in $Z\alpha$. The results of these calculations are in excellent agreement and yield a correction of 5 eV for the $5g_{9/2} - 4f_{7/2}$ transition in lead.

GYULASSY [A.46,48] has made a numerical study of the effect of finite nuclear size on the higher order vacuum polarization. He was able to calculate the finite size effect with or without the approximations of ARAFUNE and of BROWN, CAHN, and McLERRAN. The finding was that the approximations introduce a small error of 1 eV, and the finite size correction is 6 eV compared to the 5 eV quoted above. GYULASSY also examined the extent to which the finite size corrections to the third order vacuum polarization are sensitive to the shape of the nuclear charge distribution. The correc-

00004708941

tions were found to be essentially the same for a uniform spherical distribution and a shell of charge, provided the distributions have the same r.m.s. radius.

RINKER and WILETS have evaluated the higher order vacuum polarization correction by a direct numerical evaluation of the sum over eigenfunctions in (A.20). Their early work [A.72], which showed a 16 ± 2 eV finite size correction to the higher order vacuum polarization, compared to 6 eV discussed above, is incorrect due to numerical difficulties [A.73]. More recently, with improved numerical methods, they have evaluated the higher order vacuum polarization correction for many states and various values of Z in the range 26-114 [A.73]. The results in lead are consistent with the work described above.

The fourth order vacuum polarization, of order α^2 , corresponding to the Feynman diagrams in Fig. A.10, has been calculated and expressed in momentum space in terms of an integral representation by KÄLLÉN and SABRY [A.74].

The configuration space potential $V_{21}(r)$ derived from the Källén-Sabry representation was obtained by BLOMQUIST [A.65]. The complete expression for $V_{21}(r)$ is somewhat complicated, so it is convenient in calculations to employ the first terms in the power series expansion [A.65]

$$V_{21}(r) = \frac{\alpha^2 Z \alpha}{\pi^2} \left\{ -\frac{4}{9r} [\ln(m_e r) + \gamma]^2 - \frac{13}{54r} [\ln(m_e r) + \gamma] \right. \\ \left. - \left(\zeta(3) + \frac{\pi^2}{27} + \frac{65}{648} \right) \frac{1}{r} + \left(\frac{13}{9} \pi^2 + \frac{32}{9} \pi \ln 2 - \frac{766}{135} \pi \right) m_e \right. \\ \left. + \frac{5}{3} m_e^2 r [\ln(m_e r) + \gamma] - \frac{65}{18} m_e^2 r + \dots \right\} \quad (\text{A.34})$$

The power series represents $V_{21}(r)$ sufficiently well for values of r important for muonic orbits considered here to give accurate values for the energy shifts.

A numerical evaluation $V_{21}(r)$ has been made by VOGEL [A.67], who produced a table of point by point values. FULLERTON and RINKER [A.75] give a numerical approximation scheme to generate the second order potential for a finite sized nucleus based on VOGEL's tabulated values. Earlier estimates of this correction were made by FRICKE [A.70] and by SUNDARESAN and WATSON [A.69], however, these calculations erroneously counted the diagram in Fig. A.10(a) twice.

A.2.3 Additional Radiative Corrections

According to the discussion of BARRETT, BRODSKY, ERICKSON, and GOLDBABER [A.64], it is expected that the self-energy correction to muon energy levels [Fig. A.6(a)] is reasonably well approximated by the terms of lowest order in $Z\alpha$ [A.26,76].

$$\Delta E_{SE} = -\frac{4\alpha}{3\pi} \frac{(Z\alpha)^4}{n^3} \left[\ln K_0(n, \ell) + \frac{3}{8} \frac{1}{\kappa(2\ell+1)} \right] m_\mu; \quad \ell \neq 0 \quad (\text{A.35})$$

where K_0 is the Bethe average excitation energy, and the second term is due to the anomalous magnetic moment of the muon. For high- ℓ states, the point nucleus values of KLARSFELD and MAQUET [A.77] are used for K_0 . This correction contributes -7 eV for the $5g_{9/2} - 4f_{7/2}$ transition in lead.

A QED correction of order α^2 which has been the subject of recent interest is shown in Fig. A.11. In that figure, diagrams corresponding to the expansion of the electron loop in powers of the external potential are also shown. The first term in the expansion is the first vacuum polarization correction to the photon propagator. The next three terms correspond to a vacuum polarization correction of order $\alpha^2(Z\alpha)^2$ discussed in the following paragraph.

It was suggested by CHEN [A.78] that the contribution of this diagram was larger, relative to similar diagrams, than its nominal order would indicate. He estimated a value of -35 eV for the $5g-4f$ energy difference in lead. At the same time, WILETS and RINKER [A.79,73] estimated the effect and found that the $4f$ energy is shifted by an amount in the range 1-3 eV, in conflict with the result of CHEN. Subsequently, FUJIMOTO [A.80] estimated the $\alpha^2(Z\alpha)^2$ correction and found that the energy shift for the $5g_{9/2} - 4f_{7/2}$ transition in lead is approximately 0.8 eV which is consistent with the value of WILETS and RINKER. FUJIMOTO simplified the calculation considerably by treating the muon as a static point charge and setting $m_e = 0$ in the virtual electron loop. The latter approximation takes advantage of the fact that the distance between the muon and the nucleus is much less than the electron Compton wavelength. The result is then a vacuum polarization modification of the short range interaction potential between two fixed point charges given by

$$\delta V(r) = -C \frac{\alpha^2(Z\alpha)^2}{r} \quad (r \ll \lambda_e) \quad (\text{A.36})$$

where $C = 0.028(1)$. BORIE [A.81] has recently reported an approximate value of 1 eV for the correction.

Additional corrections to the muonic energy levels have been examined and found to be small. SUNDARESAN and WATSON [A.82] have estimated the contributions of hadronic intermediate states in the photon propagator, using a method due to ADLER [A.83]. BORIE has calculated various higher order QED contributions to the muonic atom energy levels, besides the $\alpha^2(Z\alpha)^2$ term just considered, and found them to be negligible compared to the experimental errors [A.84].

A.2.4 Nuclear Effects

Besides the effect of the finite nuclear charge radius which has already been discussed, the effects of nuclear motion and nuclear polarizability must be considered.

The main effect of nuclear motion is taken into account by replacing the muon mass by the reduced mass of the muon-nucleus system in the Dirac expression for the binding energy. This reduced mass correction is exact only in the non-relativistic limit. The leading relativistic correction for nuclear motion is given by [A.26,85]

$$\delta E = -\frac{m_\mu^2 (Z\alpha)^4}{8Mn^4} \quad (\text{A.37})$$

where M is the nuclear mass. The reduced mass correction to the binding energy and relativistic correction contribute -234 eV and 3 eV respectively to the $5g_{9/2} - 4f_{7/2}$ transition in lead. The main effects of the nuclear motion are correctly taken into account by using reduced mass wavefunctions in evaluating the QED corrections, most importantly in the Uehling potential correction.

Up to this point, the nucleus has been treated as a charged object with no structure. There is a small correction to the muon energy levels due to the fact that the muon can cause virtual excitations of the nucleus. This effect has been considered by COLE [A.86] and by ERICSON and HUFNER [A.87] for the case of high- l muon states. The dominant long-range effect is the static dipole polarizability of the nucleus. It can be roughly described as a separation of the center of charge from the center of mass of the nucleus induced by the electric field of the muon. The approximation that the

708942

displacement follows the motion of the muon is expected to be good, because the nuclear frequencies are much higher than the relevant muon atomic frequencies (5-20 MeV compared to a few hundred keV). The polarization in this approximation corresponds to an effective potential $V_{E1}(r)$ given by [A.87]

$$V_{E1}(r) = -\alpha_{E1} \frac{e^2}{2r^4} \quad (\text{A.38})$$

where α_{E1} is the static E1 polarizability of the nucleus. The value of α_{E1} can be obtained from the measured total γ -absorption cross section $\sigma_{E1}(\omega)$ for E1 radiation in the long wavelength limit by means of the sum rule

$$\alpha_{E1} = \frac{1}{2\pi^2} \int_{\omega_t}^{\infty} d\omega \frac{\sigma_{E1}(\omega)}{\omega^2} \quad (\text{A.39})$$

The energy shifts have been calculated by BLOMQUIST [A.65] using the experimental photonuclear cross section of HARVEY et al [A.88] for ^{208}Pb . The result is 4 eV for the $5g_{9/2} - 4f_{7/2}$ energy difference, in agreement with COLE's value [A.86].

A.2.5 Electron Screening

In the preceding discussion, the effect of the atomic electrons has been completely ignored. For the levels of the muonic atom under consideration, it is sufficiently accurate, to within a few eV, to consider the energy shift of a muon in the potential due to the charge distribution of the electron density of an atom with nuclear charge $Z-1$.

The screening potential is well approximated by a function of the form

$$V_S(r) = V_0 - Cr^K e^{-\beta r} \quad (\text{A.40})$$

The constant V_0 is relatively large and is approximately equal to the Thomas-Fermi expression $V_S(0) = 0.049 Z^{4/3}$ keV. Only the second term in (A.40) contributes to the energy differences. VOGEL has calculated and tabulated Hartree-Fock-Slater electron potentials and values for C , K , and β for which (A.40) approximates these potentials to better than 5% for the range of r relevant to muonic orbits [A.67]. VOGEL finds that screening contributes -83 eV to the $5g_{9/2} - 4f_{7/2}$ transition in lead [A.89]. Calculations have also been done by FRICKE [A.90] and by DIXIT (quoted in [A.55,91]) and are in agreement with VOGEL's results and earlier calculations in Ref. [A.64] to within a few eV. The approximation, employed in the preceding calculations, of using the Slater approximation to the exchange potential has been checked by MANN and RINKER [A.92] and is found to produce a small (1-2 eV) error. RAFELSKI, MÜLLER, SOFF, and GREINER [A.93] discuss the question of how to deal with screening and vacuum polarization corrections in a consistent way.

A source of uncertainty in the screening calculations is the lack of knowledge of the extent to which the muonic atom is ionized. During the early stages after the muon is captured, it cascades in the atom partly by radiative transitions and partly by Auger transitions. The screening corrections depend on how many electrons have been ejected by Auger transitions of the muon. This problem has been considered by VOGEL who finds that the effect of ionization is partly compensated by refilling of the empty levels, and that the uncertainty in the muon levels is only 1-3 eV [A.94].

A.2.6 Summary and Comparison with Experiment

Numerical values for the corrections described in the preceding sections are listed in detail for muonic lead in Table VI. In Table VII theoretical contributions to the transition energies for measured transitions with Z in the range 56-82 are listed. The sources of the values are as follows. The point nucleus energy differences are the Dirac values for the muon-nucleus reduced mass $m_\mu M / (m_\mu + M)$. The value in eV is based on the recent determination of the ratio $m_\mu / m_e = 206.76927(17)$ deduced from measurement of the muonium hyperfine interval by CASPERSON et al [A.95] together with $R_{\infty h} = 13.605804(36)$ eV recommended by COHEN and TAYLOR [A.96]. (There is a small change of about 2 eV in the results for the muon energy levels if the value of m_μ / m_p determined by CROWE et al [A.97] is used.) Numerical values for the contributions in Table VII are taken from Table 2 of the review by WATSON and SUNDARESAN [A.98] with the following exceptions. The finite size correction to the higher order vacuum polarization is evaluated by means of ARAFUNE's formula (with the Uehling term subtracted) in Eq. (A.32) and is included in the column labeled $\alpha(Z\alpha)^{3+}$. The $\alpha^2(Z\alpha)^2$ term is based on the results in References A.79-81. The self-energy term includes an approximate error estimate of 30% to account for higher order terms in $Z\alpha$ and finite nuclear size effects [A.64].

Table VIII lists the most recent measurements of muonic x rays for the transitions being considered. The 1971-2 experiments show substantial disagreement with theory whereas the 1975-6 experiments are generally in good agreement with theory, as is easily seen in Fig. A.12. The apparent agreement of the latest results with theory provides an impressive confirmation of strong field vacuum polarization effects in QED.

TABLE VI. Summary of contributions to energy levels in muonic lead ^{208}Pb (eV).

Contribution	Order	$4f_{7/2}$	$5g_{9/2}$
<u>Static external potential</u>			
Dirac Coulomb energy ^a		-1188314	-758970
Finite nuclear size		4	0
<u>Vacuum polarization of order α</u>			
Coulomb Uehling potential ^a	$\alpha(Z\alpha)$	-3652	-1562
Finite nuclear size corr. to Uehling		-12	-3
Second order perturbation of Uehling		-9	-3
Third order in $Z\alpha$ Coulomb	$\alpha(Z\alpha)^3$	93	50
Fifth order in $Z\alpha$ (leading term)	$\alpha(Z\alpha)^5$	16	10
Seventh order in $Z\alpha$ (leading term)	$\alpha(Z\alpha)^7$	3	2
Finite size corr. to higher order in $Z\alpha$		-8	-3
<u>Vacuum polarization of order α^2</u>			
Coulomb Källén-Sabry potential	$\alpha^2(Z\alpha)$	-25	-11
<u>Self Energy</u>			
Bethe term	$\alpha(Z\alpha)^4$	1	0
Magnetic moment	$\alpha(Z\alpha)^4$	9	3
<u>Other radiative corrections</u>			
Virtual Delbrück diagram	$\alpha^2(Z\alpha)^2$	-1	0
<u>Nuclear motion</u>			
Relativistic reduced mass	$(Z\alpha)^4 m_\mu / M$	-4	-1
<u>Nuclear Polarization</u>			
Dipole term	$\alpha(Z\alpha)^4 \alpha_{E1}$	-4	0
<u>Atomic electrons</u>			
Screening correction ^b		-89	-172
TOTAL		-1191992	-760660
TRANSITION ENERGY $\cong 431,332$ eV			

^aIncludes reduced mass correction $m_\mu \rightarrow Mm_\mu / (m_\mu + M)$.

^bConstant term V_0 is not included.

: 0 0 0 0 4 7 0 8 9 4 3

TABLE VII. Theoretical contributions to muonic atom energy separations, in eV.

Transition	Pt.Nucl.	Finite Size	Vacuum		Polarization		Self En. $\alpha(Z\alpha)^4$	Rel. Rec.	Nuc. Pol.	Elec. Scr.	Total
			$\alpha(Z\alpha)$	$\alpha(Z\alpha)^{3+}$	$\alpha^2(Z\alpha)$	$\alpha^2(Z\alpha)^2$					
^{56}Ba											
$4f_{5/2}-3d_{3/2}$	439,069±1	-146±8	2436	-21±2	17	1	9±3	3	7	-18±1	441,357±9
$4f_{7/2}-3d_{5/2}$	431,654±1	-55±5	2328	-20±2	16	1	-8±2	3	7	-18±1	433,908±6
$5g_{7/2}-4f_{5/2}$	200,544±1	0	761	-9±1	5	0	2±1	1	0	-31±2	201,273±3
$5g_{9/2}-4f_{7/2}$	199,194±1	0	747	-9±1	5	0	-2±1	1	0	-31±2	199,905±3
^{80}Hg											
$5g_{7/2}-4f_{5/2}$	414,182±1	-8±1	2047	-42±2	14	1	7±2	2	3	-78±4	416,128±5
$5g_{9/2}-4f_{7/2}$	408,465±1	-2	1972	-40±2	14	1	-6±2	2	3	-79±4	410,330±5
$^{203}_{81}\text{Tl}$											
$5g_{7/2}-4f_{5/2}$	424,850±1	-9±1	2117	-44±2	15	1	7±2	2	4	-79±4	426,864±5
$5g_{9/2}-4f_{7/2}$	418,837±1	-3	2039	-43±2	14	1	-7±2	2	4	-81±4	420,763±5
^{82}Pb											
$5g_{7/2}-4f_{5/2}$	435,666±1	-10±1	2189	-46±2	15	1	7±2	2	4	-81±4	437,747±5
$5g_{9/2}-4f_{7/2}$	429,344±1	-4	2106	-45±2	15	1	-7±2	2	4	-83±4	431,333±5

TABLE VIII. Recent measurements of muonic x rays, in eV.

	BACKENSTOSS et al. 1970	DIXIT et al. 1971	WALTER et al. 1972	TAUSCHER et al. 1975 ^a	DIXIT et al. 1975 ^b	VUILLEUMIER et al. 1976 ^b
^{56}Ba						
$4f_{5/2}-3d_{3/2}$		441,299±21		441,366±13	441,371±12	
$4f_{7/2}-3d_{5/2}$		433,829±19		433,916±12	433,910±12	
$5g_{7/2}-4f_{5/2}$		201,260±16			201,282±9	
$5g_{9/2}-4f_{7/2}$		199,902±15			199,915±9	
^{80}Hg						
$5g_{7/2}-4f_{5/2}$			416,087±23			416,100±28
$5g_{9/2}-4f_{7/2}$			410,284±24			410,292±28
$^{203}_{81}\text{Tl}$						
$5g_{7/2}-4f_{5/2}$			426,828±23			426,851±29
$5g_{9/2}-4f_{7/2}$			420,717±23			420,741±29
^{82}Pb						
$5g_{7/2}-4f_{5/2}$	437,806±40	437,687±20		437,744±16	437,762±13	
$5g_{9/2}-4f_{7/2}$	431,410±40	431,285±17		431,353±14	431,341±11	

^aThe new ^{198}Au (412 keV) standard of DESLATTES et al [A.99] would increase these values by about 10 eV.

^bBased on the new Au standard.

A.2.7 Muonic Helium

Recently, the separation of the $2P_{3/2}$ and $2S_{1/2}$ energy levels in muonic helium ($\mu^4\text{He}^+$) was measured by BERTIN et al [A.100]. In that experiment, muons were stopped in helium and in some cases formed ($\mu^4\text{He}^+$) in the metastable ($\tau = 2$ usec) $2S$ state. Transitions to the $2P_{3/2}$ state were induced by a tunable infrared pulsed dye laser, and monitored by observation of the $2P$ - $1S$ 8.2 keV x ray. A fit to the resonance curve yielded a line center corresponding to the transition energy

$$\Delta E(\text{exp}) = 1527.4(9) \text{ meV} \quad (\text{A.41})$$

The theory of the muonic helium system provides an instructive contrast to the heavy muonic atoms. The relative importance of the various corrections is quite different in the two cases. For example, in muonic lead, the electron vacuum polarization of order $\alpha(Z\alpha)^3$ plays an important role, while it is negligible in muonic helium. On the other hand, the effect of finite nuclear size, which is a small correction to high- ℓ levels in muonic lead, is the major source of uncertainty in the theoretical value of the energy separation $2P_{3/2} - 2S_{1/2}$ in muonic helium. In the following, we briefly summarize the contributions to the theoretical value of the $2P_{3/2} - 2S_{1/2}$ splitting in ($\mu^4\text{He}^+$). The numerical values are collected in Table IX.

The fine structure is qualitatively different from the fine structure of a one-electron atom; the vacuum polarization is the dominant effect in determining the muonic level spacings. The $2S_{1/2}$ level is lowered 1.7 eV by vacuum polarization compared to the Sommerfeld fine structure splitting of 0.1 eV. The finite nuclear size correction is the second largest effect and raises the $2S_{1/2}$ level by 0.3 eV.

The starting point for the theoretical contributions is the point nucleus fine structure formula

$$\Delta E_{\text{FS}} = \frac{1}{32} (Z\alpha)^4 \frac{m_\mu}{1+m_\mu/M} \left[1 + \frac{5}{8} (Z\alpha)^2 + \dots \right] \quad (\text{A.42})$$

where M is the nuclear mass. This must be corrected for the finite size of the nucleus. The nuclear charge radius is only known approximately from electron scattering experiments, so it is convenient to parameterize the size contribution to the fine structure in terms of the r.m.s. nuclear radius.

[A.101]

$$\Delta E_{\text{NS}} = -103.1 \langle r^2 \rangle \text{ meV} \cdot \text{fm}^{-2} \quad (\text{A.43})$$

The value of the sum of the above corrections is in satisfactory numerical agreement with the more recent work of RINKER [A.102].

The largest radiative correction is the electron vacuum polarization of order $\alpha(Z\alpha)$. The value has been calculated by RINKER [A.102] who numerically solves the Dirac equation with a finite-nucleus vacuum polarization potential included (see Section A.2.2). The result appears in Table IX. The order $\alpha^2(Z\alpha)$ vacuum polarization was calculated by CAMPANI [A.103], by BORIE [A.101], and by RINKER [A.102]; all of the results are in accord.

The point nucleus value for the self-energy and muon vacuum polarization is given by [A.7]

$$\Delta E_{\text{SE}} + \Delta I_{\text{VP}} = -\frac{\alpha(Z\alpha)^4 m_\mu}{6\pi} \left\{ \frac{1}{(1+m_\mu/M)^3} \left[\frac{19}{30} + \ln(Z\alpha)^{-2} + \ln(1+m_\mu/M) - \ln \frac{K_0(2,0)}{K_0(2,1)} \right] - \frac{1}{16} (1+m_\mu/M)^{-2} + 3\pi Z\alpha \left(\frac{427}{384} - \frac{1}{2} \ln 2 \right) + \dots \right\} \quad (\text{A.44})$$

The lowest order term may be partially corrected for finite nuclear size

00004708944

effects by replacing the wavefunction at the origin $|\psi(0)|^2$ by the expectation value of the nuclear charge density $\langle \rho_N(\vec{r}) \rangle$, as has been done by RINKER [A.102]. An evaluation of the finite-nucleus average excitation energy K_0 would be necessary for a complete evaluation of the effect of finite nuclear size.

A further small correction arises from the effect of the finite nuclear size on the relativistic nuclear recoil terms. RINKER [A.102] estimates a value of 0.3 meV for this correction, using the prescription of FRIAR and NEGLE [A.104] for finite nuclei. This correction is nearly cancelled by the Salpeter recoil term from the non-instantaneous transverse photon exchange of order $(Z\alpha)^5 m_\mu^2/M$.

An important effect is nuclear polarization, which has been the subject of some controversy. The simple approximation used for high- l states (see Section A.2.4) is not accurate for low- l states in muonic helium. BERNABÉU and JARLSKOG [A.105] calculated a value of 3.1 meV for the nuclear polarizability contribution using photoabsorption cross section measurements as input data. On the other hand, HENLEY, KREJS and WILETS [A.106] obtained a value of 7.0 meV based on a harmonic oscillator model for the nucleus. This value agrees with an earlier result of JOACHAIN [A.107]. However, in a subsequent analysis of the discrepancy, BERNABÉU and JARLSKOG [A.108] point out that the harmonic oscillator model predicts a value for the electric polarizability of the nucleus α_{E1} which is in substantial disagreement with the value deduced from existing measurements of the photoabsorption cross section (see Eq. (A.39)). A subsequent calculation by RINKER [A.102] confirms the conclusions of BERNABÉU and JARLSKOG and also yields a value of 3.1 meV for the nuclear polarizability contribution.

The total theoretical value for the $2P_{3/2} - 2S_{1/2}$ energy separation is

given by (see Table IX)

$$\Delta E(\text{th}) = 1815.8 \pm 1.2 \text{ meV} - 103.1 \langle r^2 \rangle \text{ fm}^{-2} - \text{meV} \quad (\text{A.45})$$

Using a weighted average of the results of electron scattering data for the ^4He charge radius ($\langle r^2 \rangle^{1/2} = 1.650 \pm 0.025 \text{ fm}$) [A.100] the theoretical energy separation is

$$\Delta E(\text{th}) = 1535(9) \text{ meV} \quad (\text{A.46})$$

in agreement with the experimental result. On the other hand, assuming that the theory is correct, one can equate (A.45) and (A.41) to obtain a measured value for the charge radius

$$\langle r^2 \rangle^{1/2} = 1.673(4) \text{ fm} \quad (\text{A.47})$$

TABLE IX. Theoretical contributions to the fine structure in muonic helium (in meV).

Source	Lowest order	Value
Fine structure	$(Z\alpha)^4$	145.7
Finite nuclear size	$(Z\alpha)^4 m_\mu^2 \langle r^2 \rangle$	$-103.1 \langle r^2 \rangle \text{ fm}^{-2}$
Electron vacuum polarization Uehling potential	$\alpha(Z\alpha)$	1666.1
Electron vacuum polarization Källén-Sabry term	$\alpha^2(Z\alpha)$	11.6
Self energy and muon vacuum polarization	$\alpha(Z\alpha)^4 \ln(Z\alpha)^{-2}$	-10.7 ± 1.0
Nuclear polarization		3.1 ± 0.6
TOTAL		1815.8 ± 1.2 $-103.1 \langle r^2 \rangle \text{ fm}^{-2}$

A.2.8 Nonperturbative Vacuum Polarization Modification
and Possible Scalar Particles

A possible deviation of QED from the ordinary perturbation theory predictions might be through a nonperturbative modification of the vacuum polarization. The corresponding change in the vacuum polarization potential would be of the form

$$\delta V(r) = -\frac{\alpha Z\alpha}{3\pi r} \int_{4m_e^2}^{\infty} dt t^{-1} \delta\rho(t) e^{-\sqrt{t} r} \quad (\text{A.48})$$

where $\delta\rho(t)$ is a nonperturbative change in the vacuum-polarization spectral function. The change $\delta\rho(t)$ excludes the ordinary electron and muon vacuum polarization contributions of order α and α^2 , but might be substantially larger than would normally be expected from perturbation theory terms of order α^3 and higher.

Phenomenological analyses of such a deviation have been given by ADLER [A.83], ADLER, DASHEN, and TREIMAN [A.109], and BARBIERI [A.110] with particular emphasis on constraints on such a deviation imposed by various comparisons of theory and experiment. ADLER finds, with the technical assumption that $\delta\rho(t)$ increases monotonically with t , that if the vacuum polarization deviation is large enough to produce a change in the muonic atom transition energies of the magnitude of the difference between ordinary QED predictions for high-Z muonic atoms and the disagreeing 1971-2 experimental values, then (a) the theoretical value of the muon magnetic moment anomaly $a_\mu = \frac{1}{2}(g_\mu - 2)$ would be reduced by at least 96×10^{-9} , and (b) there would be a reduction of order 27 meV in the theoretical value of the $2P_{3/2} - 2S_{1/2}$ transition energy in muonic helium. Prediction (a) would introduce a 2σ difference between theory and experiment in the recent results for a_μ [A.111,112]:

$$a_\mu(\text{exp}) = 1165895(27) \times 10^{-9}$$

$$a_\mu(\text{th}) = 1165918(10) \times 10^{-9}$$

Prediction (b) appears to be incompatible with the results for muonic helium discussed in Section A.2.7. However, such modifications of vacuum polarization at a level ~ 3 times smaller have not been ruled out.

A second proposed explanation for the 1971-2 discrepancy between muonic atom measurements and theory is the existence of a light weakly-coupled scalar boson ϕ . Such particles are predicted by unified gauge theories of weak and electromagnetic interactions, but the mass is not determined. It was pointed out by JACKIW and WEINBERG [A.113] and by SUNDARESAN and WATSON [A.69] that if the mass of the ϕ meson were small enough, then its effect on muonic atom energy levels could account for the discrepancy. The coupling produced by a ϕ -exchange between a muon and a nucleus of mass number A is of the Yukawa form

$$V_\phi(r) = -\frac{g_{\phi\mu\bar{\mu}} g_{\phi NN}}{4\pi} A \frac{e^{-M_\phi r}}{r} \quad (\text{A.49})$$

where $g_{\phi\mu\bar{\mu}}$ and $g_{\phi NN}$ are the ϕ -muon and ϕ -nucleon couplings respectively and M_ϕ is the mass of the ϕ . In gauge models, the ϕ -electron coupling is expected to be of order $(m_e/m_\mu)g_{\phi\mu\bar{\mu}}$ so the effect of such a potential could be observable in muon experiments without affecting the electron $g_e - 2$ or Lamb shift experiments [A.83].

WATSON and SUNDARESAN [A.98] found that the values $g_{\phi\mu\bar{\mu}} g_{\phi NN}/(4\pi) = -8 \times 10^{-7}$ and $M_\phi = 12$ MeV would explain the early muonic atom discrepancy (the sign of the coupling is changed here according to ADLER [A.83]). ADLER [A.83] found a range of values for the coupling strength and ϕ mass which explain the discrepancy. However, ADLER [A.83] and BARBIERI [A.110]

0204708945

have shown that such a particle with $M_\phi > 1$ MeV which could explain the discrepancy would also reduce the theoretical value for the muonic-helium fine structure $\Delta E (2P_{3/2} - 2S_{1/2})$ by approximately 27 meV. RESNICK, SUNDARESAN, and WATSON [A.114] pointed out that the effect of a ϕ -meson could be observed in a $0^+ - 0^+$ nuclear decay in which the ϕ is emitted and subsequently decays into an e^+e^- pair. A search for e^+e^- pairs in the decays of the ^{16}O (6.05 MeV) and ^4He (20.2 MeV) 0^+ levels to corresponding 0^+ ground states was carried out by KOHLER, BECKER, and WATSON [A.115] who concluded from the negative results that the mass of the ϕ could not be in the range 1.030 - 18.2 MeV. ADLER, DASHEN, and TREIMAN [A.109] argue that neutron-electron and electron-deuteron scattering data rules out the ϕ meson explanation for M_ϕ in the range between 0 and 0.6 MeV.

The most serious constraint, however, was derived by BARBIERI and ERICSON [A.116] who show that low energy neutron-nucleus scattering data yields a limit $g_{\phi NN}^2 M_\phi^{-4} / (4\pi) \leq 3.4 \times 10^{-11} \text{ MeV}^{-4}$. The Weinberg-Salam theory predicts $g_{\phi\mu\mu}^2 / (4\pi) = G_F m_\mu^2 / (\sqrt{2} 2\pi) = 1.3 \times 10^{-8}$; hence for $M_\phi = 1$ MeV, for example, $|g_{\phi\mu\mu} g_{\phi NN} / (4\pi)| \leq 7 \times 10^{-10}$ which is orders of magnitude smaller than the value 1.4×10^{-7} [A.83] required to explain the muonic atom discrepancy.

A.3 QUANTUM ELECTRODYNAMICS IN HEAVY-ION COLLISIONS AND SUPERCRITICAL FIELDS

A.3.1 Electrodynamics for $Z\alpha > 1$

One of the most fascinating topics in atomic physics and quantum electrodynamics is the question of what happens physically to a bound electron when the strength of the Coulomb potential increases beyond $Z\alpha = 1$. This question involves properties of quantum electrodynamics which are presumably beyond the limits of validity of perturbation theory, so it is an area of fundamental interest. Although a completely rigorous field-theoretic formulation of this strong field problem has not been given, it is easy to understand in a qualitative way what happens physically: As $Z\alpha$ increases beyond a critical value, the discrete bound electron state becomes degenerate in energy with a three-particle continuum state (consisting of two bound electrons plus an outgoing positron wave) and a novel type of pair creation can occur [A.117,118]. Remarkably, as first suggested by GERSHTEIN and ZELDOVICH [A.119], it may be possible that such "autoionizing" positron production processes of strong field quantum electrodynamics can be studied experimentally in heavy-ion collisions.

In addition to the spontaneous pair production phenomena, a number of other questions of fundamental interest also become relevant at high $Z\alpha$:

- a) What is the nature of vacuum polarization if a pair can be created without the requirement of additional energy?
- b) Do higher order radiative effects in α from vacuum polarization and self-energy corrections significantly modify the predicted high- $Z\alpha$ phenomena?

- c) How should the vacuum be defined if the gap in energy between the lowest bound state and the negative continuum states approaches zero?
- d) Can we test the non-linear aspects of QED, e.g. as contained in the Euler-Heisenberg Lagrangian [A.120] and the Wichmann-Kroll calculation [A.12]? (The conventional tests of high-Z electrodynamics are discussed in Sections A.1 and A.2.)

The high- $Z\alpha$ domain is also fascinating in that it provides a theoretical laboratory for studying the interplay of single-particle Dirac theory and quantum field theory. A speculative possibility is that it may be of considerable interest as a model for strong binding and confinement of elementary particles in gauge theories. In the non-Abelian theories, such as "quantum chromodynamics" [A.121]; the effective coupling α_s between quarks could well be beyond the critical value. In addition, theoretical work on the "psion" family of particles (J/ψ , ψ' , etc.) has focused on a fermion-antifermion potential and various gauge theory models in the strong coupling regime [A.122].

Perhaps the most practical way to create the strong fields necessary to test the exotic predictions of high- $Z\alpha$ electrodynamics is in the slow collision of two ions of high nuclear charge [A.119]. In addition to the spontaneous and induced pair phenomena, a number of interesting atomic physics questions arise concerning, among other things, the atomic spectra and radiation of the effective high- Z quasi-molecule momentarily present in the collisions. These topics are reviewed by MOKLER and FOLKMANN [A.123] in this volume. The high magnetic field aspects are also of interest (see Section A.3.11). Studies of the high- Z exotic phenomena ideally require highly-stripped ions; the physics of vacancy formation (see Section A.3.6) and recent experimental

progress is discussed by MEYERHOF [A.124] and references therein.

Historically, the first discussions of the strong field problem were concerned with the solutions of the Dirac equation for an electron in a Coulomb field,

$$\begin{aligned} (\vec{\alpha} \cdot \vec{p} + \beta m + V(r))\psi &= E\psi \\ V(r) &= -\frac{Z\alpha}{r} \end{aligned} \quad (\text{A.50})$$

This is, of course, a mathematical idealization for $r \rightarrow 0$ since the nucleus has finite mass and size. (In the case of positronium, V is effectively modified at small r by vertex corrections and relativistic finite mass corrections implicit in the Bethe-Salpeter formalism. We should emphasize that the analysis of positronium for $\alpha > 1$ remains an unsolved problem.) The spectrum of the Dirac-Coulomb equation is given by the Dirac-Sommerfeld fine-structure formula; the energy of the electron in the 1S state is

$$E = \sqrt{1 - (Z\alpha)^2} m \quad (\text{A.51})$$

$E=0$ appears to be the lower limit of the discrete spectrum as $Z\alpha \rightarrow 1$, and E is imaginary for $Z\alpha > 1$. The Dirac Hamiltonian then is apparently not self-adjoint. Actually, this result is just a mathematical problem associated with a pure Coulomb potential [A.125-127]. The solutions are well-defined when nuclear finite size is introduced [A.117,128-133].

Thus, we should consider the "realistic" potentials

$$V(r) = \begin{cases} -\frac{Z\alpha}{r} & r > R \\ -\frac{Z\alpha}{R} f(r/R) & r < R \end{cases} \quad (\text{A.52})$$

where, for example, $f(\rho) = \frac{1}{2}(3 - \rho^2)$ for the case of a uniform charge density.

00004708946

The energy eigenvalue is then found by matching the solutions for the Dirac wavefunction at $r=R$. Early discussions of the bound state problem for $Z\alpha > 1$ appear in Refs. [A.128-130]; accurate extensive calculations were given after 1968 by PIEPER and GREINER [A.117], by REIN [A.151], and by POPOV [A.133]. The energy spectrum for typical nuclear radii, from Ref. [A.117], is shown in Fig. A.13. In Fig. A.14, POPOV's [A.132,133] result for the dependence of $(Z\alpha)_{CR}$ (the value of $Z\alpha$ for which $E = -m$) on the nuclear radius R is shown. It is clear that the "limit point" $E=0$ of the point nucleus case is artificial: at sufficiently large $Z\alpha$, E reaches $-m$, the upper limit of the negative energy continuum. The critical Z for an extended superheavy nucleus with $R = 1.2 A^{1/3}$ fm is $Z \approx 170, 185,$ and 245 for the $1S_{1/2}, 2P_{1/2},$ and $2S_{1/2}$ levels, respectively [A.134]. The possibility of simulating such a nuclear state with heavy-ion collisions is discussed in the next Section.

It should be noted that the physical situation is already quite unusual if $E < 0$, let alone when E reaches the negative continuum. If $Z \geq 150$ and $E \leq 0$, then the combined energy of the nucleus and one or two electrons bound in the $1S$ state is lower than the energy of the nucleus alone! Of course, since charge is conserved, an isolated nucleus of charge $Z \geq 150$ cannot "spontaneously decay" to this lower energy state.

However, the situation becomes more intriguing if Z can be increased beyond the critical value $Z_{CR} \sim 170$ where E "dives" below $-m$ (see Fig. A.13). In this case, the total energy of a state with a bound electron and an unbound slow positron (with $E_{\text{positron}} \sim m$)

$$E_{\text{nucl}} + E_{1S} + E_{\text{positron}} < E_{\text{nucl}} \quad (\text{A.53})$$

is less than that of the nucleus alone, and an isolated nucleus may decay

to that state. In fact, for $Z \geq 170$, the nucleus will emit two positrons and fill both $1S$ levels. Clearly the physics is that of a multiparticle state and we must leave the confines of the single particle Dirac equation. However, in these first two sections we will ignore the higher order QED effects from electron self-energy corrections and vacuum polarization. (This can always be done mathematically - if we envision taking a small $Z\alpha$ fixed [A.135].) We return to the question of radiative corrections in Section A.3.8. In the remainder of this section we discuss a qualitative interpretation in terms of a new vacuum state. Quantitative results are discussed in the following sections.

The vacuum state, as originally interpreted by Dirac, is the state with all negative energy eigenstates of the wave equation occupied. Thus for fermions

$$a_{(+n)}|0\rangle = 0, \quad a_{(-n)}^\dagger|0\rangle = b_{(+n)}|0\rangle = 0 \quad (\text{A.54})$$

where $a_{(+)}$ ($a_{(-)}$) are the anticommuting annihilation operators for the positive (negative) energy single-particle states. The operators $b_{(+)}^\dagger = a_{(-)}$ can be interpreted as the positron creation (= negative energy electron annihilation) operators. Normally, the $E_n < 0$ states are continuum eigenstates. Then, up to a constant, the total energy is

$$H = \sum_{E_n > 0} a_{(+n)}^\dagger a_{(+n)} E_n + \sum_{E_n < 0} b_{(+n)}^\dagger b_{(+n)} |E_n| \quad (\text{A.55})$$

(This is just normal ordering the Hamiltonian - i.e. placing the annihilation operators to the right.)

However, in the case of nuclear Coulomb potentials with $Z > Z_0 \sim 150$, at least one bound state solution of the Dirac equation has negative energy

(see Fig. A.13). Thus it is evident that as soon as the field is strong enough to yield bound eigenstates of negative energy, one gains energy by filling these states. For example, imagine that there are two separated nuclei with charge Z and $-Z$, the latter made of antinucleons! If the charge of both nuclei were increased adiabatically beyond $Z = Z_0$ then there would be spontaneous decay of the nuclear system, to the state where two electrons in the 1S state are bound to the nucleus and two positrons are bound to the antinucleus.

Notice, incidentally, that charge conjugation symmetry is always preserved and one does not have "spontaneous symmetry breaking" in the vacuum decay. This is contrary to the claim of Ref. [A.134].

It is thus clear that when $Z > Z_0$, the state where the negative energy-bound states are filled represents the natural choice as reference state for excitations [A.136,137]. Accordingly for $Z > Z_0$, we define the "new" Dirac vacuum [A.136]

$$\begin{aligned} |0_{\text{new}}\rangle &= a_{1S}^\dagger(+)\ a_{1S}^\dagger(+)\ |0_{\text{old}}\rangle \\ &\equiv b_{1S}(+)\ b_{1S}(+)\ |0_{\text{old}}\rangle \end{aligned} \quad (\text{A.56})$$

i.e.

$$|0_{\text{old}}\rangle = b_{1S}^\dagger(+)\ b_{1S}^\dagger(+)\ |0_{\text{new}}\rangle \quad (\text{A.57})$$

where we suppose the spin up and down 1S states are the only bound states with negative energy. The charge of the new vacuum is $Q_{\text{new}} = Q_{\text{old}} - 2$.

Notice that the operator $b_{1S}^\dagger(+)\ \equiv\ a_{1S}^\dagger(+)$ creates a hole with respect to the new vacuum, and thus effectively creates a bound positron state with positive energy $E_{\text{pos}} = |E_{1S}|$. The old vacuum appears as an excited state of the system; namely, two positrons are bound with positive total energy if $Z < Z_{\text{CR}} \sim 170$.

However, if Z is raised above Z_{CR} , the positrons become unbound. Thus from the standpoint of the new picture, the phenomenon of the instability of the (old) vacuum at $Z = Z_{\text{CR}}$ is reinterpreted by the statement that the positron wavefunction becomes unbound for this value of the charge (see Fig. A.15).

The bound negative energy one-electron state may be written

$$\begin{aligned} a_{1S}^\dagger(+)\ |0_{\text{old}}\rangle &\equiv a_{1S}^\dagger(+)\ b_{1S}^\dagger(+)\ b_{1S}^\dagger(+)\ |0_{\text{new}}\rangle \\ &= b_{1S}(+)\ b_{1S}^\dagger(+)\ b_{1S}^\dagger(+)\ |0_{\text{new}}\rangle \\ &= -b_{1S}^\dagger(+)\ |0_{\text{new}}\rangle \end{aligned} \quad (\text{A.58})$$

i.e. it is equivalent (with respect to the new vacuum) to a bound positron for $Z < Z_{\text{CR}}$ and a continuum positron for $Z > Z_{\text{CR}}$. The effective potential $U_{\text{eff}}(r)$ in the relativistic Coulomb problem (see Section A.3.4) behaves like $-Ez\alpha/r$ as $r \rightarrow \infty$, i.e.: is attractive for $E > 0$ and repulsive for $E < 0$ (at sufficiently large distances from the nucleus) [A.133,138]. Thus, as shown by ZELDOVICH and POPOV [A.138], the bound positron moves in a non-monotonic effective potential which becomes shallower as Z increases (see Fig. A.16), until at $Z = Z_{\text{CR}}$ it becomes unbound. A plot of the average radius for the bound states as a function of E as computed by POPOV [A.133] is shown in Fig. A.17. The process involved in spontaneous positron production for $Z > Z_{\text{CR}}$ is then simply

$$b_{1S}^\dagger(+)\ |0_{\text{new}}\rangle = b_{1S}^\dagger(+)\ |0_{\text{new}}\rangle \quad (\text{A.59})$$

Formally, from Eqs. (A.56-58), this is equivalent, in terms of the conventional vacuum, to

$$a_{1S}^\dagger(+)\ |0_{\text{old}}\rangle = b_{1S}^\dagger(+)\ a_{1S}^\dagger(+)\ a_{1S}^\dagger(+)\ |0_{\text{old}}\rangle \quad (\text{A.60})$$

00004708947

corresponding to the degeneracy of the discrete bound electron state with a three-particle continuum. The old vacuum is, however, inappropriate for the description of the system for $Z > Z_{CR}$ simply because it is unstable. The description of high- Z electrodynamics in terms of the new vacuum thus has the advantage of displaying the continuity of the physics at $Z = Z_{CR}$. As we discuss in Section A.3.8, the vacuum polarization problem is also clarified. The formal aspects of positron autoionization are discussed in more detail in Ref. [A.139].

A.3.2 Spontaneous Pair Production in Heavy-Ion Collisions

It would be very interesting if the physical realization of an electron bound to a strong field with Z greater than $Z_{CR} \sim 170$ could be attained experimentally. It is not excluded that nuclei with $Z \sim Z_{CR}$ will eventually be synthesized, but at present this possibility seems remote. Suggestions of positron production in overcritical nuclei were discussed in 1969 by PIEPER and GREINER [A.117] and by GERSHTEIN and ZELDOVICH [A.118]. In the same year, GERSHTEIN and ZELDOVICH [A.119] proposed that the critical field condition could be attained in the close approach of two heavy ions with $Z_1 + Z_2 > Z_{CR}$. If the velocity of collision is assumed to be sufficient to approach the Coulomb barrier, then, at least in the adiabatic approximation ($v_{ion}/v_{electron} \lesssim 1/10$), a ground state electron sees an effectively coalesced nuclear potential. This pioneering paper by GERSHTEIN and ZELDOVICH and the early papers of POPOV [A.132,133,140] and GREINER et al [A.40,141-145] contain many of the fundamental physical ideas which have been subsequently discussed in more quantitative fashion over the past seven years [A.134, 139,141,144-154].

In collisions of heavy ions with several-meV/nucleon kinetic energy, the typical collision time of the ions inside the K shell of an electron is $T_C \sim 10^{-19}$ sec whereas the "orbiting" time of the electron is $T_e \sim 10^{-20}$ sec. Thus, roughly speaking, the molecular electronic states have time to adjust to the varying distance $\vec{R} = \vec{R}_2 - \vec{R}_1$ between the nuclei. One can then consider an approximate adiabatic treatment of the two-center Dirac equation

$$[\vec{\alpha} \cdot \vec{p} + \beta m + V(\vec{r} - \vec{R}_1) + V(\vec{r} - \vec{R}_2)]\psi = E\psi \quad (\text{A.61})$$

(assuming one electron is present). An extensive discussion of this problem and numerical solutions for the molecular spectra of "intermediate super-heavy molecules" are given in Refs. [A.123] and [A.134].

Let us suppose that only one ground state electron is present. For $Z_1 + Z_2 > Z_{CR}$, there will be a critical distance R_{CR} between the two nuclei for which the electron is bound with an energy $-m$. Then as the ions collide with $R < R_{CR}$, the lowest one-electron state becomes mixed with the $|e^- e^+\rangle$ continuum level (spontaneous pair production); see Fig. A.18. As the ions recede, we are left with two electrons in the 1S level plus an outgoing positron. Note that double pair production with two outgoing positrons can occur if no ground state electron is initially present. Pair production, however, is suppressed by the Pauli principle if the 1S levels are full, so preionization or stripping is necessary. The energy for the spontaneous pair production is compensated by a decrease in the kinetic energy of the outgoing nuclei. Additional pairs can in principle be produced when the 2P levels in turn reach their critical energy $E_{2P} = -m$. However, according to the calculations of RAFELSKI, MÜLLER, and GREINER [A.139] for ${}_{92}\text{U} - {}_{92}\text{U}$ molecular orbitals, the $2P_{1/2}$ level reaches the negative energy continuum at a distance R which may be too close to the Coulomb barrier for experiments

to be feasible (see Fig. A.18).

In a series of comprehensive papers, POPOV, GREINER and others have presented detailed analytic and numerical calculations of the spontaneous positron production process in heavy-ion collisions. We shall review the main points of this work which are particularly relevant to practical experiments and refer the reader to the original papers for more details.

For simplicity, we consider a beam of completely stripped nuclei Z_1 incident on an ordinary target with nuclear charge Z_2 . (The non-stripped case will be discussed in Section A.3.6.) If $Z_1 > Z_2$ then the K shell of the combined atom will generally be vacant as a result of the behavior of the molecular terms in the adiabatic approach of the nuclei [A.155]. In fact, the cross section for positron production turns out to be only slightly smaller than in the idealized case of the collision of two bare nuclei (see Ref. [A.156]). For definiteness we will usually consider U-U collisions, for which the combined Coulomb field $Z = Z_1 + Z_2 = 184$ is beyond the critical charge $Z_{cr} \approx 170$ necessary for spontaneous positron production.

As shown by MÜLLER, RAFELSKI, and GREINER [A.157] (see Section A.3.3), the critical distance for positron production in U-U collisions (where the energy of the two-center atom reaches the negative continuum) is $R_{cr} \approx 34$ fm $= 0.088 \lambda_e$. The calculation of R_{cr} can be carried out precisely and requires an analysis of the two-center Dirac problem; we return to this in Section A.3.3. Thus the lab kinetic energy of the beam at the positron production threshold is

$$E_T = \frac{1}{2} m v_L^2 = \frac{2Z_1 Z_2 \alpha}{R_{cr}} = 717 \text{ MeV} \quad (\text{A.62})$$

or ~ 3 MeV/nucleon for U-U collisions. The lab velocity is $v_L = 0.08$ which is clearly in the adiabatic non-relativistic domain, and small compared to

the velocity of a K-shell electron.

The classical orbits and Rutherford cross section of non-relativistic charged particles are, of course, well understood. Detailed discussions and kinematics are given in Refs. [A.145,158,159]. It is convenient to define $\eta = E_{LAB}/E_T$ which is also related to the distance of closest approach R_0 for backward scattering of the nuclei: $\eta = R_{cr}/R_0$. Spontaneous positron production is possible only if $\eta > 1$. If θ is the CM angle of the scattering then the requirement that the nuclei are sufficiently close, $R_{min} < R_{cr}$, where R_{min} is the distance of closest approach, is

$$\eta = \frac{E_{LAB}}{E_T} > \frac{1}{2}(1 + \text{cosec } \frac{\theta}{2}) = \eta_{min}(\theta) \quad (\text{A.63})$$

The variation of the positron production cross section as a function of η and θ gives a simple tool for testing the positron production calculations.

For nuclei approaching each other, the two-center Dirac equation can be solved in the adiabatic approximation with nuclear separation $R = R(t)$, assuming $v \ll c$. Each value $R < R_{cr}$ then gives a corresponding (complex) energy level near the lower continuum: $E = E_0 + i \Gamma/2$ [A.153]. (The unusual sign of the imaginary part is discussed in Section A.3.4.) The real part of the energy level is identified as the produced positron's kinetic energy $T = |E_0| - m$, the positron production rate is $dw/dt = \Gamma$. Integration of dw/dt over the ion's Coulomb orbit then gives the probability of positron production in the collision. Note that here we consider only spontaneous production in the adiabatic approximation; induced production will be discussed in Section A.3.5.

Clearly the maximum cross section for e^+ production is the geometric limit [A.151], $\sigma_{geom} = \pi R_{cr}^2 (1 - \eta^{-1}) = 36b(1 - \eta^{-1})$ for U-U collisions, which

8 1 6 9 0 7 0 8 9 4 8

would be attained if the Coulomb field of the nuclei succeeded in producing a positron in each collision for which $R_{\min} < R_{\text{cr}}$. (The corresponding impact parameter at $R_{\min} = R_{\text{cr}}$ is $\rho = R_{\text{cr}}(1 - \eta^{-1})^{1/2}$ and $\sigma_{\text{geom}} = \pi\rho^2$.) In fact, the actual cross section calculated by MARINOV and POPOV [A.159] is exponentially damped at threshold ($\eta + 1$) rising to a fraction of 0.1% of σ_{geom} for $\eta \geq 2$, increasing slowly thereafter. The ratio $W_{\text{av.}} = \sigma/\sigma_{\text{geom}}$ averaged over the positron spectrum is shown in Fig. A.19. The maximum energy such that there is no nuclear interaction in the collision is determined by (r_N is the nuclear radius) [A.159]

$$\eta_{\text{max}} \sim \frac{R_{\text{cr}}}{2r_N + \Delta r} \sim 2.8 \quad (\text{A.64})$$

allowing $\Delta r \sim 5$ fm for the diffuseness of the nuclear boundary. The background process of e^+e^- production due to Coulomb excitation of the nucleus is discussed in Section A.3.7.

Hence for U-U collisions, with $\eta \sim 2$, $E_{\text{LAB}} \sim 1.4$ GeV, $v_L \sim 0.1$, we have $\sigma_{\text{geom}} \sim 18\text{b}$ and $\sigma \sim 2$ mb, i.e.: spontaneous positron production occurs roughly in one out of nine thousand nuclear collisions in which the distance $R < R_{\text{cr}}$ is reached and the 1S level is unoccupied. A recent semiclassical calculation by JAKUBASSA and KLEBER [A.160] based on a one-center analysis yields a spontaneous production cross section of similar value.

The ratio of the differential cross section with positron production to the Rutherford cross section $(d\sigma/d\Omega)_R = R_{\text{cr}}^2/(4\eta)^2 \sin^4 \frac{\theta}{2}$ at $\theta = \pi$ (backward scattering) is given by an integral over the Coulomb path [A.159]

$$W_{\pi}(\eta) = \frac{d\sigma/d\Omega}{(d\sigma/d\Omega)_R} \Big|_{\theta=\pi} = C \int_{\eta^{-1}}^1 dx \left(\frac{x}{\eta x - 1} \right)^{1/2} \Gamma(x) \quad (\text{A.65})$$

where the positron width is written as a function of $x = R/R_{\text{cr}}$. Since $r_N \ll (R, R_{\text{cr}}) \ll R_K$ (R_K is the electronic K-shell radius for $Z\alpha \sim 1$) the energy E_0 and width Γ are insensitive to the detailed two-center situation; as shown by POPOV [A.153], these quantities are dependent only on the ratio R/R_{cr} . Thus the only critical parameter in the two-center problem is the actual value of R_{cr} . The constant C in Eq. (A.65) is proportional to $R_{\text{cr}}^{3/2}$ and $[(Z_1 + Z_2)\alpha]^{-1/2}$ and is equal to 2.3 for U-U collisions. The result of a numerical calculation for W_{π} is also shown in Fig. A.19. The corresponding positron spectrum $w(T)$, proportional to the integrand of Eq. (A.65), normalized to $\int_0^{T_{\text{max}}} dT w(T) = 1$, is shown in Fig. A.20 for $\theta_{\text{cm}} = \pi$. The maximum positron kinetic energy is

$$T_{\text{max}}(\eta, \theta) = |E_0(R_{\min}/R_{\text{cr}})| - m \quad (\text{A.66})$$

The distribution in T peaks sharply at T_{max} since the ion spends the most time at the point of closest approach, and $\Gamma(R/R_{\text{cr}})$ is largest there. Near the maximum energy, $w(T) \sim (T_{\text{max}} - T)^{-1/2}$. For $\eta \sim 2$, approximately 60% of the positrons have an energy above $0.9 T_{\text{max}}$. The square-root singularity is due to the fact that the radial velocity vanishes at $R = R_{\min}$. The strong peaking and maximal effect at $\theta = \pi$ is clearly favorable for experiments. For $\theta = \pi/2$, w is smaller by an order of magnitude. If the angle of the scattered ion is not measured, the peak in $w(T)$ is considerably washed out. The small value for the probability of single positron production $W_{(1)} = W_{\text{av}} \lesssim 10^{-3}$ means that the double spontaneous positron production probability $W_{(2)}$ (filling both 1S levels with electrons) is only of order $W_{(1)}^2 \lesssim 10^{-6}$, and is probably not a useful signal for spontaneous production.

A.3.3 Calculation of the Critical Internuclear Distance

An important numerical parameter for phenomena involving a supercritical Coulomb field in heavy-ion collisions is the value of the internuclear distance $R = R_{CR}$ at which the energy of the ground state of the quasi-molecule (Z_1, Z_2, e) crosses the boundary of the lower continuum. For low-velocity collisions with $Z_1 = Z_2 = Z$ it is sufficient to calculate the energy of the two-center Dirac equation with the potential $V(\vec{r}) = -Z\alpha/r_1 - Z\alpha/r_2$, where $r_i = |\vec{r} - \vec{R}_i|$ (adiabatic approximation). Since R_{CR} is substantially greater than the nucleon size, the nucleon finite size effects can be estimated from perturbation theory [A.156]. MARINOV and POPOV [A.156] and MARINOV, POPOV, and STOLIN [A.161] calculate R_{CR} using a variational method in which each component of the trial wavefunction of the two-center Dirac equation is written as a sum of terms with the correct singularity behavior at large and small distances; e.g. near the nuclei the Dirac wavefunction has the singularity

$$\psi(\vec{r}) \sim (\xi^2 - \eta^2)^{-1 + \sqrt{1 - (Z\alpha)^2}} \quad (\text{A.67})$$

where $\xi = (r_1 + r_2)/R$, $\eta = (r_1 - r_2)/R$ are elliptical coordinates. This method converges quickly with just a few terms. As shown by MARINOV et al [A.156,161], the variational method gives a lower limit on R_{CR} .

A similar variational calculation was also performed for U-U collisions by MÜLLER, RAFELSKI, and GREINER [A.157] and by MÜLLER, SMITH, and GREINER [A.162] giving the result $R_{CR} \sim 36$ fm compared to the lower limit, $R_{CR} \geq 38$ fm obtained by MARINOV et al [A.163]. (It should be noted that the published numerical results beyond the (1,0) approximation given in Refs. [A.156] and [A.161] need to be revised because of a recently discovered calculational error [A.163].) The small difference between the MÜLLER et al and MARINOV et al results could be accounted for by the absence of the relativistic

Coulomb singularity of Eq. (A.67) in the 100-term MÜLLER et al trial wavefunction [A.156].

A.3.4 Calculation of the Spontaneous Positron Production Rate

An exact calculation of spontaneous positron production by two colliding nuclei would be extremely difficult. The calculations which have been done for the two-center problem have employed a variety of approximations, which should be carefully considered. In general terms, the analytic analysis of POPOV and co-workers is based on two separated point nuclei where the combined Z is above the threshold $Z_{CR} \sim 170$ for positron production. An essential feature of the analysis of GREINER and co-workers is the assumption that the functional dependence of the decay width Γ on the positron energy E in the two-center problem is the same as the dependence in the one-center problem for a finite-size nucleus. A recent semi-classical calculation by JAKUBASSA and KLEBER [A.160] assumes that the width Γ for the two-body problem may be simulated by the width for a one-center atom with an effective nuclear charge $Z(R)$ which depends on the nuclear separation. The GREINER et al and JAKUBASSA et al analyses both depend on the nuclear size in the single-center problem which of course cannot accurately represent the effective size of the two-nucleus system.

In the work of POPOV and co-workers, as discussed in Section A.3.2, the positron production cross section is dependent on the imaginary part Γ of the energy of the level $E = E_0 + i\Gamma/2$ which for nuclear separation $R < R_{CR}$ is in the lower continuum. In principle the full complexity of the adiabatic two-center problem is required to determine E for the quasi-molecule. However, as shown by POPOV [A.133,146,149,151,153] E_0 and Γ depend, to a

6104708949

good approximation, only on R/R_{CR} , and their values can be found by matching the "inner" solution with the singularity given in Eq. (A.67) to the "outer" solution for the one-center problem: $V(\vec{r}) = -(Z_1 + Z_2)\alpha/r$. The result is the relation (valid for R_{CR} small compared to λ_e)

$$\ln \frac{R_{CR}}{R} = \psi\left(-\frac{E}{\lambda}\right) + \ln \frac{\lambda}{m} + \frac{m+E}{m+E+\lambda} \quad (\text{A.68})$$

where $\lambda = -i(E^2 - m^2)^{1/2}$ for $R < R_{CR}$ and $\psi(z)$ is the derivative of the logarithm of the gamma function. Equation (A.68) can then be solved numerically for the real and imaginary parts of E . These results are used for the calculation of the positron production cross section and spectrum given in Section A.3.2.

It is interesting to note that the solution to Eq. (A.68) gives a positive imaginary part to E , rather than the familiar position of the pole on the second sheet for a decaying state. This is due to the fact that we are dealing with the solutions of the Dirac equation in non-second-quantized form. The quasi-discrete level $E = E_0 + i\Gamma/2$ corresponds physically to a resonance for positron-scattering on a supercritical nucleus at the energy $E_{pos} = -E = |E_0| - i\Gamma/2$. This has the correct sign for the imaginary part [A.153].

An important feature of the solution of Eq. (A.68) is the dependence of the imaginary part of E near threshold:

$$\Gamma(v) \sim \gamma_0 \exp[-2\pi(Z_1 + Z_2)\alpha/v] \quad (\text{A.69})$$

where v is the positron velocity and $\gamma_0 \approx (6/5)\pi m$. This can also be written in terms of the internuclear distance [A.151]

$$\Gamma(R/R_{CR}) \sim \gamma_0 \exp[-b(1 - R/R_{CR})^{-1/2}] \quad (\text{A.70})$$

where $b \approx 5.7 (Z_1 + Z_2)\alpha$. Thus, the positron probability is exponentially small at threshold and increases rapidly with increasing $\eta = E/E_T$.

The threshold dependence of Γ is characteristic of problems involving the penetration of a Coulomb barrier. We can see the origin of the barrier by writing the equation for the large component $G(r) = rg(r)$ of the Dirac-Coulomb equation in the Schrödinger form [A.138,151]

$$\frac{1}{2m} \chi'' + [E_{eff} - U_{eff}(r)]\chi = 0 \quad (\text{A.71})$$

where $\chi = [m + E - V(r)]^{-1/2} G(r)$, $E_{eff} = \frac{1}{2}(E^2 - m^2)$, and U_{eff} (for a finite nuclear size) is shown in Fig. A.16 for $Z \sim Z_{CR}$ and $E \sim -m$. A striking feature of U_{eff} is its large distance behavior: $U_{eff}(r) = E/m V(r)$, i.e. it becomes a repulsive potential for $E < 0$. In the case of a Coulomb potential $V(r) = -Z\alpha/r$,

$$U_{eff}(r) \approx \frac{Z\alpha}{r} - \frac{(Z\alpha)^2 - 1}{2mr^2} \quad (\text{A.72})$$

for the 1S state at $E \sim -m$. At short distances, the relativistic attractive r^{-2} term dominates in U_{eff} . Note that U_{eff} has a maximum at $r = r_m = \lambda_e \times [(Z\alpha)^2 - 1]/Z\alpha$, where $U_{eff}(r_m) = \frac{1}{2}(Z\alpha)^2 m / ((Z\alpha)^2 - 1) \sim 1.4 m$ for $Z = 170$.

It is clear that for E just above $-m$ where $E_{eff} < 0$, the effective potential yields a localized discrete state with a radius of order r_m . The Schrödinger wavefunction attenuates at infinity in the form [A.138]

$$\chi(r) \sim r^{3/2} \exp[-\sqrt{8Z\alpha r/\lambda_e}] \quad (\text{A.73})$$

The radius of the localized ground state is shown in Fig. A.17. For $E_{eff} > 0$, i.e. when E dives into the lower continuum, the wavefunction extends beyond the barrier, and the width of the quasi-static level is given by the barrier penetrability [A.151,164]

$$\Gamma = \gamma_0 \exp[-2\pi(Z\alpha/v - \sqrt{(Z\alpha)^2 - 1})] \quad (\text{A.74})$$

where

$$\frac{\gamma_0}{m} = \frac{3(Z\alpha)^2(1 - e^{-2\pi v})}{[2(Z\alpha)^2 + 3]v} \rightarrow \begin{cases} 6\pi/5, & Z\alpha = 1 \\ 3/4(Z\alpha)^{-1}, & Z\alpha \gg 1. \end{cases} \quad (\text{A.75})$$

and $v = \sqrt{1 - m^2/E^2}$ is the velocity of the outgoing positron; and in Eq. (A.75) $v = 2\sqrt{(Z\alpha)^2 - 1}$. The simplest interpretation is that given in Section A.3.1: If $E < -m$, then the one electron state becomes degenerate with the two electron plus one positron state. The electron-positron pair is created near the nucleus where $V(r) > 2m$; the form of Eq. (A.74) reflects the probability that the positron can penetrate the barrier. Because Γ is small compared to m , the single particle analysis of the Dirac equation used to describe the supercritical atom can be justified [A.164].

One can now proceed to the calculation of the positron production probability by integrating over the classical ion trajectory, which is familiar from treatments by BATES and MASSEY [A.165] for autoionization in a slow collision and the level crossing formula of LANDAU and ZENER for the probability of near adiabatic transitions between discrete levels [A.166]. POPOV's result for the positron production cross section is [A.151]

$$\sigma = \frac{4\pi}{v_L} \int_{R_0}^{R_{cr}} dR R^{3/2} (R - R_0)^{1/2} \Gamma(R) \quad (\text{A.76})$$

where $\frac{1}{2}Mv_L^2$ is the lab kinetic energy of the incident nucleus and R_0 is the distance of closest approach at zero impact parameter. (If the probability $P = \sigma/\sigma_{geom}$ is not small, P should be replaced by $(1 - e^{-P})$.) The cross section for producing a positron with kinetic energy T is [A.151]

$$\frac{d\sigma}{dT} = \frac{4\pi}{v_L} \Gamma(R) R^{3/2} (R - R_0)^{1/2} \left(\frac{dE_0}{dR}\right)^{-1} \quad (\text{A.77})$$

where $T = |E_0(R/R_{cr})| - m$. Since Γ is small compared to $|E|$, the positron energy can be identified with a given internuclear distance R , and σ is correctly obtained by integrating over the complete ion orbit.

The calculation of GREINER and co-workers differs substantially in approach from that of POPOV et al. The first step is the computation of the width for positron production in a supercritical atom using the Fano autoionization method. The second step is to use these results to calculate the spontaneous and induced positron production rate, assuming that the relation between Γ and the bound state energy is the same in the one- and two-center problems.

The method used by GREINER and co-workers [A.145,158] to evaluate the positron width in the one-center problem is based on the analogy of the supercritical nucleus to that of autoionization in nuclear and atomic physics, where a bound state is imbedded in a continuum, and FANO's formalism [A.167] should be applicable. One begins by assuming that the nuclear potential is at criticality so that $|\phi_{cr}\rangle$, the single particle bound-state solution of the Dirac equation, has $E = -m$. Let $|\psi_E\rangle$ denote the s-wave negative-energy continuum solutions to the same equation with $E < -m$. If V is increased above criticality, $\Delta V = V - V_{cr} < 0$, then to first order in ΔV

$$\Delta E_{cr} = \langle \phi_{cr} | \Delta V | \phi_{cr} \rangle \quad (\text{A.78})$$

and

$$\Gamma = \tau_{pos}^{-1} = 2\pi |\langle \psi_E | \Delta V | \phi_{cr} \rangle|^2 \quad (\text{A.79})$$

Calculations [A.143] show that $\Delta E_{cr} \sim -30(Z_1 + Z_2 - Z_{cr})$ keV; see Fig. A.21.

0 0 0 0 4 7 0 8 9 5 0

Thus the bound state $|\phi_{\text{CR}}\rangle$ dives into the negative continuum with an energy shift roughly linear in $\Delta Z = Z_1 + Z_2 - Z_{\text{CR}}$ and a monotonically increasing width. If one defines the negative energy solutions $|\psi_E\rangle$ for the Dirac equation with $V_{\text{CR}} + \Delta V$, then

$$|\langle \psi_E | \phi_{\text{CR}} \rangle|^2 = \frac{1}{2\pi} \frac{\Gamma}{[E - (E_{\text{CR}} + \Delta E_{\text{CR}})]^2 + \Gamma^2/4} \quad (\text{A.80})$$

is the probability that the bound electron is promoted to $|\psi_E\rangle$ when ΔV is added adiabatically. (This Breit-Wigner form for the admixture probability neglects an extra energy shift from the energy variation of Γ .) This treatment thus far is, in principle, complementary to that given earlier in this section.

There may, however, be difficulties with using the autoionization method and a perturbation expansion near Z_{CR} for calculating the spontaneous decay width. In the papers of MÜLLER et al [A.134,145], the estimate

$$\Gamma = 2\pi |\langle \phi_{\text{CR}} | \Delta V | \psi_E \rangle|^2 \sim (\Delta Z)^2 50 \text{ eV} \quad (\text{A.81})$$

is reported to be a good approximation to the exact one-center Dirac equation width, at least for $\Delta Z = Z_1 + Z_2 - Z_{\text{CR}} \geq 3$. (For example, in the more recent work of K. SMITH et al [A.134,168] a curve is given showing numerical results based on a one-center Dirac equation calculation for the function $\gamma(T) = m\Gamma(T)/T^2$ where T is the positron kinetic energy. For $180 < Z < 210$, $R > 15$ fm, and $0.4 \text{ MeV} < T < 1.2 \text{ MeV}$, $\gamma(T)$ is roughly constant at 0.015, giving $4.7 < \Gamma(T) < 42$ keV which agrees within a factor of two with Eq. (A.81).) However, as noted by MÜLLER et al [A.145] and POPOV [A.153], the threshold behavior characteristic of the Coulomb barrier leads to strong exponential damping at zero positron momentum; for $\Delta Z \rightarrow 0$, POPOV [A.153] obtains $\Gamma \propto \exp[-b(Z_{\text{CR}}/\Delta Z)^{1/2}]$.

Thus, (A.81) should not be considered a reliable approximation for small ΔZ . The equation $\Gamma = 2\pi |\langle \phi_{\text{CR}} | \Delta V | \psi_E \rangle|^2$ is evidently invalid near threshold since it requires an expansion in ΔZ about the critical value. Furthermore, the continuum solution $|\psi_E\rangle$ which is defined to obey the Dirac equation for $V = V_{\text{CR}}$ does not see the Coulomb barrier in the effective potential U_{eff} appropriate to $V = V_{\text{CR}} + \Delta V$ and the level energy E_0 . (In the paper by POPOV and MUR [A.164], it is argued that $\Gamma/m \leq e^{-2\pi Z\alpha} \ll 1$ even for $|E_0| \gg m$ in a one-center problem because the barrier in U_{eff} increases in height as $E_0 \rightarrow \infty$. In fact, the width of the level can increase with $|E_0|$ despite the increasing barrier height because the tunneling distance becomes smaller [A.160]. This is also consistent with the barrier penetration formula (A.74) which gives $\Gamma \rightarrow \gamma_0 e^{-\pi/(Z\alpha)}$ in the limit $Z \rightarrow \infty$, $v \rightarrow 1$.)

The results of a recent one-center calculation of Γ by JAKUBASSA and KLEBER [A.160] (based on a semi-classical method) are shown in Fig. A.22. We have also indicated the values calculated from Eq. (A.81). The width computed by JAKUBASSA and KLEBER is about three times as large as that given by Eq. (A.81) at $Z \sim 200$.

It should be noted that the corresponding calculations of Γ/E_0 as a function of R/R_{CR} by POPOV [A.153] for the two-center problem yield much smaller widths, with $\Gamma/E_0 < 0.012$, i.e. an order of magnitude below those of the one-center problem results of JAKUBASSA and KLEBER. This may indicate that the one-center values, which are based on the nuclear size – and not on the actual nuclear separation – give an over-estimate of the decay width.

A.3.5 Induced Versus Adiabatic Pair Production

One of the controversial questions concerning positron production in heavy-ion collisions is the relative importance of pair production induced by the changing Coulomb field. In the review of ZELDOVICH and POPOV [A.138] and the later papers of POPOV [A.151,153], arguments are given that this mechanism can be neglected since (i) the frequency of collision ω_c (equal to the inverse of the collision time τ_c) is a small fraction of $2m$, and (ii) the characteristic electron time is much shorter than the collision time, so that the electron state can adiabatically adjust to the changing Coulomb potential. However, as emphasized in the papers by SMITH et al [A.154,168], the energy required for pair production during the collision is just the (narrow) gap between the 1S level and the negative continuum. Thus the changing Coulomb field can induce a transition (pair production) even at very low velocities. In typical inelastic atom-atom collisions, an appreciable cross section for transitions occurs when [A.169]

$$\Delta E \lesssim 2\pi \frac{v}{a} \quad (\text{A.82})$$

where v is the relative velocity and a is a length characteristic of the inducing potential. Taking $a \sim 50$ fm, $v \sim 0.05$, gives $\Delta E \sim 1$ MeV. Thus, induced pair production with a continuum positron could well be an important process even for collisions in which diving does not occur. In fact, SMITH et al [A.168] find that in typical U-U collisions, induced positron production is two orders of magnitude larger than the spontaneous cross section alone! Obviously, the induced contribution also will spread the kinetic energy spectrum of the positron, with substantial contributions occurring at kinetic energies ~ 1 MeV beyond the kinematic limit for spontaneous production.

The results of SMITH et al [A.168,170] compared with the spontaneous positron production spectrum calculated by PEITZ et al [A.158] are shown in Fig. A.23. The cross section calculated by SMITH et al for positron production in central U-U collisions at 812.5 MeV center-of-mass energy is shown in Fig. A.24. The curve denoted A is the contribution "during diving," i.e., integrated over the times when the 1S level joins the negative continuum. Curve B denotes the contribution before and after diving. The coherent sum is also shown. The Rutherford cross section for U-U scattering and the ionization probability L_0 have been divided out. By integrating over energy, one sees that roughly 5% of all the collisions with a 1S vacancy will produce a positron by the induced process. The positron production cross section for different CM kinetic energies is shown in Fig. A.25.

The during-diving positron production amplitude computed by SMITH et al [A.154,168] takes the form

$$C_D = i \int_{-t_{cr}}^{t_{cr}} dt V_E(t) \exp \left\{ \int_{-\infty}^t dt' [iE - iE_{1S}(t') - \frac{1}{2}\Gamma(t')] \right\} \quad (\text{A.83})$$

where E is the positron energy level, $\Gamma(t')$ gives the positron resonance width at time t' . The perturbing potential is taken to be

$$V_E(t) = \langle \psi_E | \Delta V(R(t)) | \phi_{cr} \rangle \quad (\text{A.84})$$

as in Section A.3.4.

As we have remarked in Section A.3.4, this expression for $V_E(t)$ and the definition $\Gamma = 2\pi |V_E(t)|^2$ are in apparent conflict with the analytic results of POPOV [A.153] for the resonance width near threshold. Hence, it is important that calculations of the induced process which avoid

15604708951

expansions in $\Delta V = V(R) - V(R_{CR})$ about the diving point be done.

Recently, JAKUBASSA and KLEBER [A.160] have also presented a method of evaluation of induced positron production in heavy-ion collisions within the WKB semi-classical approximation. Their results for both spontaneous and induced production are about ten times larger than those calculated by SMITH et al [A.168]. In particular, JAKUBASSA and KLEBER find a total cross section $\sigma = 4b$ for $v_L = 0.15$ and $\sigma = 1b$ for $v_L = 0.1$ in U-U collisions with $R_{CR} = 34$ fm.

It should be noted that so far all the calculations of the induced production rate are based on the single-center results for the widths and transition matrix elements.

We also note that the induced process may make positron production experimentally practical even for medium-Z heavy ion collisions. Diving is not critical. Further, induced pair production where both the positron and electron are in the continuum may be feasible in U-U collisions even without ionization. In fact, pair production requires not much more energy transfer than induced 1S hole production when the energy is near critical.

From a general point of view, induced and spontaneous positron production in heavy-ion collisions can be identified with the Feynman diagram shown in Fig. A.26. The physical process, however, goes beyond perturbation theory in that the production occurs as a result of the coherent energy of the Coulomb interaction in the strong field relativistic domain.

A.3.6 Vacancy Formation in Heavy-Ion Collisions

The physics of inner-shell vacancy formation is currently a subject of active experimental [A.124] and theoretical interest [A.171,172] and our discussion here can only be very brief. According to the extrapolation of BLASCHE, FRANKE and CH. SCHMELZER [A.173], completely ionized U atoms are possible at beam energies of order 300 MeV/nucleon (which should be achievable within the next five years at the LBL Bevalac). However, as we have seen, the optimum kinetic energy of the ion for the positron production experiments is in the few MeV/nucleon range. Ions with this kinetic energy could be achieved either by ion deceleration, or more ingeniously (as suggested by GREINER and CH. SCHMELZER [A.171]) by arranging low relative velocity collisions between colliding beams in storage rings, as in Fig. A.27. A similar configuration could be attained using the configuration of the CERN-ISR, with both ion beams circulating in the same direction.

At lower and more practical energies one must rely on the formation of the 1S vacancy of the combined quasi-molecule which occurs in the same atomic collision which produces the pair. (The lifetime of the vacancy is too short at high Z for collisions involving more than one target atom to be important [A.124].) For U-U collisions, estimates of the vacancy formation probability L_0 range from 0.2 for $E_{LAB} = 1600$ MeV [A.174] (using an "atomic" model in which the time variation of the Coulomb field causes energy to be transferred to the electron, which is ejected) to values between 10^{-4} to 10^{-6} depending on projectile energy [A.175,176] (using a "molecular" model in which the collision is assumed slow enough to allow the electrons to adjust themselves to the diatomic molecular levels; transitions caused by the varying Coulomb fields then produce vacancies).

However, very recently, BETZ, SOFF, MÜLLER, and GREINER [A.177] have performed an approximate calculation of the ground state vacancy production probability in U-U collisions. The vacancies are produced by the Coulomb field variation in the two-center Dirac equation. They find the vacancy production probability at 1600 MeV and zero impact parameter to be larger than 0.08 - much larger than was anticipated and very encouraging for the experiments discussed here.

Since 1S state vacancy production followed by positron production in a single collision will be accompanied by direct pair production associated with the time variation of the fields in the collision, and the latter process may have an amplitude of comparable magnitude, the cross section for $\text{atom} + \text{atom} \rightarrow \text{atom} + \text{atom} + e^- + e^+$ should be calculated from the coherent sum of both processes. In fact, all processes which produce a pair must, of course, be considered together. This includes summation over pair production processes which fill higher n vacancies. Although pair production which fills higher n vacancies may be less likely, there could be a partial compensation due to a larger probability of vacancy formation in higher n states. The relative importance of these processes has not yet been estimated for the case of collisions between neutral atoms.

A.3.7 Nuclear Excitation and Other Background Effects

There are general background effects which can complicate the experimental observation of positron production associated with the overcritical Coulomb field. We will closely follow the discussion of POPOV [A.151], OKUN [A.178], and OBERACKER et al [A.179,180] here.

When heavy particles collide, e^+e^- pairs can be produced by hard photon

bremsstrahlung and pair conversion. The cross section is small [A.151,178] because the motion of the nuclei is non-relativistic. A typical cross section for $Z = 92$, $R_0 = 40$ fm is $\sigma < 10^{-16}$ b. For identical nuclei U-U, this is suppressed by a few more orders of magnitude since the cross section for dipole radiation, proportional to $(Z_1 A_2 - Z_2 A_1)^2$, vanishes [A.151].

The most important background is the production of e^+e^- pairs by pair conversion in transitions resulting from Coulomb excitation of nuclei. An estimate given by POPOV [A.153] for U-U collisions gives $\sigma_C^{e^+e^-} \sim 10^{-4}$ b which is somewhat smaller than the estimates for the cross section for spontaneous positron production.

Extensive calculations of the nuclear and Coulomb excitation cross sections have been recently performed by OBERACKER et al [A.179,180]. The calculated differential cross section (dashed lines) for $^{238}\text{U} - ^{238}\text{U}$ collisions at the Coulomb barrier $E_{\text{cm}}^{\text{kin}} = 800$ MeV, as a function of the ion scattering angle θ_{ion} , is shown in Fig. A.28. The two dashed lines correspond to two different models for the nuclear states. The associated cross section, calculated by PEITZ (quoted in Refs. [A.179] and [A.180]), via spontaneous and induced decay (assuming $R_{\text{CT}} = 35$ fm, and the K-vacancy probability $L_0 = 10^{-2}$) is given by the solid line. Representative total nuclear and Coulomb excitation production cross sections calculated by OBERACKER et al [A.179,180] for U-U collisions range from $\sigma_C^{e^+e^-} \sim 1.25 \times 10^{-4}$ b to $\sigma_C^{e^+e^-} \sim 2.28 \times 10^{-4}$ b depending on the model for the nuclear states. This is in good agreement with the estimate of POPOV. As noted by OBERACKER et al, the nuclear background is suppressed in the backward and forward directions for symmetric systems $^{238}\text{U} - ^{238}\text{U}$. In addition, the nuclear positron spectrum terminates at $E_p \sim 800$ keV while the induced positron spectrum extends to much higher energies. Both of these characteristics should aid in separating

00004708952

out the background positrons. More complicated, but negligible backgrounds, involving conversion of gamma rays from nuclear transitions where the electron occupies the vacant ground state are also estimated by OBERACKER et al.

A.3.8 Radiative Corrections in Critical Fields

There is considerable theoretical interest in the question of whether radiative corrections could modify or even eliminate the predictions discussed here for pair production at $Z > Z_{CR}$. As we have noted in Section A.3.1, the radiative corrections are controlled by α rather than $Z\alpha$ so they are, in principle, independently controllable in their physical effects, and thus one would not expect dramatic changes in the previous description. One also would not expect that calculations based on a Feynman diagram treatment indicated by Fig. A.26, could be much affected by effects of order α . However, since virtual pairs may be produced with an arbitrarily small expenditure of energy as $Z \rightarrow Z_{CR}$, the smallness of α is not necessarily decisive. In the following, the tractable model of a single nucleus of charge Z is examined. The results for a heavy-ion collision are expected to be qualitatively similar.

The situation is well understood in the case of the order α vacuum polarization corrections; the modifications turn out to be small. For r at the maximum of the near-critical 1S probability distribution, $r_0 \sim 0.1 \lambda_e$, the Coulomb Uehling potential has the value

$$V_{11}(r_0) = -\frac{2\alpha}{3\pi} \frac{Z\alpha}{r_0} \left(\ln \frac{\lambda_e}{r_0} - \gamma - \frac{5}{6} + \dots \right) \approx -9 \text{ keV} \quad (\text{A.85})$$

Calculation of the 1S Uehling energy shift at $Z \approx Z_{CR}$ by SOFF, MÜLLER, and

RAFELSKI [A.181] gives $\Delta E = -11.8 \text{ keV}$ for $Z=171$, in good agreement with an extrapolation of the results, for $Z < 160$, of PIEPER and GREINER [A.117] and with the order-of-magnitude estimate in Eq. (A.85). The corresponding shift ΔZ_{CR} in Z_{CR} is found, with the aid of [A.47,144,145]

$$\left. \frac{dE_{1S}}{dZ} \right|_{Z_{CR}} = -27 \text{ keV} \quad (\text{A.86})$$

to be $\Delta Z_{CR} = -0.4$, i.e., the critical charge is reduced by less than one unit. The result of POPOV [A.133], $\Delta Z_{CR} = 0(10^{-3})$, appears to be an underestimate.

The higher order correction to the Uehling potential of the Wichmann-Kroll type (from the Coulomb interactions of the electron-positron pair) is an order of magnitude smaller. Arguments of POPOV [A.133] and of MÜLLER, RAFELSKI, and GREINER [A.144,145] suggest that the higher order corrections are small. A calculation has been done by GYULASSY [A.47,48] who found $\Delta E_{1S} = 1.2 \text{ keV}$ which is negligible compared to the Uehling term. GYULASSY [A.47] has also shown numerically that the vacuum polarization charge density associated with the charged vacuum, discussed by FULCHER and KLEIN [A.136], varies smoothly as Z passes through Z_{CR} . The vacuum polarization associated with the charged vacuum is formally related to the ordinary vacuum polarization by a shift in the contour of integration in the bound electron propagator as discussed in Section A.1.5 [A.47].

In the case of the self-energy corrections to the electron level, a simple heuristic argument is that a fraction α of the lepton charge is spread out over a Compton radius of the electron λ_e (modulo a logarithmic tail out to the Bohr radius $(Z\alpha m)^{-1}$ associated with the Bethe sum). Such a distribu-

tion convoluted with the nuclear size distribution could only change Z_{CR} by a small amount. Also, since the determination of the nuclear radius R derives from electron scattering experiments, the influence of radiative corrections is already partially included. The situation for the self-energy is more obscure at very high Z where higher order terms in $Z\alpha$ are important; quantitative calculation is necessary.

Results of calculations of the self-energy of the 1S state for large Z are shown in Fig. A.29. The self-energy for a Coulomb potential appears to become infinite as $Z\alpha \rightarrow 1$. This is clearly an anomaly due to the point charge singularity. CHENG and JOHNSON [A.36] have extended calculations to $Z = 160$ for a finite nucleus. By extrapolation, they find that the 1S self-energy is at least 1% of the binding energy at $Z = Z_{CR}$. Although it seems unlikely, we note that if the self-energy were to increase sufficiently rapidly as $Z \rightarrow Z_{CR}$, there might be no diving phenomenon, and further analysis would be necessary. In any case, induced positron production would still be possible (see Section A.3.5).

Calculation of radiative corrections to the positron emission rate would be very complicated, because the self-energy graph will include the long range radiative correction associated with the outgoing charged particle. The effect of photon emission would have to be separated from the energy shift.

A.3.9 Coherent Production of Photons in Heavy-Ion Collisions

Another intriguing, possibly feasible test of strong field electrodynamics utilizing high- Z ion collisions is single or multiple hard photon production. The quantum electrodynamic process is a variation of Delbrück, or light-by-light scattering (see Fig. A.30). The photons are created by the coherent

energy of the ions' Coulomb field. Unlike bremsstrahlung processes, the spectrum of the photon peaks in the electron mass (MeV) range. The production cross section for n photons should be of order α^n times the Rutherford cross section for collisions in which the potential energy at the distances of closest approach significantly exceeds the total photon energy. Such photons should be distinguishable from nuclear excitation photons and combined-atom x-rays by their (calculable) spectrum and angular distribution, and by coincidence (correlation) measurements.

Note that this photon production process occurs at ion energies and charges well below those required for spontaneous pair production. Conversely, if the photons have energies beyond 1 MeV, they provide a background for positron production from internal pair conversion, or by conversion in a nearby atom.

A.3.10 Self-Neutralization of Matter

The possibility of spontaneous pair production at high Coulomb field strength leads to a rather novel self-neutralization mechanism of ionized matter. Suppose that one could arrange a contained plasma of completely stripped uranium ions (no electrons present). For any finite temperature there will occasionally be ion-ion collisions at sufficient velocity such that the distance of closest approach is less than $R_{CR} \sim 35$ fm, where diving of the lowest electronic level of the two-center Dirac system begins. Eventually, all the bound electron atomic levels which dive will be filled by the pair production process and – assuming the continuum positrons are allowed to escape – the ionic system will be partially neutralized. Although the process can occur in principle at any finite temperature via the Maxwell

396907000000

velocity distribution, the positron production probability becomes large only at high temperatures, $kT \sim 0(1 \text{ GeV})$, i.e., $T \sim 0(10^{13} \text{ K})$. At still higher temperatures, other pair production mechanisms become important; however, the spontaneous pair production is the lowest energy mechanism.

A.3.11 Very Strong Magnetic Field Effects

RAFELSKI and MÜLLER [A.182] have suggested looking at heavy-ion collisions as a means of testing the behavior of matter in strong magnetic fields. Such tests would be sensitive to possible anomalous higher order effects of strong fields. In a heavy-ion collision, the magnetic fields are produced by the motion of the charged nuclei, with the corresponding vector potential given by

$$e\vec{A}(\vec{r}) = -Z\alpha \frac{\vec{V}_1}{|\vec{r} - \vec{R}_1|} - Z\alpha \frac{\vec{V}_2}{|\vec{r} - \vec{R}_2|} \quad (\text{A.87})$$

where \vec{V}_i are the nuclear velocities and \vec{R}_i are the position vectors of the nuclei. In a sub-Coulomb barrier heavy-ion collision, the magnetic field created in the vicinity of the colliding nuclei is of the order of 10^{14} gauss over a small volume [A.182]. The magnetic fields give rise to a splitting of the lowest quasi-molecular states through interaction with the electron spin. RAFELSKI and MÜLLER have calculated the magnetic splitting which can be expected in various heavy-ion collisions. Figure A.31 shows the energy separation of the spin-up and spin-down states relative to the binding energy for various systems. For example, the separation of the $1s\sigma$ state in a U-U collision with $T = 9 \text{ MeV/nucleon}$ and impact parameter $b = 20 \text{ fm}$ is calculated to be approximately $0.1 \text{ m} = 50 \text{ keV}$. This splitting corresponds to an average magnetic field $\bar{B} \sim 4 \times 10^{12}$ gauss. The magnetic splitting results in a difference of 3.3 fm in R_{Cr} for the two states.

We note that any model for strong magnetic field anomalies which could be evident in heavy-ion collisions would be constrained by existing fine structure measurements in exotic atoms. The determination of the magnetic moment of the anti-proton to 1% accuracy by the fine-structure measurement in $\bar{p}\text{Pb}$ by HU et al [A.183] has yielded a value which is in excellent agreement with the proton magnetic moment (in accord with the TCP theorem). The fine structure in the lower level ($n=10, \ell=9$) in that experiment arises from interaction of the anti-proton moment with an average magnetic field of order 10^{14} gauss. A similar test in somewhat stronger magnetic fields is made by muonic atoms. The measured fine structure splitting in the $2P$ state of muonic lead [A.184] agrees with theory, and the average magnetic field seen by the muon is of order 10^{16} gauss.

CONCLUSION

All of the tests of high- $Z\alpha$ quantum electrodynamics which we have discussed in this review probe in various ways the Furry bound state interaction picture description of the bound leptons. In the strong field domain where $Z\alpha$ is not small, a natural question is whether this generalization of weak field perturbation theory continues to be applicable if the binding strength is not small compared to the mass of the bound particle.

Thus far the tests of high field strength QED involving the spectra of bound electrons and muons are in extraordinary agreement with predictions, ruling out anomalous non-linear interactions, low-mass scalar particles with certain couplings; and anomalous modifications of vacuum polarization at momentum transfers $\sim Z\alpha m_\mu$. The high- $Z\alpha$ spectra also test electromagnetic interactions in the strong magnetic field regime, where the effective fields reach 10^{16} gauss. Tests of relativistic bremsstrahlung in high magnetic fields are reviewed in Ref. [A.185]. Further tests of the Furry picture of bound leptons and their radiative corrections are possible by measurements of the bound state gyromagnetic ratio via Zeeman interactions and by photon scattering from high- Z atoms. The Lamb shift measurements in heavy atoms confirm the calculations of radiative corrections for highly off-shell electrons. The measurements in high- Z few-electron ions provide a means of testing QED in strong fields with multiparticle systems for which the theory is still tractable. Precision measurements in muonic atoms are now beginning to confirm higher order vacuum polarization corrections of order $\alpha(Z\alpha)^3$, ruling out broad classes of anomalous muon-nuclear interactions [A.186].

Although the basic predictions for positron production in heavy-ion collisions appear to be understood from a fundamental point of view, there

are many quantitative questions which have not been completely settled. As we have noted, it is difficult to compare details of results based on different calculations because of the wide range of models employed. This is particularly critical in the questions concerning the absolute magnitude of both the spontaneous and induced positron production rates.

The dynamical tests of high- $Z\alpha$ QED, especially positron production (and possibly anomalous photon production) in heavy-ion collisions, are particularly interesting because they require an extension of the theory to a domain which is otherwise unexplored. For example, when the binding becomes critical, the ordinary vacuum is effectively unstable, and a new vacuum reference state is required.

There are many issues of fundamental interest which still need to be resolved. These include a complete field theoretic treatment of the positron production problem which considers the effects of radiative corrections; the problem of the Klein-Gordon equation for $Z\alpha > 1$, where Bose condensation can occur [A.138,187]; and the nature of positronium when $\alpha > 1$, and in particular, whether there is a mechanism (possibly recoil corrections) which can moderate the singular Coulomb problem.

0000470854

ACKNOWLEDGMENTS

We are grateful to R. Anholt, L. Madansky, J. Mandula, M. Marinov, R. Marrus, W. Meyerhof, and M. Weinstein for helpful conversations.

This work was supported in part by the U.S. Energy Research and Development Administration.

REFERENCES

- A.1. R. Hofstadter in Proceedings of the 1975 International Symposium on Lepton and Photon Interactions at High Energies, W. T. Kirk, ed. (SLAC, Stanford, 1975), p. 869.
- A.2. P. Papatzacos and K. Mork, Phys. Reports 21, 81 (1975).
- A.3. K. Wilson, Cornell preprint CLNS 356, 1977.
- A.4. J. Mandula, MIT preprint, 1976.
- A.5. H. Gould and R. Marrus, reported at the 5th International Conference on Atomic Physics, Berkeley, July 1976, and private communication.
- A.6. S. J. Brodsky and S. D. Drell, Ann. Rev. Nucl. Sci., 20, 147 (1970).
- A.7. B. E. Lautrup, A. Peterman, and E. de Rafael, Phys. Reports 3, 193 (1972). This paper gives complete references to the original work.
- A.8. G. W. Erickson, Phys. Rev. Letters 27, 780 (1971).
- A.9. G. W. Erickson, U. C. Davis preprint (1976).
- A.10. P. J. Mohr, Phys. Rev. Letters 34, 1050 (1975).
- A.11. P. J. Mohr, Ann. Phys. (N.Y.) 88, 26, 52 (1974).
- A.12. E. H. Wichmann and N. M. Kroll, Phys. Rev. 96, 232 (1954); 101, 843 (1956).
- A.13. W. H. Furry, Phys. Rev. 51, 125 (1937).
- A.14. R. Serber, Phys. Rev. 48, 49 (1935).
- A.15. E. A. Uehling, Phys. Rev. 48, 55 (1935).
- A.16. P. J. Mohr in Beam-Foil Spectroscopy, I. A. Sellin and D. J. Pegg, eds. (Plenum Press, New York, 1976), p. 89.

A.17. T. Appelquist and S. J. Brodsky, Phys. Rev. Letters 24, 562 (1970); Phys. Rev. A 2, 2293 (1970).

A.18. M. Leventhal, Phys. Rev. A 11, 427 (1975).

A.19. D. Dietrich, P. Lebow, R. deZafra, and H. Metcalf, Bull. Am. Phys. Soc. 21, 625 (1976).

A.20. C.Y. Fan, M. Garcia-Munoz, and I. A. Sellin, Phys. Rev. 161, 6 (1967).

A.21. H. W. Kugel, M. Leventhal, and D.E. Murnick, Phys. Rev. A 6, 1306 (1972).

A.22. G. P. Lawrence, C.Y. Fan, and S. Bashkin, Phys. Rev. Letters 28, 1612 (1972).

A.23. M. Leventhal, D. E. Murnick, and H. W. Kugel, Phys. Rev. Letters 28, 1609 (1972).

A.24. H. W. Kugel, M. Leventhal, D. E. Murnick, C. K. N. Patel, and O. R. Wood, II, Phys. Rev. Letters 35, 647 (1975).

A.25. R. Marrus in Beam-Foil Spectroscopy, S. Bashkin, ed. (Springer-Verlag, Berlin, 1976), p. 209.

A.26. Quantum Mechanics of One- and Two-Electron Atoms, H. A. Bethe and E. E. Salpeter (Springer-Verlag, Berlin, 1957).

A.27. W. A. Davis and R. Marrus, Phys. Rev. A, to be published.

A.28. H. Gould and R. Marrus in Beam-Foil Spectroscopy, I. A. Sellin and D. J. Pegg, eds. (Plenum Press, New York, 1976), p. 305.

A.29. H. Gould, R. Marrus, and P. J. Mohr, Phys. Rev. Letters 33, 676 (1974).

A.30. J. A. Bearden and A. F. Burr, Rev. Mod. Phys. 39, 125 (1967); Atomic Energy Levels (U.S. Atomic Energy Commission, Oak Ridge, 1965).

A.31. A. M. Desiderio and W. R. Johnson, Phys. Rev. A 3, 1267 (1971).

A.32. J. B. Mann and W. R. Johnson, Phys. Rev. A 4, 41 (1971).

A.33. M.S. Freedman, F. T. Porter, and J. B. Mann, Phys. Rev. Letters 28, 711 (1972).

A.34. B. Fricke, J. P. Desclaux, and J.T. Waber, Phys. Rev. Letters 28, 714 (1972).

A.35. F. T. Porter and M. S. Freedman, Phys. Rev. Letters 27, 293 (1971).

A.36. K. T. Cheng and W.R. Johnson, Phys. Rev. A 14, 1943 (1976).

A.37. K. Huang, M. Aoyagi, M. H. Chen, B. Crasemann, and H. Mark, At. Data and Nucl. Data Tables 18, 243 (1976).

A.38. M. Born and L. Infeld, Proc. Roy. Soc. (London) A 144, 425 (1934).

A.39. M. Born, Ann. Inst. Henri Poincaré 7, 155 (1937).

A.40. J. Rafelski, L. P. Fulcher, and W. Greiner, Phys. Rev. Letters 27, 958 (1971).

A.41. G. Soff, J. Rafelski, and W. Greiner, Phys. Rev. A 7, 903 (1973).

A.42. G.E. Brown and G.W. Schaefer, Proc. Roy. Soc. (London) A 233, 527 (1956).

A.43. J. Arafune, Phys. Rev. Letters 32, 560 (1974).

A.44. L. S. Brown, R.N. Cahn, and L. D. McLerran, Phys. Rev. Letters 32, 562 (1974).

A.45. L.S. Brown, R. N. Cahn, and L. D. McLerran, Phys. Rev. D 12, 609 (1975).

A.46. M. Gyulassy, Phys. Rev. Letters 32, 1393 (1974).

A.47. M. Gyulassy, Phys. Rev. Letters 33, 921 (1974).

A.48. M. Gyulassy, Nucl. Phys. A244, 497 (1975).

559704000

- A.49. L.S. Brown, R. N. Cahn, and L. D. McLerran, Phys. Rev. D 12, 581 (1975).
- A.50. L.S. Brown, R.N. Cahn, and L.D. McLerran, Phys. Rev. D 12, 596 (1975).
- A.51. G.E. Brown, J.S. Langer, and G. W. Schaefer, Proc. Roy. Soc. (London) A 251, 92 (1959).
- A.52. C.S. Wu and L. Wilets, Ann. Rev. Nucl. Sci. 19, 527 (1969).
- A.53. S. Koslov, V. Fitch, and J. Rainwater, Phys. Rev. 95, 291 (1954).
- A.54. G. Backenstoss, S. Charalambus, H. Daniel, Ch. Von der Malsburg, G. Poelz, H. P. Povel, H. Schmitt and L. Tauscher, Phys. Letters 31B, 233 (1970).
- A.55. M.S. Dixit, H. L. Anderson, C.K. Hargrove, R.J. McKee, D. Kessler, H. Mes, and A.C. Thompson, Phys. Rev. Letters 27, 878 (1971).
- A.56. H.K. Walter, J. H. Vuilleumier, H. Backe, F. Boehm, R. Engfer, A. H. v. Gunten, R. Link, R. Michaelsen, G. Petitjean, L. Schellenberg, H. Schneuwly, W. U. Schröder, and A. Zehnder, Phys. Letters 40B, 197 (1972).
- A.57. L. Tauscher, G. Backenstoss, K. Fransson, H. Koch, A. Nilsson, and J. De Raedt, Phys. Rev. Letters 35, 410 (1975).
- A.58. M. S. Dixit, A. L. Carter, E. P. Hincks, D. Kessler, J. S. Wadden, C. K. Hargrove, R. J. McKee, H. Mes, and H. L. Anderson, Phys. Rev. Letters 35, 1633 (1975).
- A.59. J.L. Vuilleumier, W. Dey, R. Engfer, H. Schneuwly, H. K. Walter, and A. Zehnder, Z. Physik A 278, 109 (1976).
- A.60. S. R. Lundeen and F. M. Pipkin, Phys. Rev. Letters 34, 1368 (1975).

- A.61. D.A. Andrews and G. Newton, Phys. Rev. Letters 37, 1254 (1976).
- A.62. J. Schwinger, Phys. Rev. 82, 664 (1951).
- A.63. W. Pauli and F. Villars, Rev. Mod. Phys. 21, 434 (1949).
- A.64. R.C. Barrett, S. J. Brodsky, G. W. Erickson, and M. H. Goldhaber, Phys. Rev. 166, 1589 (1968).
- A.65. J. Blomqvist, Nucl. Phys. B48, 95 (1972).
- A.66. K. Huang, Phys. Rev. A 14, 1311 (1976).
- A.67. P. Vogel, At. Data and Nucl. Data Tables 14, 599 (1974).
- A.68. T. L. Bell, Phys. Rev. A 7, 1480 (1973).
- A.69. M.K. Sundaresan and P. J. S. Watson, Phys. Rev. Letters 29, 15 (1972).
- A.70. B. Fricke, Z. Physik 218, 495 (1969).
- A.71. L. S. Brown, R. N. Cahn, and L. D. McLerran, Phys. Rev. Letters 33, 1591 (1974).
- A.72. G. A. Rinker, Jr. and L. Wilets, Phys. Rev. Letters 31, 1559 (1973).
- A.73. G.A. Rinker, Jr. and L. Wilets, Phys. Rev. A 12 748 (1975).
- A.74. G. Källén and A. Sabry, Dan. Mat. Fys. Medd. 29, #17 (1955).
- A.75. L. W. Fullerton and G.A. Rinker, Jr., Phys. Rev. A 13, 1283 (1976).
- A.76. H.A. Bethe and J. W. Negele, Nucl. Phys. A117, 575 (1968).
- A.77. S. Klarsfeld and A. Maquet, Phys. Letters 43B, 201 (1973).
- A.78. M. Chen, Phys. Rev. Letters 34, 341 (1975).
- A.79. L. Wilets and G. A. Rinker, Jr., Phys. Rev. Letters 34, 339 (1975).
- A.80. D. H. Fujimoto, Phys. Rev. Letters 35, 341 (1975).
- A.81. E. Borie, Bull. Am. Phys. Soc. 21, 625 (1976).
- A.82. M.K. Sundaresan and P.J.S. Watson, Phys. Rev. D 11, 230 (1975).
- A.83. S. L. Adler, Phys. Rev. D 10, 3714 (1974).
- A.84. E. Borie, Helvetica Physica Acta 48, 671 (1975).

A.85. H. Grotch and D. R. Yennie, *Rev. Mod. Phys.* 41, 350 (1969).

A.86. R. K. Cole, Jr., *Phys. Letters* 25B, 178 (1967).

A.87. T.E.O. Ericson and J. Hüfner, *Nucl. Phys.* B47, 205 (1972).

A.88. R.R. Harvey, J. T. Caldwell, R. L. Bramblett, S.C. Fultz, *Phys. Rev.* 136, B126 (1964).

A.89. P. Vogel, *Phys. Rev. A* 7, 63 (1973).

A.90. B. Fricke, *Lett. Nuovo Cim.* 2, 859 (1969).

A.91. H.L. Anderson, *Proc. of the 3rd Int. Conf. on High Energy Physics and Nuclear Structure*, New York, September 1969, ed. S. Devons (Plenum Press, New York, 1970) p. 640.

A.92. J. B. Mann and G.A. Rinker, Jr., *Phys. Rev. A* 11, 385 (1975).

A.93. J. Rafelski, B. Müller, G. Soff, and W. Greiner, *Ann. Phys. (N.Y.)* 88, 419 (1974).

A.94. P. Vogel, *Phys. Rev. A* 8, 2292 (1973).

A.95. D. E. Casperson, T. W. Crane, V. W. Hughes, P. A. Souder, R. D. Stambaugh, P. A. Thompson, H. Orth, G. zu Putlitz, H. F. Kaspar, H. W. Reist, and A. B. Denison, *Phys. Letters* 59B, 397 (1975).

A.96. E. R. Cohen and B. N. Taylor, *J. Phys. Chem. Ref. Data*, 2, 663 (1973).

A.97. K. M. Crowe, J. F. Hague, J. E. Rothberg, A. Schenck, D. L. Williams, R. W. Williams, and K. K. Young, *Phys. Rev. D* 5, 2145 (1972).

A.98. P.J.S. Watson and M.K. Sundareshan, *Can. J. Phys.* 52, 2037 (1974).

A.99. R. D. Deslattes, E. G. Kessler, W. C. Sauder, and A. Henins in *Atomic Masses and Fundamental Constants 5*, J. H. Sanders and A. H. Wapstra, eds. (Plenum Press, New York, 1976), p. 48.

A.100. A. Bertin, G. Carboni, J. Duclos, U. Gastaldi, G. Corini, G. Neri, J. Picard, O. Pitzurra, A. Placchi, E. Polacco, G. Torelli, A. Vitale, and E. Zavattini, *Phys. Letters* 55B, 411 (1975); *Nuovo Cim.* 34, 493 (1976).

A.101. E. Borie, *Z. Physik A* 275, 347 (1975).

A.102. G. A. Rinker, *Phys. Rev. A* 14, 18 (1976).

A.103. E. Campani, *Lett. Nuovo Cim.* 4, 982 (1970).

A.104. J. L. Friar and J. W. Negle, *Phys. Letters* 46B, 5 (1973).

A.105. J. Bernabéu and C. Jarlskog, *Nucl. Phys.* B75, 59 (1974).

A.106. E. M. Henley, F.R. Krejs, and L. Willets, *Nucl. Phys.* A256, 349 (1976).

A.107. C. Joachain, *Nucl. Phys.* 25, 317 (1961).

A.108. J. Bernabéu and C. Jarlskog, *Phys. Letters* 60B, 197 (1976).

A.109. S. L. Adler, R. F. Dashen, and S. B. Treiman, *Phys. Rev. D* 10, 3728 (1974).

A.110. R. Barbieri, *Phys. Letters* 56B, 266 (1975).

A.111. J. Bailey, K. Borer, F. Combley, H. Drumm, C. Eck, F.J.M. Farley, J. H. Field, W. Flegel, P.M. Hattersley, F. Krienen, F. Lange G. Petrucci, E. Picasso, H. I. Pizer, O. Runolfsson, R. W. Williams, and S. Wojcicki, *Phys. Lett.* 55B, 420 (1975).

A.112. M. A. Samuel and C. Chlouber, *Phys. Rev. Letters* 36, 442 (1976).

A.113. R. Jackiw and S. Weinberg, *Phys. Rev. D* 5, 2396 (1972).

A.114. L. Resnick, M. K. Sundareshan, and P.J.S. Watson, *Phys. Rev. D* 8, 172 (1973).

A.115. D. Kohler, B. A. Watson, and J. A. Becker, *Phys. Rev. Letters* 33, 1628 (1974).

A.116. R. Barbieri and T.E.O. Ericson, *Phys. Letters* 57B, 270 (1975).

09104708956

- A.117. W. Pieper and W. Greiner, *Z. Physik* 218, 327 (1969).
- A.118. S.S. Gershtein and Ya. B. Zel'dovich, *Lett. Nuovo Cim.* 1, 835 (1969).
- A.119. S.S. Gershtein and Ya. B. Zel'dovich, *Zh. Eksp. Teor. Fiz.* 57, 654 (1969); [*Sov. Phys. JETP* 30, 358 (1970)].
- A.120. W. Heisenberg and H. Euler, *Z. Physik* 98, 714 (1936); V. Weisskopf, *Kgl. Danske, Videnskab. Selskab, Mat. Fys. Medd.* 14, #6 (1936).
- A.121. R. Dashen in Proceedings of the 1975 International Symposium on Lepton and Photon Interactions at High Energies, W. T. Kirk, ed. (SLAC, Stanford, 1975), p. 981.
- A.122. H. Harari, op. cit., p. 317.
- A.123. Møller and Folkmann, this volume.
- A.124. W. E. Meyerhof, *Science* 193, 839 (1976).
- A.125. K. M. Case, *Phys. Rev.* 80, 797 (1950).
- A.126. A. M. Perelomov and V. S. Popov, *Teor. Mat. Fiz.* 4, 48 (1970); [*Theor. Math. Phys.* 4, 664 (1970)].
- A.127. C. Schwartz, *J. Math. Phys.* 17, 863 (1976).
- A.128. L. I. Schiff, H. Snyder and J. Weinberg, *Phys. Rev.* 57, 315 (1940).
- A.129. I. Pomeranchuk and J. Smorodinsky, *J. Phys. (USSR)* 9, 97 (1945).
- A.130. F. G. Werner and J. A. Wheeler, *Phys. Rev.* 109, 126 (1958).
- A.131. D. Rein, *Z. Physik* 221, 423 (1969).
- A.132. V. S. Popov, *Zh. ETF Pis. Red.* 11, 254 (1970); [*JETP Lett.* 11, 162 (1970)].
- A.133. V. S. Popov, *Yad. Fiz.* 12, 429 (1970); [*Sov. J. Nucl. Phys.* 12, 235 (1971)].
- A.134. B. Müller, R. K. Smith, and W. Greiner in Atomic Physics 4, G. zu Putlitz, E. W. Weber, and A. Winnacker, eds. (Plenum Press, New York, 1975), p.209.
- A.135. S. J. Brodsky, *Comments Atom. Mol. Phys.* 4, 109 (1973).
- A.136. L. Fulcher and A. Klein, *Phys. Rev. D* 8, 2455 (1973).

- A.137. J. S. Greenberg, C. K. Davis, B. Müller, and W. Greiner in Proceedings of the International Conference on Reactions Between Complex Nuclei, Vol. 2, R. L. Robinson, ed., June 1974, at Nashville, Tennessee (American Elsevier Publ. Co., New York, 1974), p. 67.
- A.138. Ya. B. Zel'dovich and V. S. Popov, *Usp. Fiz. Nauk.* 105, 403 (1971); [*Sov. Phys. Usp.* 14, 673 (1972)].
- A.139. J. Rafelski, B. Müller, and W. Greiner, *Nucl. Phys.* B68, 585 (1974).
- A.140. V. S. Popov, *Zh. Eksp. Teor. Fiz.* 59, 965 (1970); [*Sov. Phys. JETP* 32, 526 (1971)].
- A.141. L. P. Fulcher and W. Greiner, *Lett. Nuovo Cim.* 2, 279 (1971).
- A.142. P. G. Reinhard, W. Greiner, and H. Arenhövel, *Nucl. Phys.* A166, 173 (1971).
- A.143. B. Müller, H. Peitz, J. Rafelski, and W. Greiner, *Phys. Rev. Letters* 28, 1235 (1972).
- A.144. B. Müller, J. Rafelski and W. Greiner, *Z. Physik.* 257, 62 (1972).
- A.145. B. Müller, J. Rafelski and W. Greiner, *Z. Physik.* 257, 183 (1972).
- A.146. V. S. Popov, *Yad. Fiz.* 14, 458 (1971); [*Sov. J. Nucl. Phys.* 14, 257 (1972)].
- A.147. V. S. Popov, *Yad. Fiz.* 15, 1069 (1972); [*Sov. J. Nucl. Phys.* 15, 595 (1972)].
- A.148. V. S. Popov, *Zh. ETF Pis. Red.* 16, 355 (1972); [*JETP Lett.* 16, 251 (1972)].
- A.149. V. S. Popov, *Yad. Fiz.* 17, 621 (1973); [*Sov. J. Nucl. Phys.* 17, 322 (1973)].
- A.150. J. Rafelski, W. Greiner, and L. P. Fulcher, *Nuovo Cim.* 13B, 135 (1973).
- A.151. V. S. Popov, *Zh. Eksp. Teor. Fiz.* 65, 35 (1973); [*Sov. Phys. JETP* 38, 18 (1974)].

- A.152. B. Müller, J. Rafelski and W. Greiner, *Nuovo Cim.* 18A, 551 (1975).
- A.153. V. S. Popov, *Yad. Fiz.* 19, 155 (1974); [*Sov. J. Nucl. Phys.* 19, 81 (1974)].
- A.154. K. Smith, B. Müller and W. Greiner, *J. Phys. B* 8, 75 (1975).
- A.155. S. S. Gershtein and V. S. Popov, *Lett. Nuovo Cim.* 6, 593 (1973).
- A.156. M. S. Marinov and V. S. Popov, *Zh. Eksp. Teor. Fiz.* 68, 421 (1975); [*Sov. Phys. JETP* 41, 205 (1975)].
- A.157. B. Müller, J. Rafelski and W. Greiner, *Phys. Letters* 47B, 5 (1973).
- A.158. H. Peitz, B. Müller, J. Rafelski and W. Greiner, *Lett. Nuovo Cim.* 8, 37 (1973).
- A.159. M. S. Marinov and V. S. Popov, *Yad. Fiz.* 20, 1223 (1974); [*Sov. J. Nucl. Phys.* 20, 641 (1975)].
- A.160. D. H. Jakubassa and M. Kleber, *Z. Physik A* 277, 41 (1976).
- A.161. M. S. Marinov, V. S. Popov and V. L. Stolin, *J. Comp. Phys.* 19, 241 (1975).
- A.162. B. Müller, R. K. Smith and W. Greiner, *Phys. Letters* 53B, 401 (1975).
- A.163. M. S. Marinov, private communication (1976).
- A.164. V. S. Popov and V. D. Mur, *Yad. Fiz.* 18, 684 (1973); [*Sov. J. Nucl. Phys.* 18, 350 (1974)].
- A.165. D. R. Bates and H. S. W. Massey, *Phil. Mag.* 45, 111 (1954);
D. R. Bates in *Atomic and Molecular Processes*, D. R. Bates, ed., (Academic Press, New York, 1962), p.613.
- A.166. D. R. Bates, op. cit., p. 608.
- A.167. U. Fano, *Phys. Rev.* 124, 1866 (1961).
- A.168. K. Smith, H. Peitz, B. Müller and W. Greiner, *Phys. Rev. Letters* 32, 554 (1974).
- A.169. M. S. W. Massey, *Rep. Prog. Phys.* 12, 248 (1949).

- A.170. J. Rafelski and A. Klein in *Proceedings of the International Conference on Reactions Between Complex Nuclei, Vol. 2*, R. L. Robinson, ed., June 1974, at Nashville, Tennessee (American Elsevier Publ. Co., New York, 1974), p. 397.
- A.171. W. Greiner, in *Proceedings of the Third General European Physical Society Conference*, Bucharest, Romania (1975).
- A.172. J. S. Briggs, *Reports on Prog. in Phys.* 39, 217 (1976).
- A.173. Blasche, Franke, and Ch. Schmelzer, quoted in Ref. A.171.
- A.174. D. Burch, W. B. Ingalls, H. Wieman and R. Vandenbosch, *Phys. Rev. A* 10, 1245 (1974).
- A.175. W. E. Meyerhof, *Phys. Rev. A* 10, 1005 (1974).
- A.176. C. Foster, T. Hoogkamer, P. Worlee and F. W. Saris, Abstracts submitted to IX International Conference on Physics of Electronic and Atomic Collisions, J.S. Risley and R. Geballe, eds. (University of Washington Press, 1975), p.511.
- A.177. W. Betz, G. Soff, B. Müller, W. Greiner, Frankfurt/Main preprint (1976).
- A.178. L. B. Okun, *Dokl. Akad. Nauk. SSSR* 89, 883 (1953).
- A.179. V. Oberacker, G. Soff and W. Greiner, *Phys. Rev. Letters* 36, 1024 (1976).
- A.180. V. Oberacker, G. Soff and W. Greiner, *Nucl. Phys.* A259, 324 (1976).
- A.181. G. Soff, B. Müller and J. Rafelski, *Z. Naturforsch.* A29, 1267 (1974).
- A.182. J. Rafelski and B. Müller, *Phys. Rev. Letters* 36 517 (1976).
- A.183. E. Hu, Y. Asano, M. Y. Chen, S. C. Cheng, G. Dugan, L. Lidofsky, W. Patton, C. S. Wu, V. Hughes, and D. Lu, *Nucl. Phys.* A254, 403 (1975).
- A.184. H. L. Anderson, C. K. Hargrove, E. P. Hincks, J. D. McAndrew, R. J. McKee, R. D. Barton, and D. Kessler, *Phys. Rev.* 187, 1565 (1969).
- A.185. T. Erber, D. White, W. Tsai, and H. G. Iatal, *Ann. Phys. (N.Y.)* 102, 405 (1976).
- A.186. R. Staffin, private communication.
- A.187. A. B. Migdal, *Zh. Eksp. Teor. Fiz.* 61, 2209 (1972); [*Sov. Phys. JETP* 34, 1184 (1972)].

FIGURE CAPTIONS

Fig. A.1. Feynman diagrams for the lowest order self-energy (a) and vacuum polarization (b). The double line represents an electron in the external Coulomb field.

Fig. A.2. Calculated values of $G_{SE}(Z\alpha)$ for $Z=10$ to 50 and the extrapolated value at $Z=1$. From MOHR [A.10].

Fig. A.3. Feynman diagrams which contribute to the Lamb shift in helium-like ions.

Fig. A.4. Comparison of theory and experiment for the $L_I - L_{II}$ level splitting in heavy atoms. The error bars give the probable error in the experimental values. Estimated experimental errors smaller than the data points are not shown. See text for explanation.

Fig. A.5. Possible contours of integration in Eq. (A.11) for $Z\alpha > 1$. The contour labelled C_{He} corresponds to a vacuum state with both $1S$ levels filled.

Fig. A.6. Lowest order QED corrections to the energy levels of a bound muon.

Fig. A.7. Expansion of the vacuum polarization in powers of the external field.

Fig. A.8. Sum over all orders in perturbation theory for $V_{11}(r)$.

Fig. A.9. The function $F_0(Z\alpha)$ which describes the charge induced at the nucleus by the higher order vacuum polarization in a Coulomb field. From BROWN et al [A.49].

Fig. A.10. Fourth order vacuum polarization diagrams.

Fig. A.11. Higher order radiative correction to muon levels.

Fig. A.12. Difference between theory and experiment for muonic atom x rays plotted as a function of x-ray energy. Experimental values from Refs. A.54-59.

Fig. A.13. Energy levels for the Dirac-Coulomb equation as a function of Z . A uniform charge density with $R = 1.2 A^{1/3}$ fm is assumed. From PIEPER and GREINER [A.117].

Fig. A.14. Critical value of $Z\alpha$ in the Dirac-Coulomb equation for $E_{1S} = -m$ as a function of nuclear radius (in units of $\lambda_e = 386$ fm). From POPOV [A.133].

Fig. A.15. Spontaneous positron production from the viewpoint of the old and new vacuum. The old vacuum is unstable due to the adiabatic introduction of $\Delta V \propto Z - Z_{CR}$.

Fig. A.16. The effective potential $U_{eff}(r)$ of the effective Schrödinger equation (A.71) for $Z > Z_{CR}$, $E > -m$. The potential $V(r)$ is the potential in the Dirac equation. From ZELDovich and POPOV [A.138].

Fig. A.17. The mean radius \bar{r} of the ground state as a function of its energy E . The radius contracts to $\bar{r} = 0.13 \lambda_e$ at $E = -m$. From POPOV [A.133].

Fig. A.18. The combined atom relativistic molecular states for $92^{II} - 92^{II}$ collisions as a function of the internuclear distance R ; from MÜLLER et al [A.134]. The lowest state reaches the negative continuum at $R_{CR} \sim 34$ fm.

Fig. A.19. The probability of spontaneous positron production for scattering of uranium nuclei at 180° (W_{π}) and the probability averaged over all angles ($W_{av} = \sigma/\sigma_{geom}$). From MARINOV and POPOV [A.159]. These curves should be multiplied by the factor 0.54 for $R_{CR} = 34$ fm (see Section A.3.3).

Fig. A.20. The energy spectrum of spontaneously-produced positrons for backward ion scattering ($\theta = 180^\circ$). The curves labeled 1,2,3 refer to $\eta = 2, 2.8,$ and 4 respectively. From MARINOV and POPOV [A.159].

Fig. A.21. Dependence of the atomic levels on nuclear charge. The positron escape width, which gives the rate for spontaneous decay, increases monotonically with $\Delta Z = Z - Z_{CR}$. Adapted from MÜLLER et al [A.143].

Fig. A.22. Energy and width of the supercritical 1S state calculated by JAKUBASSA and KLEBER [A.160]. The solid lines labeled $|E_1|$ and Γ_1 give the energy and width in the WKB approximation; the dashed lines give the corresponding results when the effective potential is modified by adding a centrifugal term. The results of MÜLLER et al [A.134,145], labeled Γ_2 , for the width of the 1S state (Eq. (A.81)) have been added to the figure for comparison. Adapted from JAKUBASSA and KLEBER [A.160].

Fig. A.23. Probability $W(E)$ for production of a positron with energy E per $\Delta E = 1$ keV. Comparison of the spontaneous and spontaneous-plus-induced spectrum as calculated by SMITH et al. From the review of RAFELSKI and KLEIN [A.170].

Fig. A.24. Cross section for positron production as a function of positron energy, divided by the ionization probability L_0 and Rutherford cross section for U-U central collisions at 812.5 MeV. From SMITH et al [A.168,170].

Fig. A.25. (a) The positron cross sections calculated for U-U central collisions, with L_0 set equal to 10^{-2} . The ion center-of-mass kinetic energies are: [1] 815.5 MeV (distance of closest approach, 15 fm); [2] 609.4 MeV (20 fm); [3] 478.5 MeV (25 fm); [4] 706.3 MeV (30 fm); [5] 398.2 MeV (35 fm). The vertical scale here is corrected according to the relevant footnote in Ref. [A.134]. (b) The total positron cross section dependence on the ion CM energy. From SMITH et al [A.168].

Fig. A.26. Feynman diagram for positron production in ion-ion collisions. The produced electron becomes bound to the nucleus with charge $Z_1|e|$.

Fig. A.27. Schematic diagram of a heavy ion storage ring configuration, suggested in Ref. [A.171], arranged to obtain low relative velocity collisions. By changing θ , the relative velocity can be adjusted. From GREINER [A.171].

Fig. A.28. Differential pair production cross sections (CM) as a function of ion angle for $^{238}\text{U} - ^{238}\text{U}$ collisions. Spontaneous and induced positron production cross section (solid line) and pair production from Coulomb and nuclear excitation cross sections (dashed lines corresponding to two nuclear models) are shown. From OBERACKER et al [A.179].

Fig. A.29. Results of various calculations of the 1S self-energy at high Z . The energy shift is given by $\Delta E = (\alpha/\pi)(Z\alpha)^4 F(Z\alpha)m$. The results are from Refs. [A.8,11,36]. Error estimates smaller than 2% are not shown. From CHENG and JOHNSON [A.36].

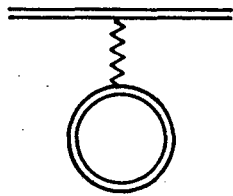
Fig. A.30. Feynman diagrams for production of photons by vacuum polarization in high- Z collision.

Fig. A.31. Relative magnetic splitting $(E_{\downarrow} - E_{\uparrow})/E_B$ (E_B is the binding energy) for selected quasi-molecular states. Collision parameters are $E_{\text{LAB}} = 9$ MeV/nucleon and impact parameter $b = 13$ fm. From RAFELSKI and MÜLLER [A.182].

00004708958



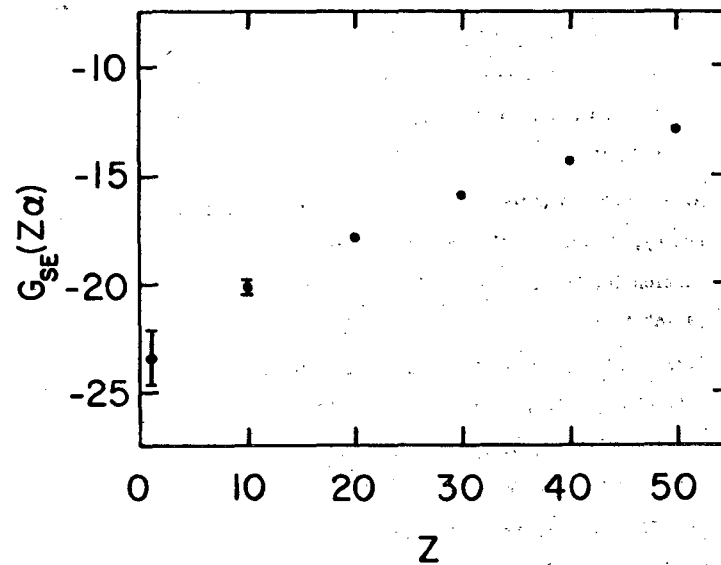
(a)



(b)

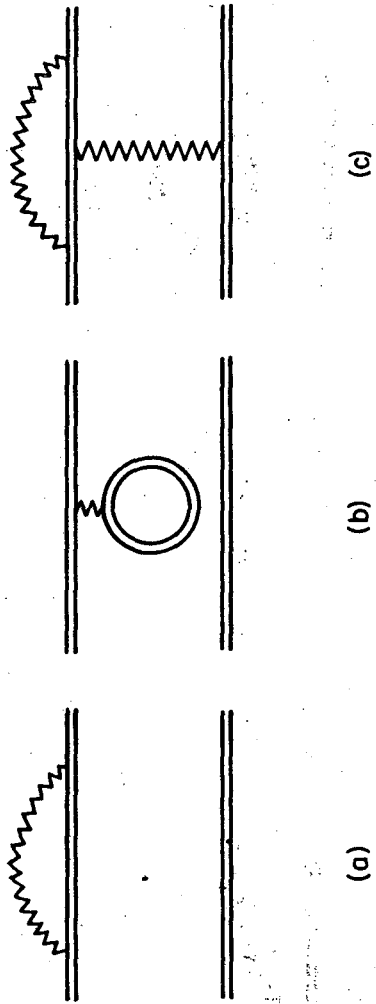
XBL 772-7448

Figure A.1



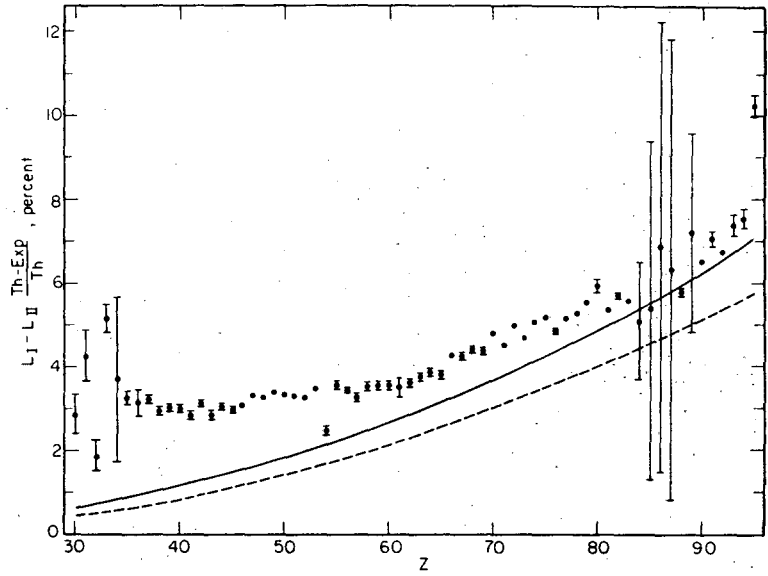
XBL 751-83

Figure A.2



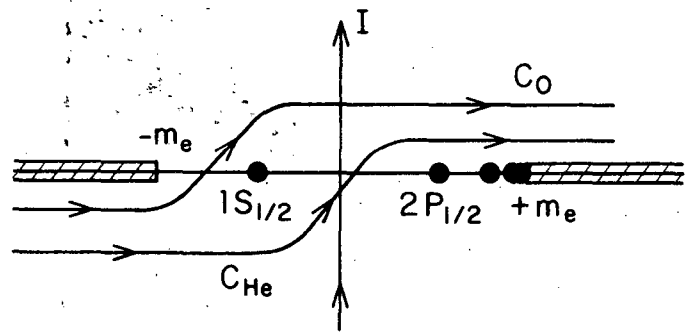
XBL 772-7449

Figure A.3



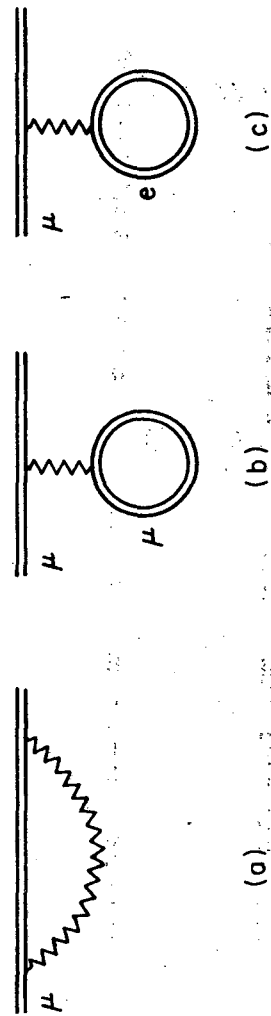
XBL 772-5032

Figure A.4



XBL 747-3588

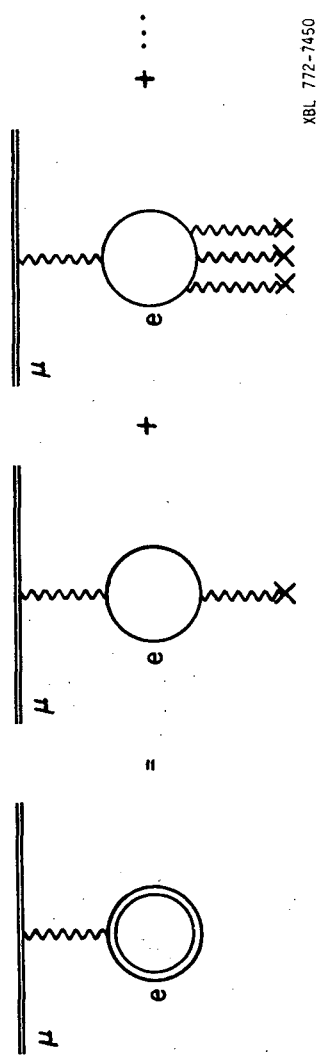
Figure A.5



XBL 767-9112

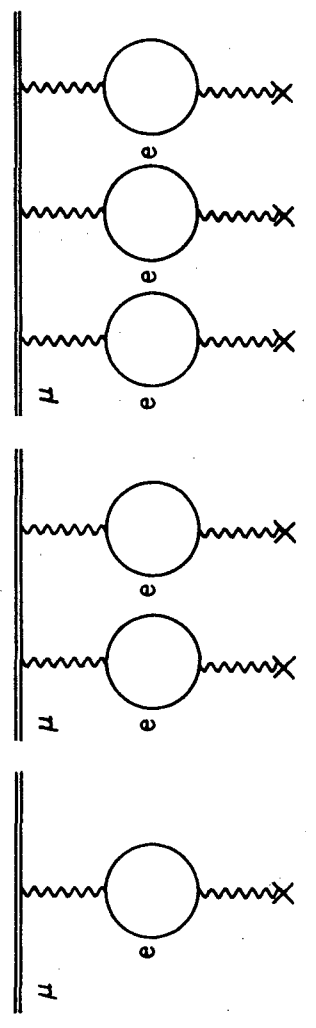
Figure A.6

00004708959



XBL 772-7450

Figure A.7

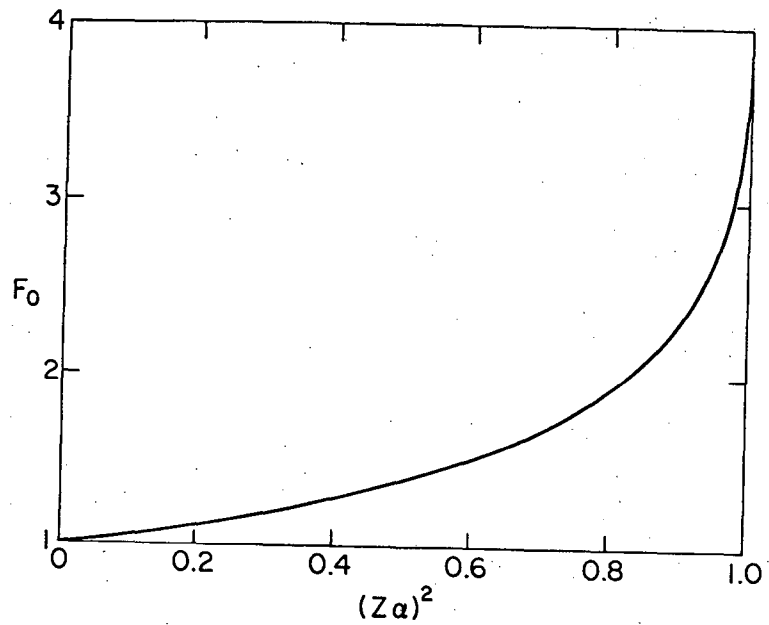


(a)

(b)

(c)

XBL 772-7451



XBL 772-7446

Figure A.9

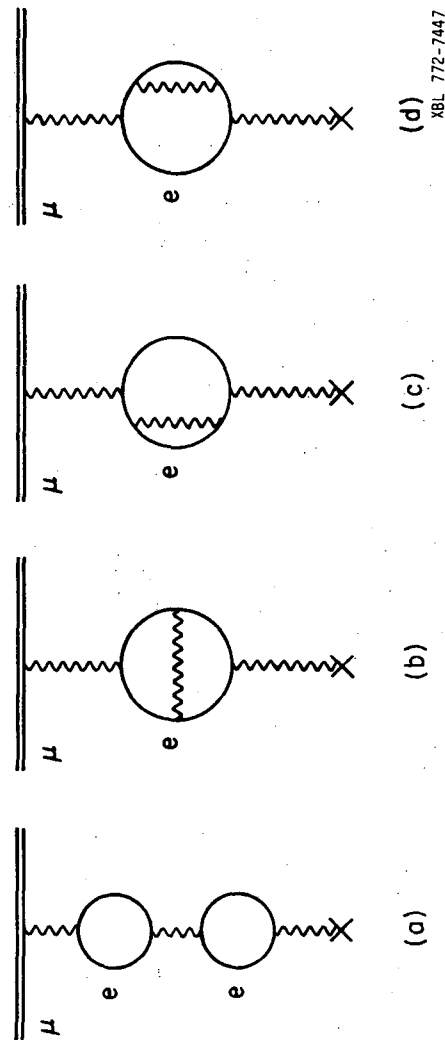
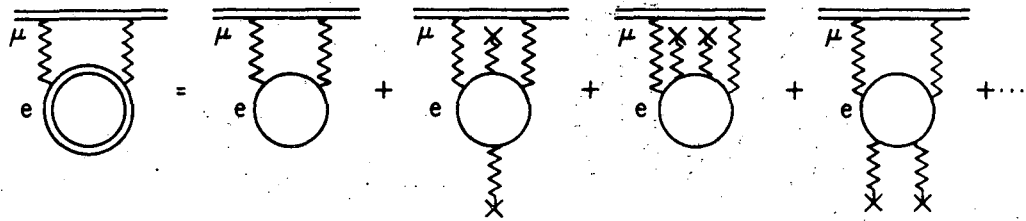
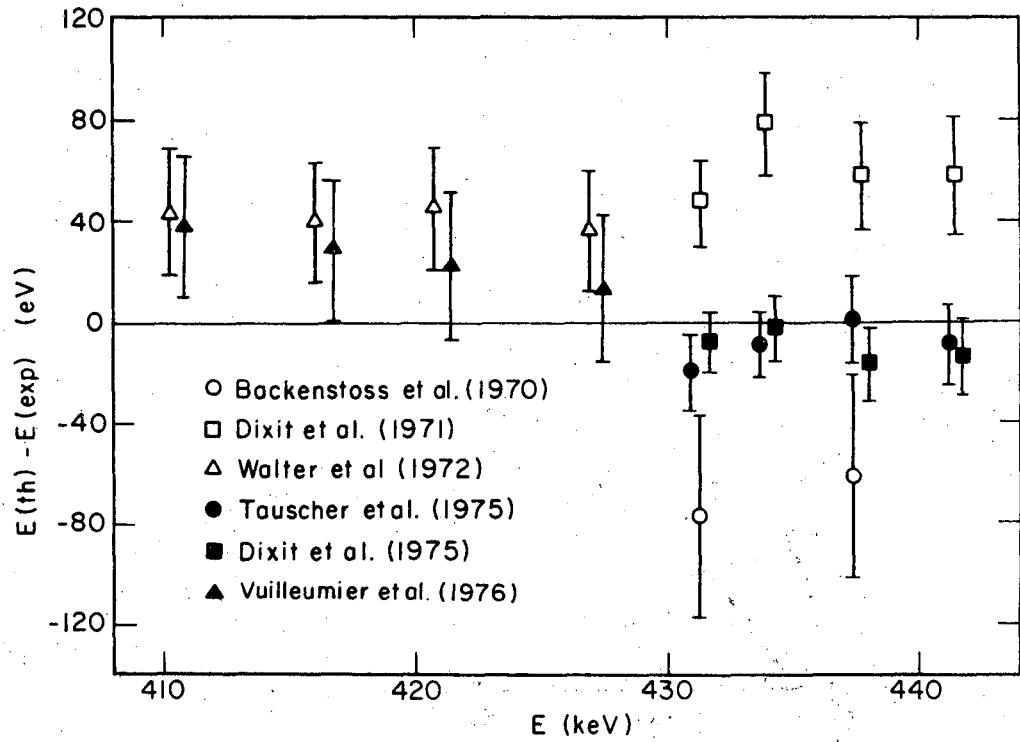


Figure A.10



XBL767-9111

Figure A.11



XBL767-9113A

Figure A.12

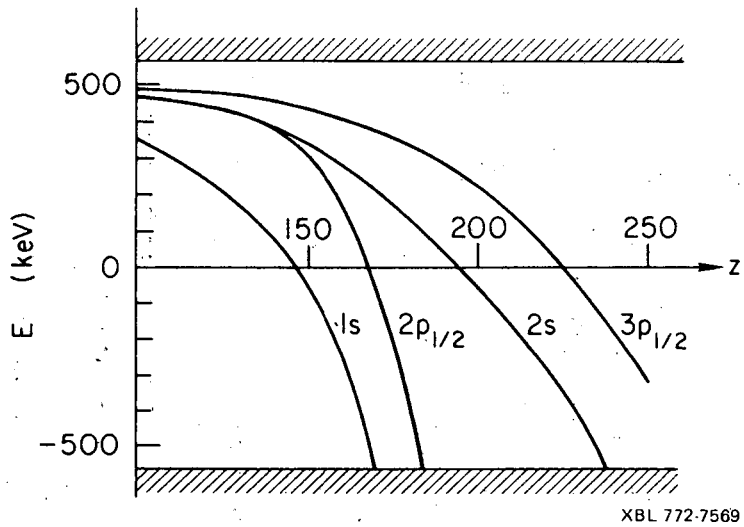


Figure A.15

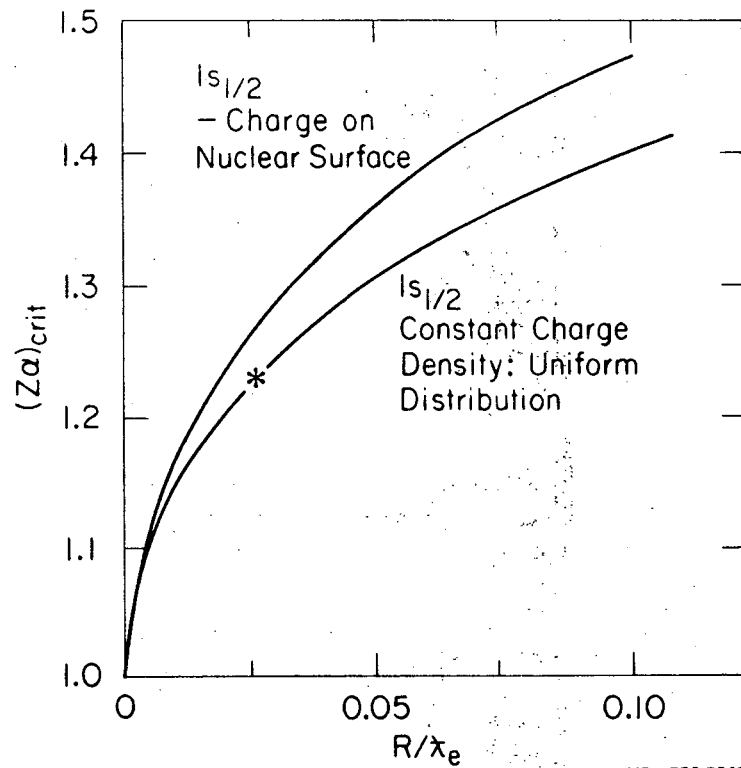
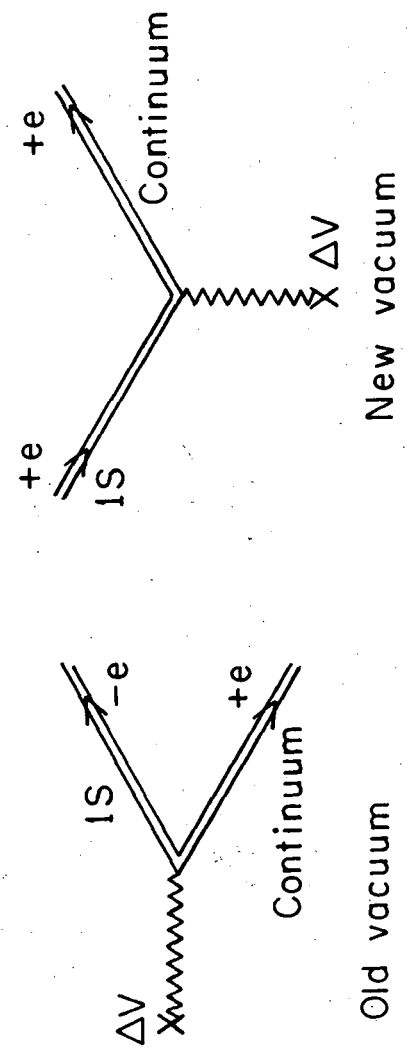


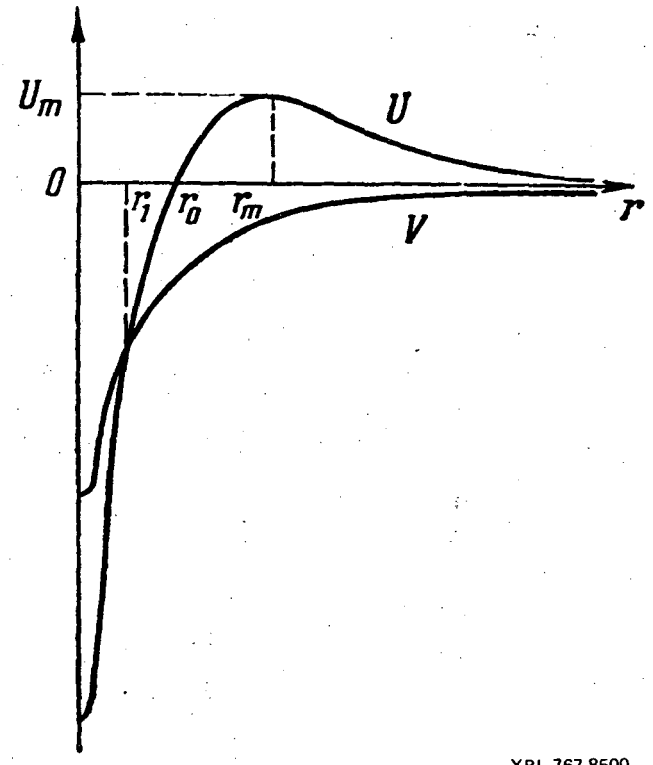
Figure A.14

100004708961



XBL 767-3105

Figure A.15



XBL 767-8500

Figure A.16

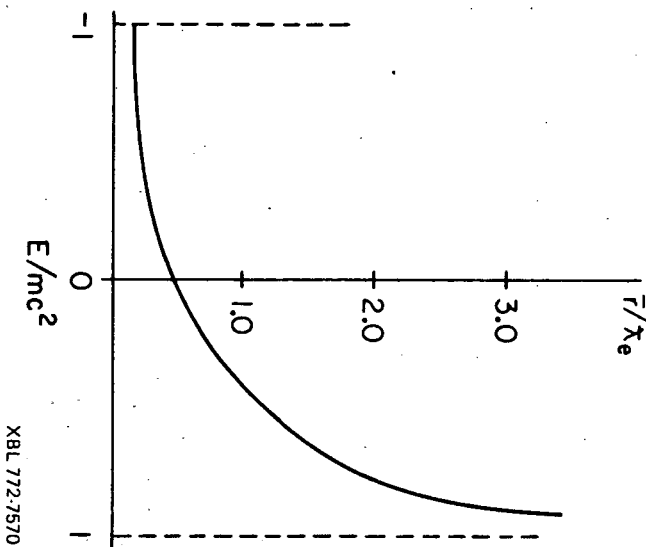
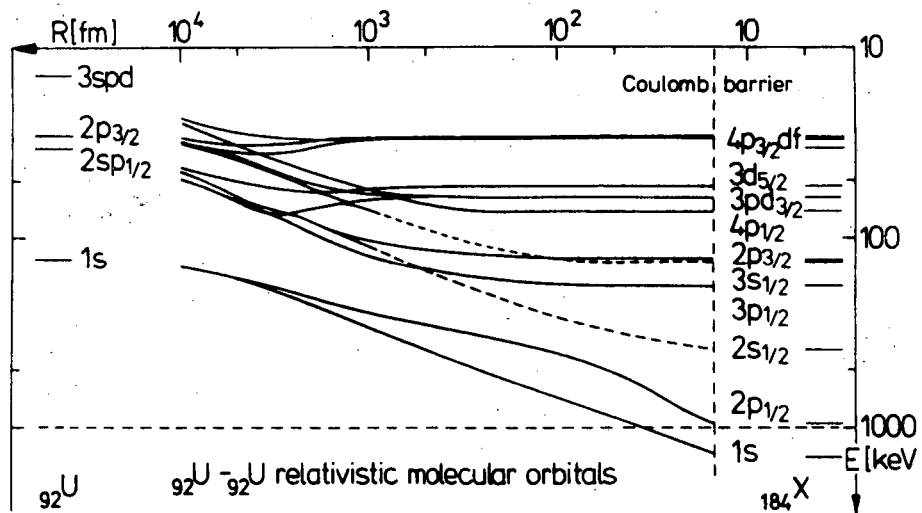


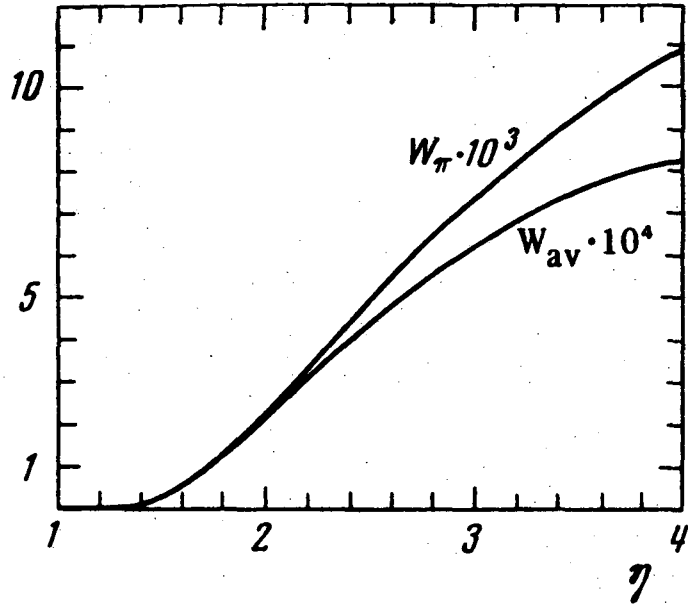
Figure A.17

XBL 772-7570



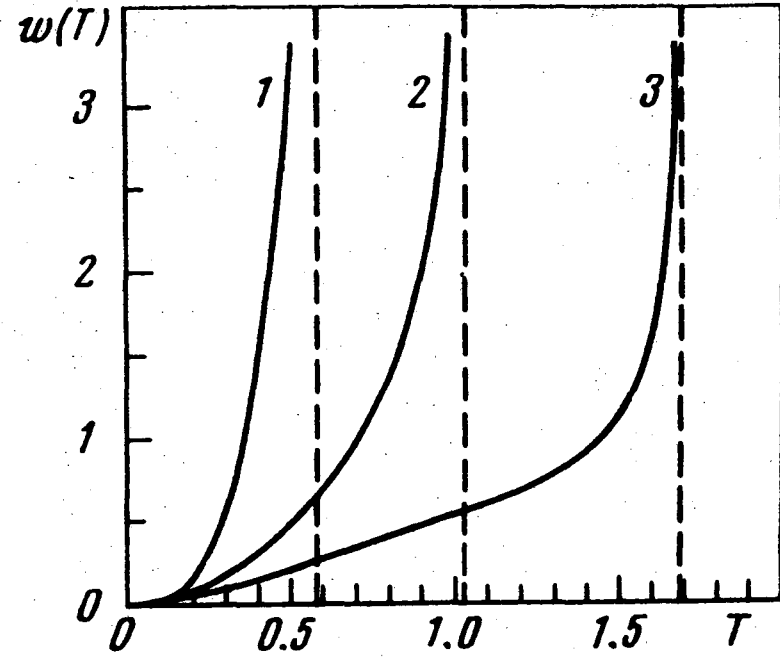
XBL 767-8502

Figure A.18



XBL 767-8501

Figure A.19



XBL 767-8496

Figure A.20

00404708962

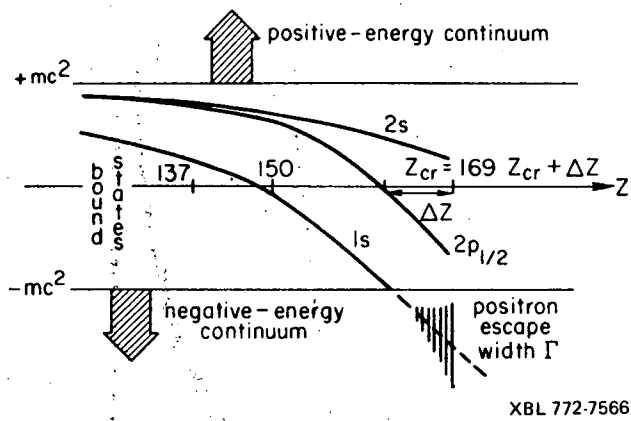


Figure A.21

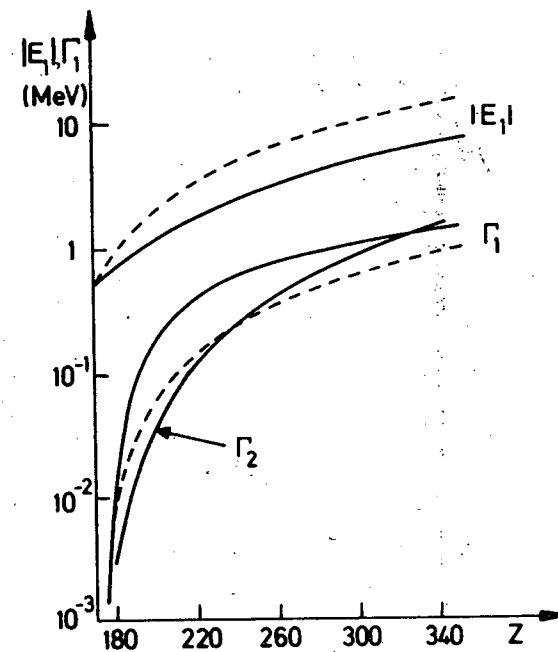
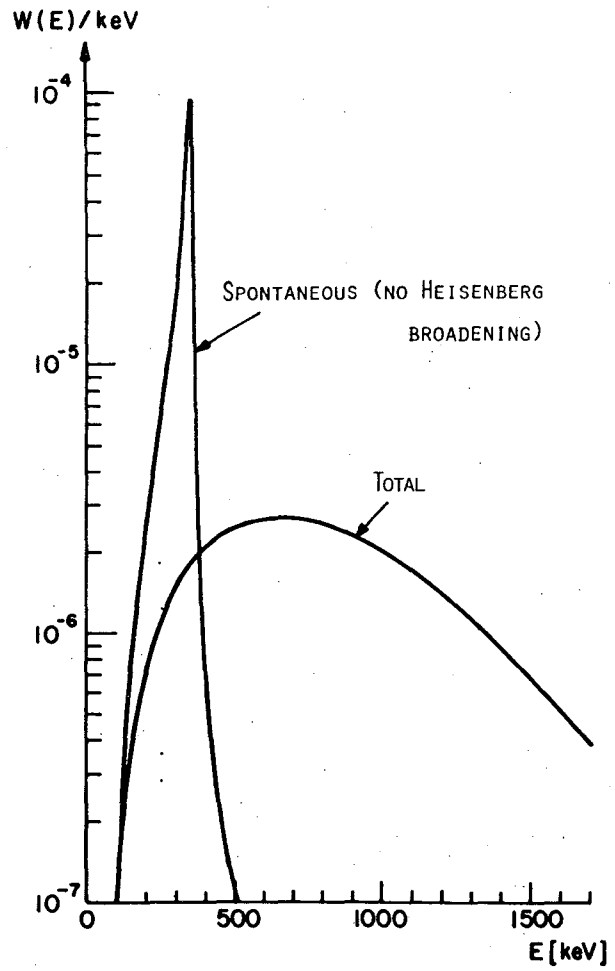
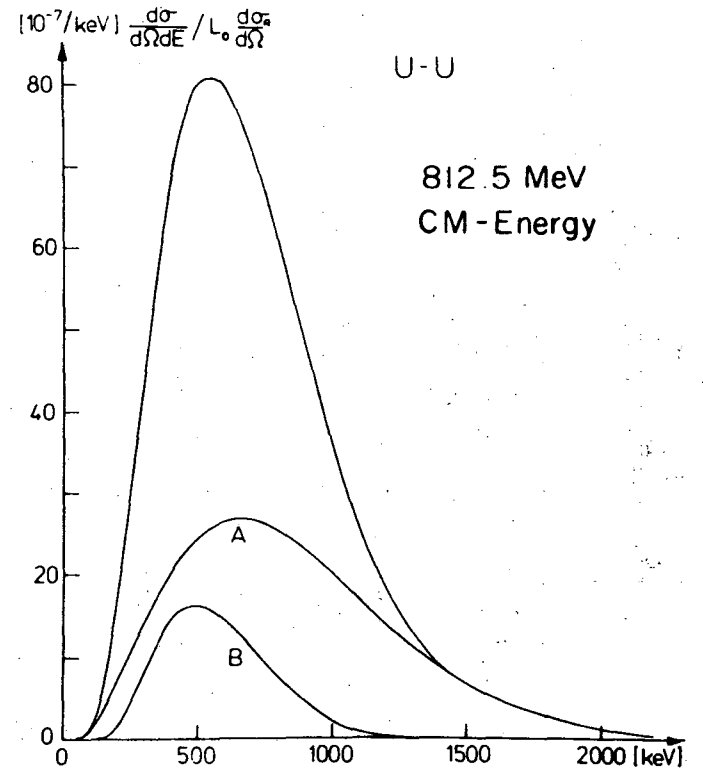


Figure A.22



XBL 767-8497

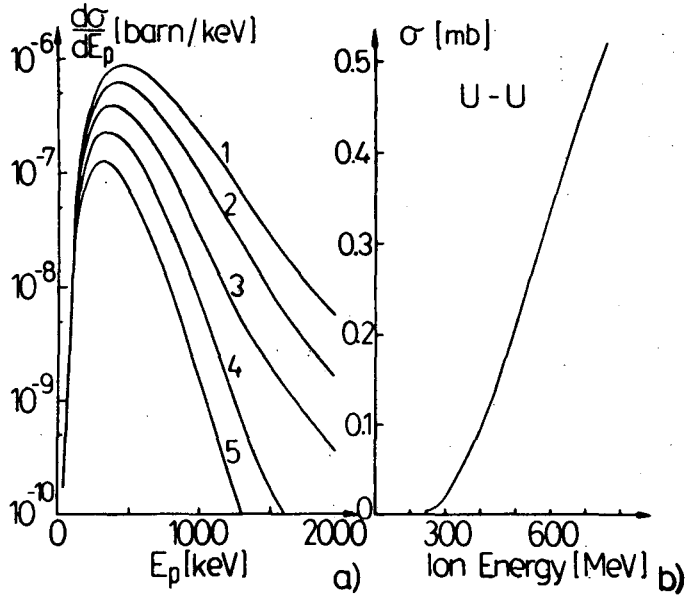
Figure A.23



XBL 767-8499

Figure A.24

00104708963



XBL 767-8493

Figure A.25

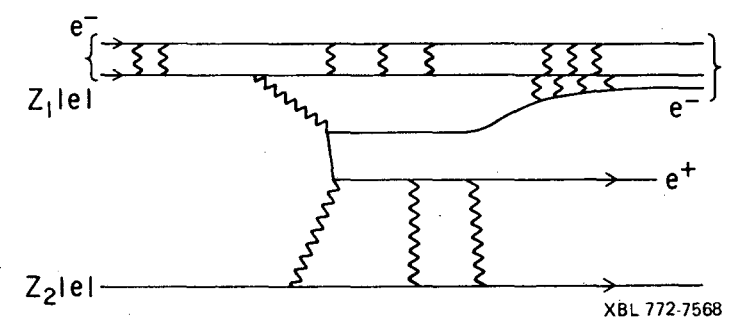
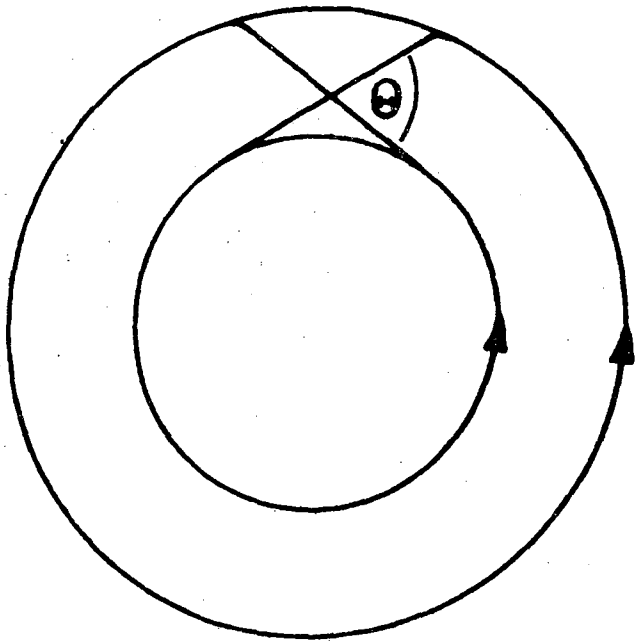
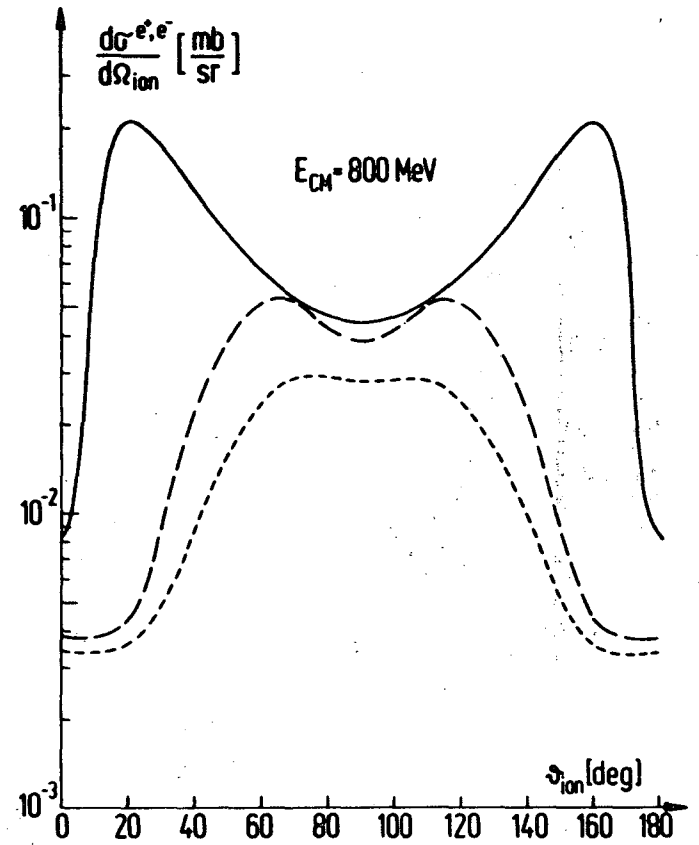


Figure A.26



XBL 767-8492

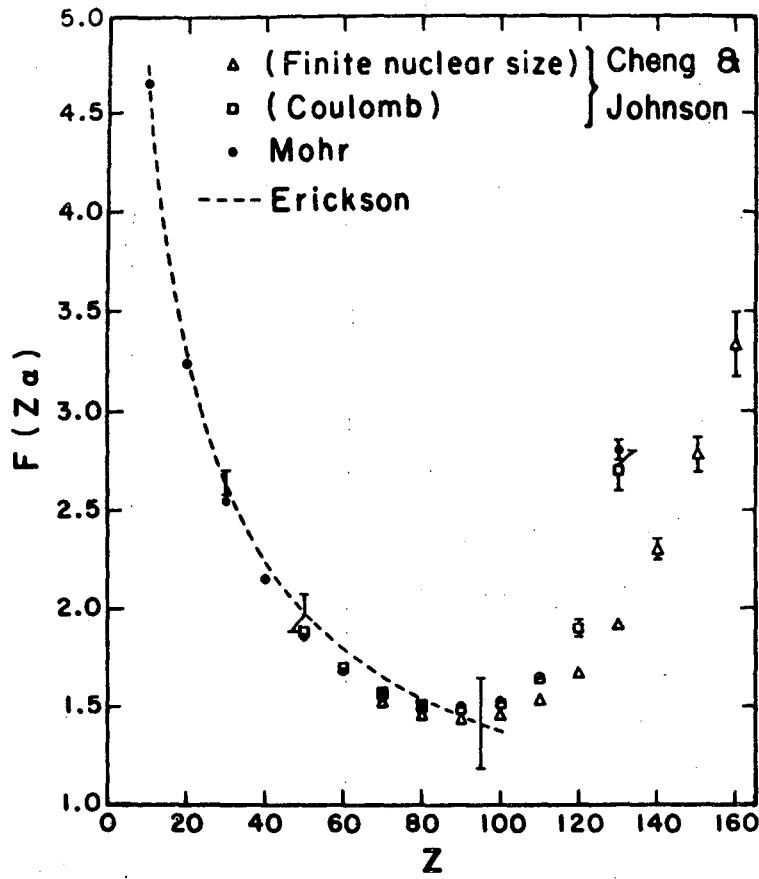
Figure A.27



XBL 767-8494

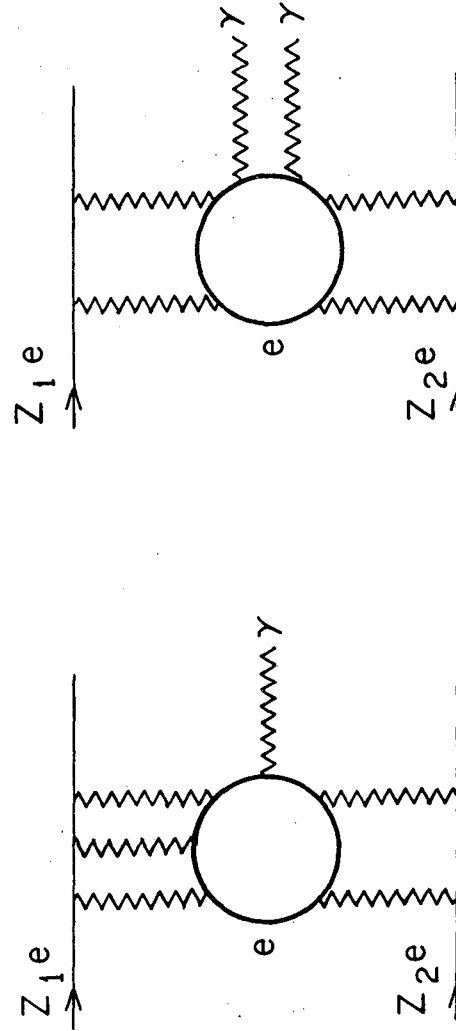
Figure A.28

102004708964



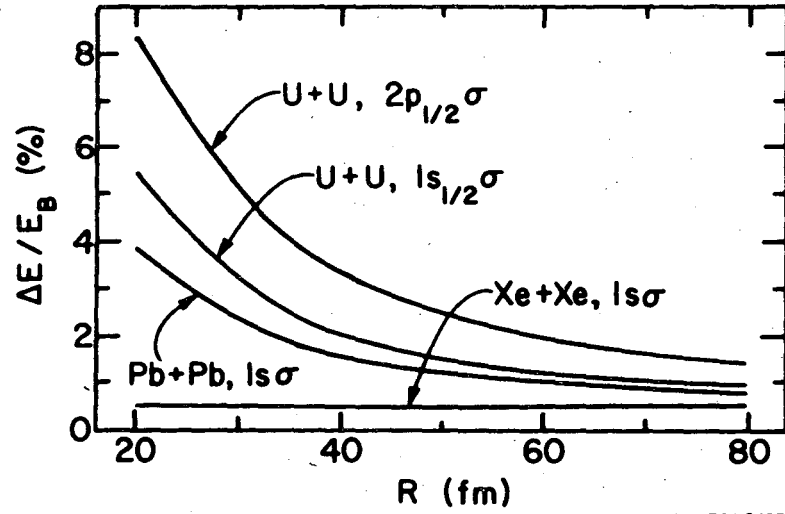
XBL 7610-4685

Figure A.29



XBL 767-3107

Figure A.30



XBL 767-8495

Figure A.31

00004708965

TECHNICAL INFORMATION DIVISION
LAWRENCE BERKELEY LABORATORY
UNIVERSITY OF CALIFORNIA
BERKELEY, CALIFORNIA 94720